Studies on internal rarefied gas flows on the basis of kinetic theory(Dissertation_全文)

AUTHOR(S):

Funagane, Hitoshi

Studies on internal rarefied gas flows on the basis of kinetic theory

Hitoshi Funagane

2012

Contents

Preface **v**

1 Fluid modeling for the Knudsen compressor: Case of polyatomic gases **1**

1.1 Introduction 1

1.2 Fluid-dynamic model for a single channel 3

1.2.1 Problem and assumptions 3

1.2.2 Basic equation and boundary conditions 3

1.2.3 Dimensionless form 6

1.2.4 Macroscopic equation 8

1.2.4.1 Zeroth order 9

1.2.4.2 First order 10

1.2.4.3 Second order and macroscopic equation 13

1.3 Connected channels and connection condition 14

1.4 Data for M_{P} and M_{T}: Reduction to BGK model 15

1.5 Knudsen pump and its performance 17

1.6 Concluding remarks 20

1.7 Appendix A: Equations for ϕ_{P} and ϕ_{T} 21

2 Poiseuille flow and thermal transpiration of a rarefied polyatomic gas through a circular tube with applications to microflows **27**

2.1 Introduction 27

2.2 Poiseuille flow and thermal transpiration through a circular tube 29

2.2.1 Problem, assumptions, and notations 29

2.2.2 Basic equations 31

2.2.3 Similarity solutions 32

2.2.4 Further transformation and reduction to the BGK model 34

2.2.5 Mass-flow and heat-flow rates 36

2.2.6 Numerical results 37

2.3 Diffusion-type system 39
2.4 Applications of diffusion-type system 42
2.4.1 Flow caused by a large pressure difference 42
2.4.2 Knudsen compressor 43
2.5 Concluding remarks 47
2.6 Appendix A: ES model of the Boltzmann equation 49

3 Poiseuille and thermal transpiration flows of a highly rarefied gas: over-concentration in the velocity distribution function 57

3.1 Introduction 57
3.2 Problem and formulation 59
3.3 Preliminary arguments 61
3.4 Structure of the over-concentration and solution method 63
3.4.1 Iterative approximation: method and error estimate 63
3.4.2 Structure of over-concentration 64
3.4.3 Overview of computational method 66
3.5 Numerical results and discussions 68
3.5.1 Velocity distribution functions 68
3.5.2 Net mass flows 69
3.6 Further discussions on asymptotic behaviour as $k \to \infty$ 71
3.6.1 Grad's hard potential and asymptotic formula for $M[\phi_J]$ 71
3.6.2 Similarity between $u[\phi_T]$ and $Q[\phi_P]$ 73
3.7 Conclusion 74
3.8 Appendix A: Sketch of proofs of the statements in § 3.3and § 3.4.1 75
3.9 Appendix B: Database of the net mass flows for the HS model 76
3.10 Appendix C: Grad's hard potential 78

Conclusion 81

Acknowledgment 83

List of Publications 85

Preface

In order to describe ordinary gas flows, one uses fluid dynamics (or gas dynamics), which is a macroscopic and continuum model based on phenomenological assumptions, and it works quite well in most situations. However, in low pressure gases, the gas molecules do not undergo sufficient intermolecular collisions, so that the gas deviates from a local equilibrium state. In such a case, the macroscopic approach is not valid, and one has to use kinetic theory of gases, in which the velocity distribution of gas molecules is taken into account. More specifically, kinetic theory is necessary when the molecular mean free path is not negligibly small compared with characteristic length of the considered system. Therefore, the same situation occurs when the system is of microscale even if the pressure of the gas is ordinary. A gas in which the mean free path is not negligibly small compared with the characteristic length is called a rarefied gas (even if the pressure of the gas is not low). The fundamental equation of kinetic theory of gases is the celebrated Boltzmann equation, and gas dynamics based on kinetic theory is called rarefied gas dynamics or molecular gas dynamics.

Molecular gas dynamics achieved great progress in the 1960's and 1970's in connection with the rapid space development at that time. In the meanwhile, it has spread to other fields such as vacuum technology and micro engineering. Nowadays it is a hot research topic in these fields.

External gas flows are of importance in aerospace applications, whereas internal gas flows appear much more frequently in vacuum technology and micro engineering. In addition, some internal flows have played a role of fundamental problems, which have promoted understanding of physical properties of rarefied gas flows as well as mathematical structures of the solution of the Boltzmann equation. Among such internal flows are the Poiseuille and thermal transpiration flows through a channel or pipe. The former, which is familiar also in ordinary fluid dynamics, is a flow driven by a pressure gradient, and the latter, which is peculiar to rarefied gases, is caused by a temperature gradient imposed on the channel or pipe wall. These two flows have been extensively studied by many researchers since the early stage of modern molecular gas dynamics, and important and useful information has been

accumulated. In these flows, however, there is still enough room for research, for instance, on mathematical structures of the solution of the Boltzmann equation, accurate numerical methods with mathematical basis, etc.

On the other hand, these classical flows of rarefied gases have attracted attentions in recent years, since it turned out that they provided potential mechanisms for vacuum pumps and microscale flow controllers. An example is the revived Knudsen compressor (or pump) without any mechanical or moving parts. A typical configuration of the Knudsen pump is a periodic structure consisting of alternately arranged narrow and wide pipes with a saw-tooth temperature distribution along the pump wall. The Poiseuille and thermal transpiration flows form the basis of the mechanism of the Knudsen pump. Therefore, a theoretical and numerical study of the Knudsen compressor based on the accumulated knowledge of the Poiseuille and thermal transpiration flows is highly desirable at this moment.

The present thesis contains the results of some studies on internal rarefied gas flows performed with the motivation given by the above facts. Chapters 1 and 2 are devoted to a study of Knudsen compressor, whereas Chapter 3 to a fundamental study of linearized Poiseuille and thermal transpiration flows. A more detailed description of these chapters follows.

In Chapter 1, Knudsen compressor consisting of a periodic arrangement of narrower and wider two-dimensional channels, having a periodic saw-tooth temperature distribution, is considered. The properties of the Knudsen compressor, when the gas is a polyatomic gas, are investigated. A macroscopic equation of convection-diffusion type, describing the behavior of a polyatomic gas in the Knudsen compressor, is derived, on the basis of the polyatomic version of the ellipsoidal statistical (ES) model of the Boltzmann equation, by a systematic asymptotic analysis under the assumption that the channel width is much shorter than the length of the pump. The properties of the Knudsen compressor, containing the effect of the internal structure of a gas molecule, are shown by some numerical results based on the macroscopic model.

In Chapter 2, as the first step, Poiseuille and thermal transpiration flows of a rarefied polyatomic gas in a long circular tube is investigated, using the ES model of the Boltzmann equation for a polyatomic gas. It is shown that the solutions to these problems can be reduced to those based on the Bhatnagar, Gross & Krook (BGK) model for a monatomic

gas. As the second step, a rarefied polyatomic gas in a long circular pipe in the following situations is considered: (i) the pressure and temperature variations along the pipe can be arbitrary and large; (ii) the length scale of variations is much longer than the radius of the pipe; (iii) the pipe may consist of circular tubes with different radii. By the same procedure as in the case of two-dimensional channels (Chapter 1), a macroscopic equation is derived. The equation is applied to a polyatomic gas flow through a single long pipe caused by a large pressure difference imposed at both ends, and to a Knudsen compressor consisting of alternately arranged narrower and wider circular tubes.

In Chapter 3, Poiseuille and thermal transpiration flows of a highly rarefied gas between two parallel plates are investigated on the basis of the linearized Boltzmann equation, with a special interest in the phenomenon of over-concentration of gas molecules on velocities parallel to the plates. An iterative approximation method with an explicit convergence estimate is presented, by which the structure of the over-concentration is clarified. A numerical computation on the basis of the method is performed for a hard-sphere molecular gas to construct a database that promptly gives the induced net mass flow for an arbitrary value of large Knudsen numbers (the ratio of the molecular mean free path to the characteristic length). An asymptotic formula of the net mass flow is also presented for molecular models belonging to Grad's hard potential. Finally, the resemblance of the profiles between the heat flow in the Poiseuille flow and the flow velocity in the thermal transpiration is pointed out, and its cause is explained.

Chapter 1

Fluid modeling for the Knudsen compressor: Case of polyatomic gases

1.1 Introduction

The Knudsen pump (or compressor) is a non-mechanical thermal pump for gases, the prototype of which is the device made by Knudsen in 1910 [24,25]. The driving mechanism is the thermal transpiration, a gas flow caused by a temperature gradient along the wall of a pipe, which is peculiar to rarefied gases (gases in low-density circumstances or in micro scales). Since the pump does not contain any moving parts, it has a potential applicability for specific purposes in vacuum and micro technologies. Therefore, the properties of the pump have been investigated in detail numerically and experimentally [30,41,43,23,39,4,37,40,20,19].

A typical configuration of the Knudsen pump is a long tube, consisting of alternately arranged thin and thick pipes, with an imposed periodic temperature distribution along the pipe wall (say, saw-tooth distribution increasing in the thin pipes and decreasing in the thick pipes). Because of the opposite temperature gradients, the flows induced in the thick pipes are in the opposite direction to the flows induced in the thin pipes. However, these flows in the opposite directions do not cancel out completely because of the different thickness of the pipes. As a result, the flows in the thin pipes become dominant and cause a global one way flow, which has a pumping effect. As is seen from this mechanism, the performance of the pump can be improved by a cascade system using many thick and thin pipes (i.e., many units).

Since the thermal transpiration is an effect of a rarefied gas, one has to use kinetic theory to analyze the behavior of the gas in the Knudsen pump. The most widely used tool for simulations of rarefied gas flows is the direct simulation Monte Carlo (DSMC) method [8]. However, for the pump consisting of large number of units, the computational cost required for the DSMC method makes it impossible to perform practical computations. The same is true for other numerical methods, such as finite-difference methods based on

the model Boltzmann equations. In contrast, a simple and convenient macroscopic system, composed of an equation of convection-diffusion type and a connection condition at the junctions of the thick and thin pipes, was proposed recently for the purpose of overcoming the computational difficulty [2,42,3]. The system, which is valid for any Knudsen number (the mean free path of the gas molecules divided by the characteristic length of the system), was derived systematically from the Boltzmann equation under the assumption that the pipes are sufficiently thin compared with their length. The convection-diffusion-type equation contains variable coefficients (say, transport coefficients), which correspond to the mass-flow rate of the thermal transpiration and that of the Poiseuille flow (the flow caused by the pressure gradient along the pipe axis) in an infinitely long single pipe as the functions of the Knudsen number. Applying the macroscopic system with the transport coefficients based on the model Boltzmann equations, some quantitative results for two-dimensional Knudsen pumps composed of wider and narrower channels between two plates have been obtained [42,3]. For instance, the fact that the Knudsen pump is applicable to gas separation was pointed out in [42].

The previous results are formally based on the Boltzmann equation for a single gas or a mixture of gases of monatomic molecules, and the quantitative results are based on the transport coefficients obtained by using the model Boltzmann equations for monatomic molecules [the Bhatnagar–Gross–Krook (BGK) model [7,44] for a single gas in [3], the ellipsoidal statistical (ES) model [21,22] for a single gas in [5], and the McCormack model [26] for a gaseous mixture in [42]]. The aim of the present paper is to extend the macroscopic system to a single polyatomic gas and clarify the effect of the polyatomic molecules on the properties of the Knudsen pump. We employ the ES model for a polyatomic gas [1] as the basic equation and derive the macroscopic system following the procedure in [2,42,3]. As in the examples in [42,3], we restrict ourselves to the case of a two-dimensional Knudsen pump consisting of wider and narrower channels between two plates.

The paper is organized as follows. In Sec. 1.2, we first formulate the flow of a rarefied polyatomic gas between two parallel infinite plates using the ES model and then derive a convection-diffusion-type equation by a formal asymptotic analysis, under the assumption that the channel width is much smaller than the length scale of variation of the wall temperature along the channel. In Sec. 1.3, we derive the connection condition at the junctions

of wider and narrower channels for the convection-diffusion-type equation when it is applied to each channels. In Sec. 1.4, we show that the transport coefficients in the convection-diffusion-type equation can be obtained readily from the corresponding quantities for the BGK model for a monatomic gas by a simple conversion. Finally in Sec. 1.5, the behavior of a polyatomic gas in the Knudsen pump is investigated with the help of the macroscopic system.

1.2 Fluid-dynamic model for a single channel

In this section, we consider a rarefied gas in a single channel between two parallel plates, and following the analysis in [42], [3], we derive a macroscopic equation of convection-diffusion type in the case where the channel width is much smaller than the length scale of variation along the channel.

1.2.1 Problem and assumptions

Let us consider a rarefied gas in a channel between two infinite parallel plates. We take the X_1 axis (of a rectangular coordinate system X_i) perpendicular to the plates and X_2 axis along them and let the plates be located at $X_1 = \pm D/2$. The temperature of the plates, which is common to both plates and depends only on X_2, is denoted by $T_{\rm w}(X_2)$.

We investigate the motion of the gas in the channel under the following assumptions:

(i) The behavior of the gas is described by the ES model [1] of the Boltzmann equation for a polyatomic gas.

(ii) The gas molecules undergo diffuse reflection on the plates.

(iii) The problem is two dimensional, i.e., the physical quantities do not depend on X_3.

(iv) The scale of variation L_* of the plate temperature is much longer than the width of the channel D, i.e., $L_* \gg D$.

1.2.2 Basic equation and boundary conditions

Let us consider a polyatomic gas consisting of molecules with internal degree of freedom δ. The number of the molecules with position in $d\boldsymbol{X}$ around $\boldsymbol{X}$, velocity in $d\boldsymbol{\xi}$ around $\boldsymbol{\xi}$, and

energy related to the internal degree of freedom in $d\mathcal{E}$ around $\mathcal{E}$ at time t is written as

$$\frac{1}{m} f(t, \boldsymbol{X}, \boldsymbol{\xi}, \mathcal{E}) d\boldsymbol{X} d\boldsymbol{\xi} d\mathcal{E}, \tag{1.1}$$

where f is the velocity and energy distribution function of the gas molecules, and m is the mass of a molecule. The equation for f, the ES model for a polyatomic gas, can be written in the following form [1] (see the last paragraph of this subsection for the difference in notations between [1] and the present paper):

$$\frac{\partial f}{\partial t} + \xi_1 \frac{\partial f}{\partial X_1} + \xi_2 \frac{\partial f}{\partial X_2} = A_{\rm c}(T)\rho(\mathcal{G} - f), \tag{1.2a}$$

$$\mathcal{G} = \frac{\rho \Lambda_\delta \mathcal{E}^{\delta/2-1}}{(2\pi)^{3/2} |\underline{\mathcal{T}}|^{1/2} (RT_{\rm rel})^{\delta/2}} \exp\Big(-\frac{1}{2} {}^t(\boldsymbol{\xi} - \boldsymbol{v}) \cdot \underline{\mathcal{T}}^{-1} \cdot (\boldsymbol{\xi} - \boldsymbol{v}) - \frac{\mathcal{E}}{RT_{\rm rel}} \Big), \tag{1.2b}$$

$$\underline{\mathcal{T}} = (1-\eta)\Big\{ (1-\nu) RT_{\rm tr} \underline{Id} + \nu \underline{\Theta} \Big\} + \eta RT \underline{Id}, \tag{1.2c}$$

$$\underline{\Theta} = \frac{1}{\rho} \iint_0^\infty (\boldsymbol{\xi} - \boldsymbol{v}) \cdot {}^t(\boldsymbol{\xi} - \boldsymbol{v}) f d\mathcal{E} d\boldsymbol{\xi}, \tag{1.2d}$$

$$\rho = \iint_0^\infty f d\mathcal{E} d\boldsymbol{\xi}, \tag{1.2e}$$

$$v_i = \frac{1}{\rho} \iint_0^\infty \xi_i f d\mathcal{E} d\boldsymbol{\xi}, \tag{1.2f}$$

$$T_{\rm tr} = \frac{1}{3\rho R} \iint_0^\infty (\xi_i - v_i)^2 f d\mathcal{E} d\boldsymbol{\xi}, \tag{1.2g}$$

$$T_{\rm int} = \frac{2}{\delta \rho R} \iint_0^\infty \mathcal{E} f d\mathcal{E} d\boldsymbol{\xi}, \tag{1.2h}$$

$$T = \frac{3T_{\rm tr} + \delta T_{\rm int}}{3+\delta}, \tag{1.2i}$$

$$T_{\rm rel} = \eta T + (1-\eta) T_{\rm int}. \tag{1.2j}$$

Here, ρ is the mass density of the gas, v_i is the flow velocity, T is the temperature, $T_{\rm tr}$ is the temperature related to the translational energy, $T_{\rm int}$ is the temperature related to the energy of the internal degree of freedom, and R is the specific gas constant (the Boltzmann constant divided by the mass of a molecule); $\nu \in [-1/2, 1)$ and $\eta \in (0, 1]$ are the parameters to adjust the Prandtl number and the bulk viscosity to the gas under consideration [see Eqs. (1.6c) and (1.6d)]; $A_{\rm c}(T)$ is a function of T such that $A_{\rm c}(T)\rho$ is the collision frequency of the gas molecules, and Λ_δ is a dimensionless constant defined by

$$\Lambda_\delta^{-1} = \int_0^\infty s^{\delta/2-1} e^{-s} ds. \tag{1.3}$$

In addition, $\underline{\mathcal{T}}$ and $\underline{\Theta}$ are 3×3 symmetric matrices, $\underline{Id}$ is the 3×3 identity matrix, $|\underline{\mathcal{T}}|$ and $\underline{\mathcal{T}}^{-1}$ are the determinant and the inverse matrix of $\underline{\mathcal{T}}$, respectively, and the symbol ^{t} indicates

the transpose operation. In what follows, for an arbitrary matrix $\underline{A}$, its (i, j) component, determinant, inverse matrix, and transposed matrix are denoted by A_{ij}, $|\underline{A}|$, $\underline{A}^{-1}$, and ${}^t\underline{A}$, respectively. In the above equations, $d\boldsymbol{\xi} = d\xi_1 d\xi_2 d\xi_3$, and the domain of integration with respect to ξ_i is the whole space of ξ_i. It should be noted that the pressure p and the stress tensor p_{ij} are given by

$$p = \rho RT, \tag{1.4a}$$

$$p_{ij} = \rho\Theta_{ij} = \iint_0^\infty (\xi_i - v_i)(\xi_j - v_j) f d\mathcal{E} d\boldsymbol{\xi}. \tag{1.4b}$$

The vanishing right-hand side of Eq. (1.2a) is equivalent to the fact that f is a local equilibrium distribution $f_{\rm eq}$ [1]:

$$f_{\rm eq} = \frac{\rho\Lambda_\delta}{(2\pi RT)^{3/2}(RT)^{\delta/2}} \mathcal{E}^{\delta/2-1} \exp\Big(-\frac{(\xi_i - v_i)^2}{2RT} - \frac{\mathcal{E}}{RT}\Big). \tag{1.5}$$

It is also known [1] that Eq. (1.2) leads to the viscosity μ, the thermal conductivity κ, the Prandtl number Pr, and the bulk viscosity $\mu_{\rm b}$ in the following form:

$$\mu = \frac{1}{1 - \nu + \eta\nu} \frac{RT}{A_{\rm c}(T)}, \tag{1.6a}$$

$$\kappa = \frac{\gamma}{\gamma - 1} R \frac{RT}{A_{\rm c}(T)}, \tag{1.6b}$$

$$\Pr = \frac{\gamma}{\gamma - 1} \frac{R\mu}{\kappa} = \frac{1}{1 - \nu + \eta\nu}, \tag{1.6c}$$

$$\mu_{\rm b} = \frac{1}{\eta}\Big(\frac{5}{3} - \gamma\Big) \frac{\mu}{\Pr}, \tag{1.6d}$$

with γ the ratio of the specific heats given by

$$\gamma = \frac{\delta + 5}{\delta + 3}. \tag{1.7}$$

Equation (1.2a) contains the set of parameters (ν, η, δ) characterizing the gas under consideration. In place of this set, we may use another set $(\Pr, \mu_{\rm b}/\mu, \delta)$ because of relations (1.6c), (1.6d), and (1.7) (cf. Secs. 1.2.4 and 1.4 and 1.7).

The diffuse-reflection condition [10,11,35,36], adapted to the present polyatomic case, on the channel walls are expressed as

$$f = \frac{\rho_{\rm w}\Lambda_\delta}{(2\pi RT_{\rm w})^{3/2}(RT_{\rm w})^{\delta/2}} \mathcal{E}^{\delta/2-1} \exp\Big(-\frac{\xi_i^2}{2RT_{\rm w}} - \frac{\mathcal{E}}{RT_{\rm w}}\Big), \qquad (X_1 = \pm D/2,\ \ \xi_1 \lessgtr 0), \tag{1.8a}$$

$$\rho_{\rm w} = \pm\Big(\frac{2\pi}{RT_{\rm w}}\Big)^{1/2} \int_{\xi_1 \gtrless 0} \int_0^\infty \xi_1 f d\mathcal{E} d\boldsymbol{\xi}, \qquad (X_1 = \pm D/2), \tag{1.8b}$$

where the upper (or lower) signs go together. The initial condition is given by

$$f(0, X_1, X_2, \boldsymbol{\xi}, \mathcal{E}) = f^0(X_1, X_2, \boldsymbol{\xi}, \mathcal{E}). \tag{1.9}$$

The mass-flow rate M in the X_2 direction (per unit time and per unit length in X_3) is expressed as

$$M = \int_{-D/2}^{D/2} \rho \upsilon_2 dX_1. \tag{1.10}$$

In [1], the energy $\mathcal{E}$, which is denoted by ε there, is assumed to be expressed as $\mathcal{E} = I^{2/\delta}$ in terms of a variable I, and I is used as an independent variable. More specifically, the distribution function in [1], which we denote by $\overline{f}(t, \boldsymbol{X}, \boldsymbol{\xi}, I)$ here, is defined in such a way that

$$\frac{1}{m}\overline{f}(t, \boldsymbol{X}, \boldsymbol{\xi}, I) d\boldsymbol{X} d\boldsymbol{\xi} dI, \tag{1.11}$$

indicates the number of the molecules with position in $d\boldsymbol{X}$ around $\boldsymbol{X}$, velocity in $d\boldsymbol{\xi}$ around $\boldsymbol{\xi}$, and the variable I in dI around I at time t. Therefore, the relation between $\overline{f}$ and the present f is as follows:

$$f(t, \boldsymbol{X}, \boldsymbol{\xi}, \mathcal{E}) = (\delta/2)\mathcal{E}^{\delta/2-1}\overline{f}(t, \boldsymbol{X}, \boldsymbol{\xi}, \mathcal{E}^{\delta/2}). \tag{1.12}$$

In addition, Λ_δ in [1], which we denote $\overline{\Lambda}_\delta$ here, is related to Λ_δ in Eq. (1.3) as

$$\Lambda_\delta^{-1} = (2/\delta)(\overline{\Lambda}_\delta)^{-1}. \tag{1.13}$$

1.2.3 Dimensionless form

Let us introduce the following dimensionless quantities:

$$\begin{aligned}
&\hat{t} = t/t_*, \qquad x_1 = X_1/D_*, \qquad x_2 = X_2/L_*, \\
&\zeta_i = \xi_i/(2RT_*)^{1/2}, \qquad \hat{\mathcal{E}} = \mathcal{E}/RT_*, \\
&(\hat{f},\ \hat{\mathcal{G}}) = (f,\ \mathcal{G})/2\rho_*(2RT_*)^{-5/2}, \\
&\hat{\rho} = \rho/\rho_*, \qquad \hat{\upsilon}_i = \upsilon_i/(2RT_*)^{1/2}, \\
&(\hat{T}_{\rm tr},\ \hat{T}_{\rm int},\ \hat{T},\ \hat{T}_{\rm rel}) = (T_{\rm tr},\ T_{\rm int},\ T,\ T_{\rm rel})/T_*, \\
&\hat{p} = p/p_*, \qquad \hat{p}_{ij} = p_{ij}/p_*, \qquad \hat{M} = M/\rho_*(2RT_*)^{1/2}D_*, \\
&\hat{\rho}_{\rm w} = \rho_{\rm w}/\rho_*, \qquad \hat{T}_{\rm w} = T_{\rm w}/T_*, \qquad a = D/D_*, \\
&\hat{A}_{\rm c}(\hat{T}) = A_{\rm c}(T)/A_{\rm c}(T_*), \qquad (\underline{\hat{\mathcal{I}}},\ \underline{\hat{\Theta}}) = (\underline{\mathcal{I}},\ \underline{\Theta})/RT_*,
\end{aligned} \tag{1.14}$$

where t_* is the reference time, $D_*\,(\ll L_*)$ is the reference width of the channel, ρ_* is the reference density, T_* is the reference temperature, $p_* = R\rho_* T_*$ is the reference pressure. The mean free path l_* of the gas molecules in the equilibrium state at rest is given as $l_* = (2/\sqrt{\pi})(2RT_*)^{1/2}/A_{\rm c}(T_*)\rho_*$.

Then, Eq. (1.2) is transformed to the following dimensionless form:

$$\mathrm{Sh}\frac{\partial \hat{f}}{\partial \hat{t}} + \zeta_1 \frac{\partial \hat{f}}{\partial x_1} + \epsilon\zeta_2 \frac{\partial \hat{f}}{\partial x_2} = \frac{2}{\sqrt{\pi}} \frac{1}{K_*} \hat{A}_{\rm c} \hat{\rho} (\hat{\mathcal{G}} - \hat{f}), \tag{1.15a}$$

$$\hat{\mathcal{G}} = \frac{\hat{\rho}\Lambda_\delta}{\pi^{3/2} |\underline{\hat{\mathcal{I}}}|^{1/2} \hat{T}_{\rm rel}^{\delta/2}} \hat{\mathcal{E}}^{\delta/2-1} \exp\Big(-{}^t(\boldsymbol{\zeta} - \hat{\boldsymbol{v}}) \cdot \underline{\hat{\mathcal{I}}}^{-1} \cdot (\boldsymbol{\zeta} - \hat{\boldsymbol{v}}) - \frac{\hat{\mathcal{E}}}{\hat{T}_{\rm rel}} \Big), \tag{1.15b}$$

$$\underline{\hat{\mathcal{I}}} = (1-\eta)\{(1-\nu)\hat{T}_{\rm tr}\underline{Id} + \nu\underline{\hat{\Theta}}\} + \eta\hat{T}\underline{Id}, \tag{1.15c}$$

$$\underline{\hat{\Theta}} = \frac{2}{\hat{\rho}} \iint_0^\infty (\boldsymbol{\zeta} - \hat{\boldsymbol{v}}) \cdot {}^t(\boldsymbol{\zeta} - \hat{\boldsymbol{v}}) \hat{f} d\hat{\mathcal{E}} d\boldsymbol{\zeta}, \tag{1.15d}$$

$$\hat{\rho} = \iint_0^\infty \hat{f} d\hat{\mathcal{E}} d\boldsymbol{\zeta}, \tag{1.15e}$$

$$\hat{v}_i = \frac{1}{\hat{\rho}} \iint_0^\infty \zeta_i \hat{f} d\hat{\mathcal{E}} d\boldsymbol{\zeta}, \tag{1.15f}$$

$$\hat{T}_{\rm tr} = \frac{2}{3}\frac{1}{\hat{\rho}} \iint_0^\infty (\zeta_i - \hat{v}_i)^2 \hat{f} d\hat{\mathcal{E}} d\boldsymbol{\zeta}, \tag{1.15g}$$

$$\hat{T}_{\rm int} = \frac{2}{\delta}\frac{1}{\hat{\rho}} \iint_0^\infty \hat{\mathcal{E}} \hat{f} d\hat{\mathcal{E}} d\boldsymbol{\zeta}, \tag{1.15h}$$

$$\hat{T} = \frac{3\hat{T}_{\rm tr} + \delta\hat{T}_{\rm int}}{3+\delta}, \tag{1.15i}$$

$$\hat{T}_{\rm rel} = \eta\hat{T} + (1-\eta)\hat{T}_{\rm int}, \tag{1.15j}$$

where $d\boldsymbol{\zeta} = d\zeta_1 d\zeta_2 d\zeta_3$, and the domain of integration with respect to ζ_i is the whole space of ζ_i. The Sh, ϵ, and K_* in Eq. (1.15) are the dimensionless parameters defined by

$$\mathrm{Sh} = \frac{D_*}{t_*(2RT_*)^{1/2}}, \qquad \epsilon = \frac{D_*}{L_*}, \qquad K_* = \frac{l_*}{D_*}, \tag{1.16}$$

where Sh is the reference Strouhal number, and K_* is the reference Knudsen number. Corresponding to Eqs. (1.4a) and (1.4b), we have

$$\hat{p} = \hat{\rho}\,\hat{T}, \tag{1.17a}$$

$$\hat{p}_{ij} = \hat{\rho}\,\hat{\Theta}_{ij} = \iint_0^\infty 2(\zeta_i - \hat{v}_i)(\zeta_j - \hat{v}_j)\hat{f} d\hat{\mathcal{E}} d\boldsymbol{\zeta}. \tag{1.17b}$$

The dimensionless form of the boundary condition (1.8) is given by

$$\hat{f} = \frac{\hat{\rho}_{\rm w}\Lambda_\delta}{(\pi\hat{T}_{\rm w})^{3/2}\hat{T}_{\rm w}^{\delta/2}}\hat{\mathcal{E}}^{\delta/2-1}\exp\Big(-\frac{\zeta_i^2}{\hat{T}_{\rm w}}-\frac{\hat{\mathcal{E}}}{\hat{T}_{\rm w}}\Big) \quad (x_1=\pm a/2, \quad \zeta_1 \lessgtr 0), \tag{1.18a}$$

$$\hat{\rho}_{\rm w} = \pm 2\sqrt{\frac{\pi}{\hat{T}_{\rm w}}}\int_{\zeta_1\gtrless 0}\int_0^\infty \zeta_1 \hat{f} d\hat{\mathcal{E}} d\boldsymbol{\zeta}, \tag{1.18b}$$

and that of the initial condition (1.9) is given by

$$\hat{f}(0, x_1, x_2, \boldsymbol{\zeta}, \hat{\mathcal{E}}) = \hat{f}^0(x_1, x_2, \boldsymbol{\zeta}, \hat{\mathcal{E}}). \tag{1.19}$$

From Eq. (1.10), we have, for the dimensionless mass-flow rate $\hat{M}$,

$$\hat{M} = \int_{-a/2}^{a/2} \hat{\rho}\hat{v}_2 dx_1. \tag{1.20}$$

Because of assumption (iv) in Sec. 1.2.1, ϵ in Eq. (1.16) is the small parameter in our problem, whereas the reference Knudsen number K_* is arbitrary. In this situation, the induced gas flow is expected to be slow. If we assume that $\hat{v}_i$ is of the order of ϵ, the reference time t_* and thus the Strouhal number Sh may be chosen as

$$t_* = L_*/(2RT_*)^{1/2}\epsilon, \qquad {\rm Sh} = \epsilon^2. \tag{1.21}$$

Therefore, Eq. (1.15a) becomes

$$\epsilon^2\frac{\partial \hat{f}}{\partial \hat{t}} + \zeta_1\frac{\partial \hat{f}}{\partial x_1} + \epsilon\zeta_2\frac{\partial \hat{f}}{\partial x_2} = \frac{2}{\sqrt{\pi}}\frac{1}{K_*}\hat{A}_{\rm c}\hat{\rho}(\hat{\mathcal{G}} - \hat{f}). \tag{1.22}$$

1.2.4 Macroscopic equation

We analyze the problem (1.22) [with Eqs. (1.15b)–(1.15j)], (1.18), and (1.19) by expanding $\hat{f}$ in terms of ϵ:

$$\hat{f} = \hat{f}_{(0)} + \hat{f}_{(1)}\epsilon + \hat{f}_{(2)}\epsilon^2 + \cdots. \tag{1.23}$$

Correspondingly, the moments of $\hat{f}$ occurring in Eq. (1.22), i.e., $\hat{\rho}$, $\hat{v}_i$, $\hat{T}_{\rm tr}$, $\hat{T}_{\rm int}$, and $\underline{\hat{\Theta}}$, and thus all the other (macroscopic) quantities that are defined in terms of these moments are expanded as

$$\hat{h} = \hat{h}_{(0)} + \hat{h}_{(1)}\epsilon + \hat{h}_{(2)}\epsilon^2 + \cdots. \tag{1.24}$$

Here, $\hat{h}$ stands for $\hat{\rho}$, $\hat{v}_i$, $\hat{T}_{\rm tr}$, $\hat{T}_{\rm int}$, and $\underline{\hat{\Theta}}$ and also $\hat{T}$, $\hat{T}_{\rm rel}$, $\hat{A}_{\rm c}$, $|\underline{\hat{\mathcal{I}}}|$, $\underline{\hat{\mathcal{I}}}^{-1}$, $\hat{p}$ and $\hat{p}_{ij}$. For instance, for $\hat{\rho}$, $\underline{\hat{\Theta}}$, $\hat{A}_{\rm c}$, we write

$$\hat{\rho} = \hat{\rho}_{(0)} + \hat{\rho}_{(1)}\epsilon + \hat{\rho}_{(2)}\epsilon^2 + \cdots , \tag{1.25a}$$

$$\underline{\hat{\Theta}} = \underline{\hat{\Theta}}_{(0)} + \underline{\hat{\Theta}}_{(1)}\epsilon + \underline{\hat{\Theta}}_{(2)}\epsilon^2 + \cdots , \tag{1.25b}$$

$$\hat{A}_{\rm c} = \hat{A}_{{\rm c}(0)} + \hat{A}_{{\rm c}(1)}\epsilon + \hat{A}_{{\rm c}(2)}\epsilon^2 + \cdots . \tag{1.25c}$$

The expansion of the macroscopic quantities (1.24) leads to the corresponding expansion of the Gaussian $\hat{\mathcal{G}}$:

$$\hat{\mathcal{G}} = \hat{\mathcal{G}}_{(0)} + \hat{\mathcal{G}}_{(1)}\epsilon + \hat{\mathcal{G}}_{(2)}\epsilon^2 + \cdots . \tag{1.26}$$

In addition, $\hat{\rho}_{\rm w}$ in the boundary condition (1.18) and the dimensionless mass-flow rate $\hat{M}$ [Eq. (1.20)] are expanded as well:

$$\hat{\rho}_{\rm w} = \hat{\rho}_{{\rm w}(0)} + \hat{\rho}_{{\rm w}(1)}\epsilon + \hat{\rho}_{{\rm w}(2)}\epsilon^2 + \cdots , \tag{1.27a}$$

$$\hat{M} = \hat{M}_{(0)} + \hat{M}_{(1)}\epsilon + \hat{M}_{(2)}\epsilon^2 + \cdots . \tag{1.27b}$$

The explicit expressions of the coefficients in the expansions (1.24), (1.26), and (1.27), some of which will be given when necessary in the sequel, are omitted here. By the substitution of these expansions in Eqs. (1.22) [with Eqs. (1.15b)–(1.15j)], (1.18), and (1.19), we can solve the problem from the lowest order of ϵ.

1.2.4.1 Zeroth order

The equation at the zeroth order in ϵ is as follows:

$$\zeta_1 \frac{\partial \hat{f}_{(0)}}{\partial x_1} = \frac{2}{\sqrt{\pi}} \frac{1}{K_*} \hat{A}_{{\rm c}(0)} \hat{\rho}_{(0)} (\hat{\mathcal{G}}_{(0)} - \hat{f}_{(0)}), \tag{1.28}$$

where $\hat{A}_{{\rm c}(0)} = \hat{A}_{\rm c}(\hat{T}_{(0)})$, and the explicit forms of $\hat{\rho}_{(0)}$ and $\hat{\mathcal{G}}_{(0)}$, which can be obtained from Eqs. (1.15b)–(1.15j) straightforwardly, are omitted here. The corresponding boundary condition is given by

$$\hat{f}_{(0)} = \frac{\hat{\rho}_{{\rm w}(0)} \Lambda_\delta}{(\pi \hat{T}_{\rm w})^{3/2} \hat{T}_{\rm w}^{\delta/2}} \hat{\mathcal{E}}^{\delta/2-1} \exp\Big(-\frac{\zeta_i^2}{\hat{T}_{\rm w}} - \frac{\hat{\mathcal{E}}}{\hat{T}_{\rm w}}\Big) \quad (x_1 = \pm a/2,\ \ \zeta_1 \lessgtr 0), \tag{1.29a}$$

$$\hat{\rho}_{{\rm w}(0)} = \pm 2 \sqrt{\frac{\pi}{\hat{T}_{\rm w}}} \int_{\zeta_1 \gtrless 0} \int_0^\infty \zeta_1 \hat{f}_{(0)} d\hat{\mathcal{E}} d\boldsymbol{\zeta}. \tag{1.29b}$$

It should be noted that $\hat{t}$ and x_2 appear only as parameters in the problem (1.28) and (1.29). It is seen by the direct substitution that Eqs. (1.28) and (1.29) have a solution of the following form:

$$\hat{f}_{(0)} = \frac{\sigma_{(0)}(\hat{t}, x_2)\Lambda_\delta}{[\pi \hat{T}_{\rm w}(x_2)]^{3/2}[\hat{T}_{\rm w}(x_2)]^{\delta/2}} \hat{\mathcal{E}}^{\delta/2-1} \exp\Big(-\frac{\zeta_i^2 + \hat{\mathcal{E}}}{\hat{T}_{\rm w}(x_2)}\Big), \tag{1.30}$$

where $\sigma_{(0)}$ is an arbitrary function of $\hat{t}$ and x_2 to be determined later. In fact, Eq. (1.30) gives the following macroscopic quantities:

$$\begin{aligned}
&\hat{\rho}_{(0)} = \sigma_{(0)}(\hat{t}, x_2), \qquad \hat{\upsilon}_{i(0)} = 0, \\
&\hat{T}_{{\rm tr}(0)} = \hat{T}_{{\rm int}(0)} = \hat{T}_{(0)} = \hat{T}_{{\rm rel}(0)} = \hat{T}_{\rm w}(x_2), \\
&\hat{p}_{(0)} = \sigma_{(0)}(\hat{t}, x_2)\hat{T}_{\rm w}(x_2), \qquad \hat{p}_{ij(0)} = \hat{p}_{(0)}\delta_{ij}, \qquad \hat{M}_{(0)} = 0,
\end{aligned} \tag{1.31}$$

which reduce $\hat{\mathcal{G}}_{(0)}$ and $\hat{A}_{{\rm c}(0)}$ to

$$\hat{\mathcal{G}}_{(0)} = \hat{f}_{(0)}, \quad \hat{A}_{{\rm c}(0)} = \hat{A}_{\rm c}(\hat{T}_{\rm w}). \tag{1.32}$$

Moreover, we can show, by following [14], that Eq. (1.30) is the unique solution (up to the arbitrariness of $\sigma_{(0)}$).

1.2.4.2 First order

The equation in the first order of ϵ is obtained as follows:

$$\zeta_1 \frac{\partial \hat{f}_{(1)}}{\partial x_1} + \zeta_2 \frac{\partial \hat{f}_{(0)}}{\partial x_2} = \frac{2}{\sqrt{\pi}} \frac{1}{K_*} \hat{A}_{{\rm c}(0)} \sigma_{(0)} (\hat{\mathcal{G}}_{(1)} - \hat{f}_{(1)}), \tag{1.33a}$$

$$\begin{aligned}
\hat{\mathcal{G}}_{(1)} = \hat{\mathcal{G}}_{(0)} \Big[&\frac{\hat{\rho}_{(1)}}{\sigma_{(0)}} - \frac{1}{2}\frac{|\underline{\hat{\mathcal{I}}}|_{(1)}}{\hat{T}_{\rm w}^3} - \frac{\delta}{2}\frac{\hat{T}_{{\rm rel}(1)}}{\hat{T}_{\rm w}} + \frac{\hat{\mathcal{E}}\hat{T}_{{\rm rel}(1)}}{\hat{T}_{\rm w}^2} \\
&+ 2\frac{\zeta_i \hat{\upsilon}_{i(1)}}{\hat{T}_{\rm w}} - {}^t\boldsymbol{\zeta} \cdot (\underline{\hat{\mathcal{I}}}^{-1})_{(1)} \cdot \boldsymbol{\zeta} \Big],
\end{aligned} \tag{1.33b}$$

$$|\underline{\hat{\mathcal{I}}}|_{(1)} = \hat{T}_{\rm w}^2 \Big[3(1-\eta)\hat{T}_{{\rm tr}(1)} + 3\eta \hat{T}_{(1)} \Big], \tag{1.33c}$$

$$\begin{aligned}
{}^t\boldsymbol{\zeta} \cdot (\underline{\hat{\mathcal{I}}}^{-1})_{(1)} \cdot \boldsymbol{\zeta} = -\frac{1}{\hat{T}_{\rm w}^2} \Big[&\Big((1-\eta)\hat{T}_{{\rm tr}(1)} + \eta \hat{T}_{(1)} \Big) \zeta_i^2 \\
&+ (1-\eta)\nu \frac{\hat{p}_{ij(1)}}{\sigma_{(0)}} (\zeta_i \zeta_j - \frac{1}{3}\zeta_k^2 \delta_{ij}) \Big],
\end{aligned} \tag{1.33d}$$

$$\hat{\rho}_{(1)} = \iint_0^\infty \hat{f}_{(1)} d\hat{\mathcal{E}} d\boldsymbol{\zeta}, \tag{1.33e}$$

$$\sigma_{(0)} \hat{\upsilon}_{i(1)} = \iint_0^\infty \zeta_i \hat{f}_{(1)} d\hat{\mathcal{E}} d\boldsymbol{\zeta}, \tag{1.33f}$$

$$\sigma_{(0)} \hat{T}_{{\rm tr}(1)} = \frac{2}{3} \iint_0^\infty \zeta_i^2 \hat{f}_{(1)} d\hat{\mathcal{E}} d\boldsymbol{\zeta} - \hat{\rho}_{(1)} \hat{T}_{\rm w}, \tag{1.33g}$$

$$\sigma_{(0)}\hat{T}_{\mathrm{int}(1)} = \frac{2}{\delta}\iint_0^\infty \hat{\mathcal{E}}\hat{f}_{(1)}d\hat{\mathcal{E}}d\boldsymbol{\zeta} - \hat{\rho}_{(1)}\hat{T}_{\mathrm{w}}, \tag{1.33h}$$

$$\hat{T}_{(1)} = \frac{3\hat{T}_{\mathrm{tr}(1)} + \delta\hat{T}_{\mathrm{int}(1)}}{3+\delta}, \tag{1.33i}$$

$$\hat{T}_{\mathrm{rel}(1)} = \eta\hat{T}_{(1)} + (1-\eta)\hat{T}_{\mathrm{int}(1)}. \tag{1.33j}$$

The corresponding boundary condition is given by

$$\hat{f}_{(1)} = \frac{\hat{\rho}_{\mathrm{w}(1)}\Lambda_\delta}{(\pi\hat{T}_{\mathrm{w}})^{3/2}\hat{T}_{\mathrm{w}}^{\delta/2}}\hat{\mathcal{E}}^{\delta/2-1}\exp\Big(-\frac{\zeta_i^2}{\hat{T}_{\mathrm{w}}} - \frac{\hat{\mathcal{E}}}{\hat{T}_{\mathrm{w}}}\Big) \quad (x_1 = \pm a/2, \quad \zeta_1 \lessgtr 0), \tag{1.34a}$$

$$\hat{\rho}_{\mathrm{w}(1)} = \pm 2\sqrt{\frac{\pi}{\hat{T}_{\mathrm{w}}}}\int_{\zeta_1 \gtrless 0}\int_0^\infty \zeta_1\hat{f}_{(1)}d\hat{\mathcal{E}}d\boldsymbol{\zeta}. \tag{1.34b}$$

In addition, the pressure, the stress tensor, and the mass-flow rate in the first order of ϵ are expressed as follows:

$$\hat{p}_{(1)} = \sigma_{(0)}\hat{T}_{(1)} + \hat{\rho}_{(1)}\hat{T}_{\mathrm{w}}, \tag{1.35a}$$

$$\hat{p}_{ij(1)} = \iint_0^\infty 2\zeta_i\zeta_j\hat{f}_{(1)}d\hat{\mathcal{E}}d\boldsymbol{\zeta}, \tag{1.35b}$$

$$\hat{M}_{(1)} = \int_{-a/2}^{a/2}\sigma_{(0)}\hat{v}_{2(1)}dx_1. \tag{1.35c}$$

Here again, the problem (1.33) and (1.34) contains $\hat{t}$ and x_2 only as parameters [see Eqs. (1.31) and (1.32)]. Now we can show, as in the same way as [42], that the solution to Eqs. (1.33) and (1.34) is obtained in the following form:

$$\begin{aligned}\hat{f}_{(1)} = \hat{f}_{(0)}\Big[&\phi_g(\hat{t},x_2) + \frac{\zeta_2}{\zeta_r}a\phi_{\mathrm{P}}\Big(\frac{x_1}{a},\frac{\zeta_1}{\hat{T}_{\mathrm{w}}^{1/2}},\frac{\zeta_r}{\hat{T}_{\mathrm{w}}^{1/2}},\frac{\hat{\mathcal{E}}}{\hat{T}_{\mathrm{w}}};K(\hat{t},x_2)\Big)\frac{1}{\hat{p}_{(0)}}\frac{\partial\hat{p}_{(0)}}{\partial x_2}\\ &+\frac{\zeta_2}{\zeta_r}a\phi_{\mathrm{T}}\Big(\frac{x_1}{a},\frac{\zeta_1}{\hat{T}_{\mathrm{w}}^{1/2}},\frac{\zeta_r}{\hat{T}_{\mathrm{w}}^{1/2}},\frac{\hat{\mathcal{E}}}{\hat{T}_{\mathrm{w}}};K(\hat{t},x_2)\Big)\frac{1}{\hat{T}_{\mathrm{w}}}\frac{d\hat{T}_{\mathrm{w}}}{dx_2}\Big],\end{aligned} \tag{1.36}$$

where

$$\zeta_r = (\zeta_2^2+\zeta_3^2)^{1/2}, \tag{1.37a}$$

$$K(\hat{t},x_2) = \frac{K_*\hat{T}_{\mathrm{w}}^{3/2}(x_2)}{\hat{p}_{(0)}(\hat{t},x_2)\hat{A}_{\mathrm{c}(0)}(x_2)a}, \tag{1.37b}$$

$\phi_g(\hat{t},x_2)$ is an arbitrary function of $\hat{t}$ and x_2, and ϕ_{P} and ϕ_{T} are, respectively, the solutions of the specific boundary-value problems for the linearized ES model. The equation and boundary condition for ϕ_{P} and those for ϕ_{T} are given in Sec. 1.7, where the parameter set $(\mathrm{Pr},\mu_{\mathrm{b}}/\mu,\delta)$ is used in place of (ν,η,δ) in Eq. (1.67) [see the comment following Eq. (1.7)]. The ϕ_{P} corresponds to the solution for the flow induced between two parallel plates by the

uniform pressure gradient (Poiseuille flow) [36], whereas $\phi_{\rm T}$ corresponds to the solution for the flow induced between two parallel plates by the uniform temperature gradient along the plates (thermal transpiration) [36]. They are fundamental and classical problems in rarefied gas dynamics and have been investigated by many authors by various methods. Since an exhaustive list of references is beyond the scope of the present paper, we only mention some early works, [12], [28], [29], and more recent works, [34], [15] (see also [36], [32] and references therein). We will discuss these problems in Sec. 1.4.

The macroscopic quantities in the first order of ϵ, i.e., those corresponding to the solution (1.36), are obtained as follows:

$$
\begin{aligned}
&\hat\rho_{(1)} = \sigma_{(0)}(\hat t, x_2)\phi_g(\hat t, x_2), \qquad \hat\upsilon_{1(1)} = \hat\upsilon_{3(1)} = 0,\\
&\hat\upsilon_{2(1)} = a\hat T_{\rm w}^{1/2}\Big(u_{\rm P}\frac{1}{\hat p_{(0)}}\frac{\partial \hat p_{(0)}}{\partial x_2} + u_{\rm T}\frac{1}{\hat T_{\rm w}}\frac{d\hat T_{\rm w}}{dx_2}\Big),\\
&\hat T_{{\rm tr}(1)} = \hat T_{{\rm int}(1)} = \hat T_{(1)} = \hat T_{{\rm rel}(1)} = 0,\\
&\hat p_{(1)} = \hat p_{(0)}(\hat t, x_2)\phi_g(\hat t, x_2),\\
&\hat p_{ij(1)} = \hat p_{(1)}\delta_{ij} + a\hat p_{(0)}\Big(\Sigma_{\rm P}\frac{1}{\hat p_{(0)}}\frac{\partial \hat p_{(0)}}{\partial x_2} + \Sigma_{\rm T}\frac{1}{\hat T_{\rm w}}\frac{d\hat T_{\rm w}}{dx_2}\Big)(\delta_{i1}\delta_{j2} + \delta_{i2}\delta_{j1}),
\end{aligned}
\tag{1.38}
$$

where, with $\alpha = {\rm P},\ {\rm T}$,

$$
\begin{aligned}
u_\alpha &= u_\alpha\Big(\frac{x_1}{a};\ K(\hat t, x_2)\Big)\\
&= \int_{-\infty}^{\infty}\int_0^\infty\int_0^\infty c_r^2 Y^{\delta/2-1}\phi_\alpha\Big(\frac{x_1}{a},\ c_1,\ c_r,\ Y;\ K(\hat t, x_2)\Big)\tilde E_Y\, dY dc_r dc_1, \qquad (1.39a)\\
\Sigma_\alpha &= \Sigma_\alpha\Big(\frac{x_1}{a};\ K(\hat t, x_2)\Big)\\
&= 2\int_{-\infty}^{\infty}\int_0^\infty\int_0^\infty c_1 c_r^2 Y^{\delta/2-1}\phi_\alpha\Big(\frac{x_1}{a},\ c_1,\ c_r,\ Y;\ K(\hat t, x_2)\Big)\tilde E_Y\, dY dc_r dc_1, \qquad (1.39b)\\
\tilde E_Y &= \Lambda_\delta \pi^{-1/2}\exp(-c_1^2 - c_r^2 - Y). \qquad (1.39c)
\end{aligned}
$$

[It turns out that $\Sigma_{\rm P} = -x_1/a$ and $\Sigma_{\rm T} = 0$ (see Sec. 1.7).] In addition, the corresponding mass-flow rate is given as

$$
\hat M_{(1)} = a^2\frac{\hat p_{(0)}}{\hat T_{\rm w}^{1/2}}\Big(M_{\rm P}\frac{1}{\hat p_{(0)}}\frac{\partial \hat p_{(0)}}{\partial x_2} + M_{\rm T}\frac{1}{\hat T_{\rm w}}\frac{d\hat T_{\rm w}}{dx_2}\Big), \tag{1.40}
$$

where

$$
M_\alpha = M_\alpha(K(\hat t, x_2)) = \int_{-1/2}^{1/2} u_\alpha(y;\ K(\hat t, x_2))dy, \qquad (\alpha = {\rm P},\ {\rm T}). \tag{1.41}
$$

1.2.4.3 Second order and macroscopic equation

The equation in the second order of ϵ reads as follows:

$$\frac{\partial \hat{f}_{(0)}}{\partial \hat{t}} + \zeta_1 \frac{\partial \hat{f}_{(2)}}{\partial x_1} + \zeta_2 \frac{\partial \hat{f}_{(1)}}{\partial x_2} = \frac{2}{\sqrt{\pi}} \frac{1}{K_*} \Big[\hat{A}_{\mathrm{c}(0)} \sigma_{(0)} (\hat{\mathcal{G}}_{(2)} - \hat{f}_{(2)}) + (\hat{A}_{\mathrm{c}(0)} \hat{\rho}_{(1)} + \hat{A}_{\mathrm{c}(1)} \sigma_{(0)}) (\hat{\mathcal{G}}_{(1)} - \hat{f}_{(1)}) \Big], \tag{1.42}$$

where the explicit form of $\hat{\mathcal{G}}_{(2)}$ is omitted. The boundary condition for Eq. (1.42) is given by

$$\hat{f}_{(2)} = \frac{\hat{\rho}_{\mathrm{w}(2)} \Lambda_\delta}{(\pi \hat{T}_{\mathrm{w}})^{3/2} \hat{T}_{\mathrm{w}}^{\delta/2}} \hat{\mathcal{E}}^{\delta/2-1} \exp\Big(-\frac{\zeta_i^2}{\hat{T}_{\mathrm{w}}} - \frac{\hat{\mathcal{E}}}{\hat{T}_{\mathrm{w}}} \Big) \quad (x_1 = \pm a/2, \ \ \zeta_1 \lessgtr 0), \tag{1.43a}$$

$$\hat{\rho}_{\mathrm{w}(2)} = \pm 2 \sqrt{\frac{\pi}{\hat{T}_{\mathrm{w}}}} \int_{\zeta_1 \gtrless 0} \int_0^\infty \zeta_1 \hat{f}_{(2)} d\hat{\mathcal{E}} d\boldsymbol{\zeta}. \tag{1.43b}$$

We now integrate Eq. (1.42) with respect to ζ_i and $\hat{\mathcal{E}}$ over their whole ranges and then with respect to x_1 from $-a/2$ to $a/2$. If we take into account, in this process, the explicit forms of $\hat{f}_{(0)}$ [Eq. (1.30)] and $\hat{f}_{(1)}$ [Eq. (1.36)], as well as the relation

$$\iint_0^\infty \zeta_1 \hat{f}_{(2)}|_{x_1 = \pm a/2} d\hat{\mathcal{E}} d\boldsymbol{\zeta} = 0, \tag{1.44}$$

obtained from the boundary condition (1.43), then we have the following equation:

$$\frac{\partial \hat{p}_{(0)}}{\partial \hat{t}} + \hat{T}_{\mathrm{w}} \frac{\partial \mathcal{M}}{\partial x_2} = 0, \tag{1.45a}$$

$$\mathcal{M} = \frac{\hat{p}_{(0)}}{\hat{T}_{\mathrm{w}}^{1/2}} a \Big[M_{\mathrm{P}}(K;\, \delta,\, \mathrm{Pr}) \frac{1}{\hat{p}_{(0)}} \frac{\partial \hat{p}_{(0)}}{\partial x_2} + M_{\mathrm{T}}(K;\, \delta) \frac{1}{\hat{T}_{\mathrm{w}}} \frac{d\hat{T}_{\mathrm{w}}}{dx_2} \Big], \tag{1.45b}$$

$$K = K_* \hat{T}_{\mathrm{w}}^{3/2} / \hat{p}_{(0)} \hat{A}_{\mathrm{c}(0)} a, \quad \hat{A}_{\mathrm{c}(0)} = \hat{A}_{\mathrm{c}}(\hat{T}_{\mathrm{w}}), \tag{1.45c}$$

where, $\hat{p}_{(0)} = \sigma_{(0)} \hat{T}_{\mathrm{w}}$, rather than $\sigma_{(0)}$, has been used as the unknown function. In Eq. (1.45), $\hat{p}_{(0)}$, $\mathcal{M}$, and K are the functions of $\hat{t}$ and x_2, whereas $\hat{T}_{\mathrm{w}}$ and $\hat{A}_{\mathrm{c}(0)}$ are the functions of x_2 only. As shown in Sec. 1.7, ϕ_{P} depends only on (Pr, δ) and ϕ_{T} only on δ among the set of parameters $(\mathrm{Pr}, \mu_{\mathrm{b}}/\mu, \delta)$. Thus, the same dependency holds for M_{P} and M_{T}. This fact is shown explicitly in Eq. (1.45). Further relevant properties of M_{P} and M_{T} will be shown in Sec. 1.4. The original (dimensional) mass-flow rate M [cf. Eq. (1.10)] is expressed as

$$M/\rho_* (2RT_*)^{1/2} D_* = a\mathcal{M}\epsilon + O(\epsilon^2). \tag{1.46}$$

Thus, $\mathcal{M}$ is the dimensionless first-order mass flux.

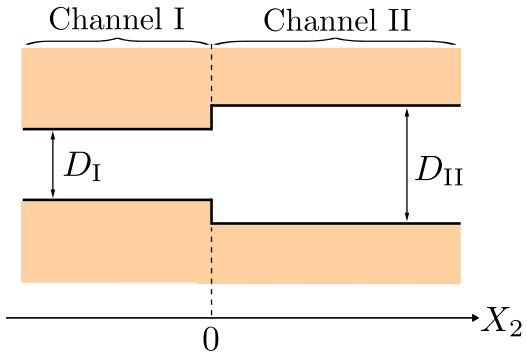

Figure 1.1: Junction of two channels with different width.

In summary, Eq. (1.45) is the equation of convection-diffusion type for the pressure $\hat{p}_{(0)}$ at the zeroth order in ϵ if we have the data of $M_{\rm P}$ and $M_{\rm T}$ as the functions of K. The construction of the database will be made in Sec. 1.4.

The steady version of Eq. (1.45) is essentially the same as the generalized Reynolds equation derived in [17] and often used in micro-fluid applications [33,13]. Mathematical study of the derivation of diffusion-type equations from the Boltzmann equation is found, for instance, in Refs. [6,18,16]. In Ref. [3], the term corresponding to ϕ_g in Eq. (1.36) is set to be zero because this setting does not make any change in the resulting equation of convection-diffusion type.

1.3 Connected channels and connection condition

Let us consider a long channel composed of several (or many) channels with different width connected linearly one after another. If each channel is long enough compared with its width, the macroscopic equation (1.45) should be valid in each channel except the regions near the junctions. If we assume that the macroscopic equation is valid even in the junction regions, it should be complemented by an appropriate connection condition at the junctions. This condition can be derived by the analysis of the original kinetic equation in the junction regions (see [2,42,3]). Here, we only give the result thus obtained.

Let us consider the junction of two channels shown in Fig. 1.1. That is, the channel I with width $D_{\rm I}$ ($X_2 < 0$) is connected with the channel II with width $D_{\rm II}$ ($X_2 > 0$) at $X_2 = 0$. We assume the diffuse reflection on the wall at $X_2 = 0$ and that the temperature of the channel wall is continuous at $X_2 = 0$ though its derivative may be discontinuous. Then, the

connection condition for Eq. (1.45) applied to each channel is given by

$$\hat{p}^{\mathrm{I}}_{(0)}(\hat{t}, x_2 = 0_-) = \hat{p}^{\mathrm{II}}_{(0)}(\hat{t}, x_2 = 0_+), \tag{1.47a}$$

$$\mathcal{M}^{\mathrm{I}}(\hat{t}, x_2 = 0_-)a_{\mathrm{I}} = \mathcal{M}^{\mathrm{II}}(\hat{t}, x_2 = 0_+)a_{\mathrm{II}}, \tag{1.47b}$$

with

$$a_{\mathrm{I}} = D_{\mathrm{I}}/D_*, \qquad a_{\mathrm{II}} = D_{\mathrm{II}}/D_*. \tag{1.48}$$

Here, $\hat{p}^J_{(0)}$ and $\mathcal{M}^J$ ($J = \mathrm{I}$, II) are the zeroth-order pressure and the first-order mass flux in the channel J, respectively. The condition (1.47) is valid irrespective of the positions of the center lines of the two channels (i.e., the center lines do not need to be common).

In the case of a channel composed of many channels with different width, the condition (1.47) is to be applied at each junction.

1.4 Data for M_{P} and M_{T}: Reduction to BGK model

The convection-diffusion-type equation (1.45) is of the same form as in the case of a monatomic gas [42,3]. In other words, the effect of the polyatomic gas is confined in the transport coefficients M_{P} and M_{T}. As we have seen in Sec. 1.2.4.2, M_{P} and M_{T} are obtained by Eqs. (1.39a) and (1.41) from the solutions ϕ_{P} and ϕ_{T} to Eq. (1.67) with boundary condition (1.66). In this section, we investigate this problem in detail.

We first note that we can eliminate the variable Y from our problem by introducing the following marginal velocity distribution functions:

$$\Phi_\alpha(y, c_1, c_r;\, K(\hat{t}, x_2)) = \Lambda_\delta \int_0^\infty Y^{\delta/2-1}\phi_\alpha(y, c_1, c_r, Y;\, K(\hat{t}, x_2))\exp(-Y)dY, \qquad (\alpha = \mathrm{P},\, \mathrm{T}). \tag{1.49}$$

More specifically, if we multiply Eq. (1.67a) by $\Lambda_\delta Y^{\delta/2-1}\exp(-Y)$ and integrate with respect to Y from 0 to ∞, we obtain the boundary-value problems for Φ_{P} and Φ_{T}. That is, the problem for Φ_{P} is

$$c_1\frac{\partial \Phi_{\mathrm{P}}}{\partial y} = \frac{2}{\sqrt{\pi}}\frac{1}{K}\Big[-\Phi_{\mathrm{P}} + 2c_r u_{\mathrm{P}} - 2\Big(1 - \frac{1}{\mathrm{Pr}}\Big)c_1 c_r y\Big] - c_r, \tag{1.50a}$$

$$u_{\mathrm{P}} = \int_{-\infty}^{\infty}\int_0^\infty c_r^2 \Phi_{\mathrm{P}} E_c dc_r dc_1, \tag{1.50b}$$

$$\Phi_{\mathrm{P}} = 0, \qquad (y = \pm 1/2,\ \ c_1 \lessgtr 0), \tag{1.50c}$$

where

$$E_c = \pi^{-1/2} \exp(-c_1^2 - c_r^2), \tag{1.51}$$

and the problem for $\Phi_{\rm T}$ is

$$c_1 \frac{\partial \Phi_{\rm T}}{\partial y} = \frac{2}{\sqrt{\pi}} \frac{1}{K} (-\Phi_{\rm T} + 2c_r u_{\rm T}) - c_r \Big(c_1^2 + c_r^2 - \frac{5}{2} \Big), \tag{1.52a}$$

$$u_{\rm T} = \int_{-\infty}^{\infty} \int_{0}^{\infty} c_r^2 \Phi_{\rm T} E_c dc_r dc_1, \tag{1.52b}$$

$$\Phi_{\rm T} = 0, \qquad (y = \pm 1/2, \ \ c_1 \lesseqgtr 0). \tag{1.52c}$$

In addition, we have

$$M_{\rm P} = \int_{-1/2}^{1/2} u_{\rm P} dy, \qquad M_{\rm T} = \int_{-1/2}^{1/2} u_{\rm T} dy. \tag{1.53}$$

It should be remarked that the parameter δ of the internal degree of freedom of a molecule has been eliminated from the problems (1.50) and (1.52). As seen from Eqs. (1.50) and (1.52), $\Phi_{\rm P}$ depends only on Pr and $\Phi_{\rm T}$ on none of the parameters $({\rm Pr}, \mu_{\rm b}/\mu, \delta)$. Thus, we may write $M_{\rm P}$ and $M_{\rm T}$ as $M_{\rm P}(K, {\rm Pr})$ and $M_{\rm T}(K)$.

In fact, Eqs. (1.50) and (1.52) are of the same form as the equations and boundary conditions corresponding to the plane Poiseuille flow and thermal transpiration based on the ES model for a monatomic gas. The only difference lies in the different values of Pr in the former. Furthermore, Eq. (1.52) is identical to the equation and boundary condition corresponding to the thermal transpiration based on the BGK model for a monatomic gas. Therefore, we can just exploit the existing data of $M_{\rm T}$ based on the BGK model [38]. On the other hand, the problem (1.50) differs from that based on the BGK model. However, if we let

$$\Phi_{\rm P} = \Psi_{\rm P} - \frac{2}{\sqrt{\pi}} \frac{1}{K} \left(1 - \frac{1}{\rm Pr} \right) c_r \left(y^2 - \frac{1}{4} \right), \tag{1.54}$$

then we have the following equation and boundary condition for $\Psi_{\rm P}$:

$$c_1 \frac{\partial \Psi_{\rm P}}{\partial y} = \frac{2}{\sqrt{\pi}} \frac{1}{K} (-\Psi_{\rm P} + 2c_r u_{\rm P}[\Psi_{\rm P}]) - c_r, \tag{1.55a}$$

$$u_{\rm P}[\Psi_{\rm P}] = \int_{-\infty}^{\infty} \int_{0}^{\infty} c_r^2 \Psi_{\rm P} E_c dc_r dc_1, \tag{1.55b}$$

$$\Psi_{\rm P} = 0, \qquad (y = \pm 1/2, \ \ c_1 \lesseqgtr 0), \tag{1.55c}$$

which does not contain Pr and is identical to the equation and boundary condition for the plane Poiseuille flow based on the BGK model for a single-component gas. Let $u_{\rm P}[\Phi_{\rm P}]$ and $M_{\rm P}[\Phi_{\rm P}]$ denote $u_{\rm P}$ and $M_{\rm P}$ based on $\Phi_{\rm P}$, and $u_{\rm P}[\Psi_{\rm P}]$ and $M_{\rm P}[\Psi_{\rm P}]$ those based on $\Psi_{\rm P}$. Then, they are related as

$$u_{\rm P}[\Phi_{\rm P}] = u_{\rm P}[\Psi_{\rm P}] - \frac{1}{\sqrt{\pi}}\frac{1}{K}\Big(1-\frac{1}{\rm Pr}\Big)\Big(y^2-\frac{1}{4}\Big), \tag{1.56}$$

$$M_{\rm P}[\Phi_{\rm P}] = M_{\rm P}[\Psi_{\rm P}] + \frac{1}{6}\frac{1}{\sqrt{\pi}}\frac{1}{K}\Big(1-\frac{1}{\rm Pr}\Big). \tag{1.57}$$

Since $M_{\rm P}[\Psi_{\rm P}]$ is independent of Pr, the functional form of $M_{\rm P}(K, {\rm Pr})$, as the function of Pr, is given by the last term on the right-hand side of Eq. (1.57). In this way, the data of $M_{\rm P}(K, {\rm Pr})$ can be obtained readily from the existing data of $M_{\rm P}[\Psi_{\rm P}]$ for the BGK model for a monatomic gas [38]. The same conversions as (1.54), (1.56), and (1.57) can be used even when the boundary condition other than the diffuse reflection (e.g., Cercignani–Lampis model [10]) is used in the formulation of the problem [or in place of (1.50c)]. It should be noted that, for a monatomic gas, the conversion between the ES and BGK models is mentioned in [9,10], where a conversion formula corresponding to Eq. (1.57) is given for the cylindrical Poiseuille flow, assuming the diffuse reflection boundary condition.

In summary, we can obtain the database for $M_{\rm P}(K, {\rm Pr})$ and $M_{\rm T}(K)$ without any new computation.

1.5 Knudsen pump and its performance

In this section, we apply the macroscopic equation (1.45) and connection condition (1.47) to a Knudsen pump. We take the nitrogen gas (N_2), for which the experimental values of Pr and $\mu_{\rm b}/\mu$ are available (${\rm Pr} = 0.718$ [27] and $\mu_{\rm b}/\mu = 0.731$ [31]). We set the values of ν and η in such a way that the resulting Pr and $\mu_{\rm b}/\mu$ are close to the above experimental values, that is, $\nu = -0.50$ and $\eta = 0.46$, which lead to ${\rm Pr} = 0.787$ and $\mu_{\rm b}/\mu = 0.722$.

Now, let us consider a Knudsen pump (or compressor) shown in Fig. 1.2, that is, a long channel consisting of alternately arranged $\mathcal{N}$ narrower channels (Channel I: length $L_{\rm I}$ and width $D_{\rm I}$) and $\mathcal{N}$ wider channels [Channel II: length $L_{\rm II}$ and width $D_{\rm II}(> D_{\rm I})$] along the X_2 axis. We let $L = L_{\rm I} + L_{\rm II}$ and assume that $D_{\rm I} \ll L_{\rm I}$ and $D_{\rm II} \ll L_{\rm II}$. In addition, we assume that the temperature $T_{\rm w}(X_2)$ of the channel walls is a piecewise linear and continuous

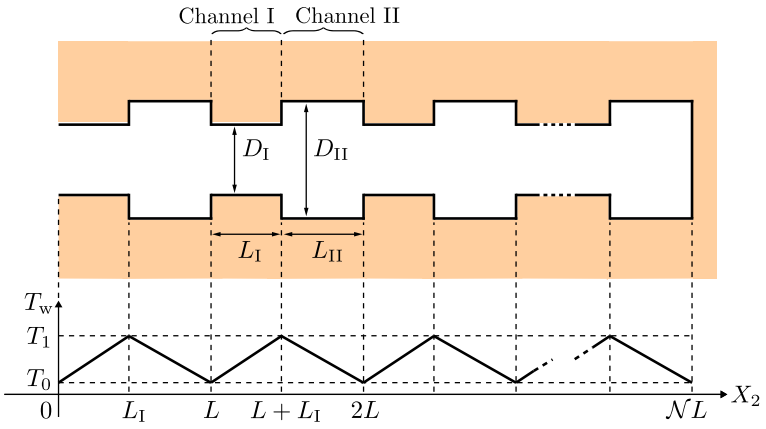

Figure 1.2: Knudsen pump composed of Channel I and Channel II.

periodic function (period L) of X_2, varying between T_0 and $T_1(>T_0)$. With this setting, we can apply Eq. (1.45) to each channel and Eq. (1.47) to each junction. To be more specific, if we denote the dimensionless pressure $\hat{p}_{(0)}$ in Channel J ($J=$ I, II) by $\hat{p}^J_{(0)}$, we have

$$\frac{\partial \hat{p}^J_{(0)}}{\partial \hat{t}} + \hat{T}_{\rm w}\frac{\partial \mathcal{M}^J}{\partial x_2} = 0, \tag{1.58a}$$

$$\mathcal{M}^J = \frac{\hat{p}^J_{(0)}}{\hat{T}_{\rm w}^{1/2}} a_J \Big[M_{\rm P}(K_J,{\rm Pr})\frac{1}{\hat{p}^J_{(0)}}\frac{\partial \hat{p}^J_{(0)}}{\partial x_2} + M_{\rm T}(K_J)\frac{1}{\hat{T}_{\rm w}}\frac{d\hat{T}_{\rm w}}{dx_2}\Big], \tag{1.58b}$$

$$a_J = \frac{D_J}{D_*}, \qquad K_J = \frac{K_* \hat{T}_{\rm w}^{3/2}}{\hat{p}^J_{(0)} a_J}, \tag{1.58c}$$

where

$$J = \begin{cases} {\rm I} & \text{for } mL/L_* < x_2 < (L_{\rm I}+mL)/L_*, \\ {\rm II} & \text{for } (L_{\rm I}+mL)/L_* \le x_2 \le (1+m)L/L_*, \end{cases} \qquad (m=0,\,\ldots,\,\mathcal{N}-1). \tag{1.59}$$

Here, we have assumed that $A_{\rm c}(T)$ does not depend on T, so that $\hat{A}_{\rm c}=1$ (or $\hat{A}_{{\rm c}(0)}=1$). We also have to impose the following conditions at the junctions:

$$\hat{p}^{\rm I}_{(0)} = \hat{p}^{\rm II}_{(0)}, \qquad \mathcal{M}^{\rm I} a_{\rm I} = \mathcal{M}^{\rm II} a_{\rm II}, \\ \text{at } \; x_2 = L_{\rm I}/L_*,\ (L_{\rm I}+mL)/L_* \ \text{ and } \ mL/L_*, \qquad (m=1,\,\ldots,\,\mathcal{N}-1). \tag{1.60}$$

If we assign the appropriate initial condition and conditions at both ends, we can describe the time evolution of the pressure distribution along the Knudsen pump. Here, we consider the following two types of end condition that are simple and natural:

(i) Open end: the pressure of the gas is specified there.

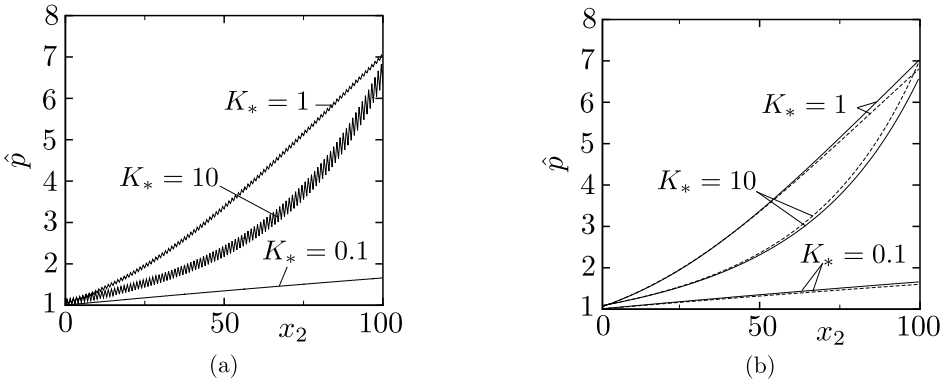

Figure 1.3: Steady pressure distribution along the Knudsen pump in Problem (A). (a) Pressure distribution for the N_2 gas, (b) Averaged pressure distribution for the N_2 and monatomic gases. In (b), the solid line indicates the result for the N_2 gas, and the dashed line that for the monatomic gas.

(ii) Closed end: the mass flow vanishes there.

Let us consider the following two problems for the Knudsen pump:

(A) The left end ($X_2 = 0$) is open, and the right end ($X_2 = \mathcal{N}L$) is closed. The pressure at the left end is kept at p_0. The initial condition is that the density is uniform at $t = 0$.

(B) Both ends are open. The pressure at the left end is kept at p_0 and that at the right end is kept at $p_1\,(> p_0)$. The initial condition is that the density is uniform at $t = 0$.

We take p_0, T_0, $D_{\rm I}$, and L as the reference pressure p_*, temperature T_*, channel width D_*, and channel length L_*, respectively. Therefore, the reference mean free path becomes $l_* = (2/\sqrt{\pi})(2RT_0)^{1/2}/A_{\rm c}\rho_0$ (with $\rho_0 = p_0/RT_0$), and thus the reference Knudsen number $K_* = l_*/D_{\rm I}$. In what follows, we show the steady pressure distribution for Problem (A) and the steady mass-flow rate for Problem (B), obtained as the long-time limits of the time-dependent solutions. The results for the N_2 gas (Pr = 0.787) are compared with those for a monatomic gas with Pr = 0.666 (Note that the values of Pr obtained experimentally as well as theoretically are very close to 2/3 for any monatomic gas).

The steady pressure distribution $p/p_0\,(= \hat{p})$ along the pump at $K_* = 0.1$, 1, and 10 in Problem (A) is shown in Fig. 1.3 for $D_{\rm II}/D_{\rm I} = 2$, $L_{\rm I}/L = 0.5$, $T_1/T_0 = 1.5$, and $\mathcal{N} = 100$. Figure 1.3(a) shows the result for the N_2 gas. Figure 1.3(b) shows the distribution of the pressure averaged over each unit. The result for the monatomic gas is also shown in Fig. 1.3(b) for comparison. In this problem, we observe the property of the Knudsen pump

Table 1.1: Steady mass-flow rate $\mathcal{M}^{\mathrm{I}}a_{\mathrm{I}}$ versus the number of the units $\mathcal{N}$ in Problem (B).

	$\mathcal{M}^{\mathrm{I}}(0.666)a_{\mathrm{I}}$			$\mathcal{M}^{\mathrm{I}}(0.787)a_{\mathrm{I}}$		
$\mathcal{N}$	$K_*=10$	$K_*=1$	$K_*=0.1$	$K_*=10$	$K_*=1$	$K_*=0.1$
10	-0.1107	$-0.7529(-1)$[1]	-0.3029	-0.1112	$-0.7321(-1)$	-0.2664
50	$0.3414(-2)$	$0.1970(-1)$	$-0.4618(-1)$	$0.2783(-2)$	$0.1875(-1)$	$-0.3905(-1)$
100	$0.1595(-1)$	$0.2910(-1)$	$-0.1410(-1)$	$0.1539(-1)$	$0.2788(-1)$	$-0.1064(-1)$
150	$0.1917(-1)$	$0.3097(-1)$	$-0.3410(-2)$	$0.1867(-1)$	$0.2971(-1)$	$-0.1182(-2)$
200	$0.2031(-1)$	$0.3142(-1)$	$0.1928(-2)$	$0.1984(-1)$	$0.3017(-1)$	$0.3542(-2)$

[1] Read as -0.7529×10^{-1}.

as a compressor. If the Knudsen number K_*, which is the Knudsen number at the left end, is not small, the pressure ratio of $6.5\sim7$ is obtained at the right end. The difference between the pressure at the right end for the N_2 gas and that for the monatomic gas is relatively small: the difference is around 6% at $K_*=10$, 3% at $K_*=1$, and 4% at $K_*=0.1$.

Table 1.1 shows the (dimensionless) steady mass-flow rate $\mathcal{M}^{\mathrm{I}}a_{\mathrm{I}}$ [cf. Eq. (1.46)] versus the number of the units $\mathcal{N}$ in Problem (B) at three different Knudsen numbers ($K_*=10$, 1, 0.1) for $D_{\mathrm{II}}/D_{\mathrm{I}}=2$, $L_{\mathrm{I}}/L=0.5$, $T_1/T_0=1.5$, and $p_1/p_0=2$: $\mathcal{M}^{\mathrm{I}}(0.787)a_{\mathrm{I}}$ indicates the result for the N_2 gas, whereas $\mathcal{M}^{\mathrm{I}}(0.666)a_{\mathrm{I}}$ that for the monatomic gas. In this problem, we can see the pumping effect against the pressure difference. As the number of units increases, the pumping effect finally overcomes the flow caused by the pressure difference, and the gas flows from the low-pressure circumstances to the high-pressure ones. The mass-flow rate of the N_2 gas does not differ much from that of the monatomic gas.

1.6 Concluding remarks

In the present study, we considered the Knudsen pump consisting of alternately arranged wider and narrower channels between two parallel plates and investigated its properties when the working gas is a polyatomic gas, using a polyatomic version of the ES model. We first derived, under the assumption that the width of each channel is sufficiently small compared with its length, the macroscopic system composed of a differential equation of convection-diffusion type and its connection condition at the junctions of the wider and narrower channels. The resulting macroscopic system is the same form as that derived from the BGK model for a monatomic gas, and the effect of the polyatomic gas is confined only in the transport coefficients in the equation. We also showed that the transport coefficients

can be obtained readily from those corresponding to the BGK model for a monatomic gas by a simple conversion. Finally, we applied the macroscopic system to investigate numerically the properties of the Knudsen pump for a diatomic N_2 gas. As the result, we confirmed that the polyatomic-gas effect on the performance of the Knudsen pump is quite limited, so that the existing macroscopic system derived for a monatomic gas can be applied safely also to a polyatomic gas in the level of practical applications.

1.7 Appendix A: Equations for $\phi_{\rm P}$ and $\phi_{\rm T}$

Let us consider Eqs. (1.33) and (1.34). We note that, with the help of Eq. (1.30), the inhomogeneous term of Eq. (1.33a), i.e., the term $-\zeta_2 \partial \hat{f}_{(0)}/\partial x_2$, can be expressed as the sum of two terms, one in proportion to $(1/\hat{p}_{(0)})(\partial \hat{p}_{(0)}/\partial x_2)$ and the other to $(1/\hat{T}_{\rm w})(d\hat{T}_{\rm w}/dx_2)$.

We first introduce the following new variables:

$$\phi = \frac{\hat{f}_{(1)}}{\hat{f}_{(0)}}, \quad \psi = \frac{\hat{\mathcal{G}}_{(1)}}{\hat{f}_{(0)}}, \quad c_i = \frac{\zeta_i}{\hat{T}_{\rm w}^{1/2}}, \quad Y = \frac{\hat{\mathcal{E}}}{\hat{T}_{\rm w}}, \quad y = \frac{x_1}{a}, \tag{1.61}$$

so that $\phi = \phi(\hat{t},\, y,\, x_2,\, c_i,\, Y)$. Then, taking into account the form of the inhomogeneous term, we let

$$\phi = \phi_g + \frac{1}{\hat{p}_{(0)}} \frac{\partial \hat{p}_{(0)}}{\partial x_2} \phi_s^{\rm P} + \frac{1}{\hat{T}_{\rm w}} \frac{d\hat{T}_{\rm w}}{dx_2} \phi_s^{\rm T}. \tag{1.62}$$

From the form of the equation and boundary condition for ϕ_g, it is easy to show that ϕ_g is independent of y, c_i, and Y (cf. [42]), i.e.,

$$\phi_g = \phi_g(\hat{t},\, x_2). \tag{1.63}$$

On the other hand, it can be shown that $\phi_s^{\rm P}$ and $\phi_s^{\rm T}$ of the following form:

$$\phi_s^\alpha = a(c_2/c_r)\phi_\alpha(y, c_1, c_r, Y; K(\hat{t}, x_2)), \qquad (\alpha = {\rm P},\, {\rm T}), \tag{1.64a}$$

$$c_r = (c_2^2 + c_3^2)^{1/2}, \tag{1.64b}$$

are compatible with their equations and boundary conditions (similarity solutions). The

resulting equation and boundary condition for $\phi_\alpha(y, c_1, c_r, Y; K(\hat{t}, x_2))$ are as follows:

$$c_1 \frac{\partial \phi_\alpha}{\partial y} = \frac{2}{\sqrt{\pi}} \frac{1}{K} \Big[-\phi_\alpha + 2c_r u_\alpha + 2(1-\eta)\nu c_1 c_r \Sigma_\alpha \Big] + I_\alpha \quad (\alpha = \mathrm{P},\, \mathrm{T}), \tag{1.65a}$$

$$u_\alpha = \int_{-\infty}^{\infty} \int_0^{\infty} \int_0^{\infty} c_r^2 Y^{\delta/2-1} \phi_\alpha \tilde{E}_Y \, dY dc_r dc_1, \tag{1.65b}$$

$$\Sigma_\alpha = 2 \int_{-\infty}^{\infty} \int_0^{\infty} \int_0^{\infty} c_1 c_r^2 Y^{\delta/2-1} \phi_\alpha \tilde{E}_Y \, dY dc_r dc_1, \tag{1.65c}$$

$$I_\mathrm{P} = -c_r, \qquad I_\mathrm{T} = -c_r \Big(c_1^2 + c_r^2 + Y - \frac{5+\delta}{2} \Big), \tag{1.65d}$$

$$\tilde{E}_Y = \Lambda_\delta \pi^{-1/2} \exp(-c_1^2 - c_r^2 - Y), \tag{1.65e}$$

and

$$\phi_\alpha = 0, \qquad (y = \pm 1/2, \;\; c_1 \lessgtr 0). \tag{1.66}$$

But, by integrating Eq. (1.65a) multiplied by $2c_r^2 Y^{\delta/2-1} \tilde{E}_Y$ over the whole ranges of Y, c_r, and c_1, we have $\Sigma_\mathrm{P} = -y$ and $\Sigma_\mathrm{T} = 0$ because of the symmetry $\phi_\alpha(y, c_1, c_r, Y) = \phi_\alpha(-y, -c_1, c_r, Y)$. Therefore, Eq. (1.65) is recast as

$$c_1 \frac{\partial \phi_\alpha}{\partial y} = \frac{2}{\sqrt{\pi}} \frac{1}{K} \Big[-\phi_\alpha + 2c_r u_\alpha + 2\Big(1 - \frac{1}{\mathrm{Pr}}\Big) c_1 c_r \Sigma_\alpha \Big] + I_\alpha \quad (\alpha = \mathrm{P},\, \mathrm{T}), \tag{1.67a}$$

$$u_\alpha = \int_{-\infty}^{\infty} \int_0^{\infty} \int_0^{\infty} c_r^2 Y^{\delta/2-1} \phi_\alpha \tilde{E}_Y \, dY dc_r dc_1, \tag{1.67b}$$

$$\Sigma_\mathrm{P} = -y, \qquad \Sigma_\mathrm{T} = 0, \tag{1.67c}$$

$$I_\mathrm{P} = -c_r, \qquad I_\mathrm{T} = -c_r \Big(c_1^2 + c_r^2 + Y - \frac{5+\delta}{2} \Big), \tag{1.67d}$$

where (Pr, μ_b/μ, δ), rather than (ν, η, δ), has been used as the set of parameters characterizing the gas under consideration [see the comment following Eq. (1.7)]. It is seen from Eq. (1.67) that ϕ_P does not depend on μ_b/μ and ϕ_T depends on neither μ_b/μ nor Pr.

References

1 P. Andries, P. Le Tallec, J.-P. Perlat and B. Perthame, *The Gaussian-BGK model of Boltzmann equation with small Prandtl number*, Eur. J. Mech. B/Fluids, **19** (2000), 813–830.

2 K. Aoki and P. Degond, *Homogenization of a flow in a periodic channel of small section*, Multiscale Model. Simul., **1** (2003), 304–334.

3 K. Aoki, P. Degond, S. Takata and H. Yoshida, *Diffusion models for Knudsen compressors*, Phys. Fluids, **19** (2007), 117103.

4 K. Aoki, Y. Sone, S. Takata, K. Takahashi and G. A. Bird, *One-way flow of a rarefied gas induced in a circular pipe with a periodic temperature distribution*, in "Rarefied Gas Dynamics" (eds. T. J. Bartel and M. A. Gallis), AIP, (2001), 940–947.

5 K. Aoki, S. Takata and K. Kugimoto, *Diffusion approximation for the Knudsen compressor composed of circular tubes*, in "Rarefied Gas Dynamics" (ed. T. Abe), AIP, (2009), 953–958.

6 H. Babovsky, C. Bardos and T. Platkowski, *Diffusion approximation for a Knudsen gas in a thin domain with accommodation on the boundary*, Asymptotic Analysis, **3** (1991), 265–289.

7 P. L. Bhatnagar, E. P. Gross and M. Krook, *A model for collision processes in gases. I. Small amplitude processes in charged and neutral one-component systems*, Phys. Rev., **94** (1954), 511–525.

8 G. A. Bird, "Molecular Gas Dynamics and the Direct Simulation of Gas Flows," Oxford University Press, Oxford, 1994.

9 C. Cercignani, "Mathematical Methods in Kinetic Theory," Plenum Press, New York, 1969, Chap. VIII, Sec. 5.

10 C. Cercignani, "The Boltzmann Equation and its Applications," Springer-Verlag, Berlin, 1988.

11 C. Cercignani, "Rarefied Gas Dynamics, From Basic Concepts to Actual Calculations," Cambridge Univ. Press, Cambridge, 2000.

12 C. Cercignani and A. Daneri, *Flow of a rarefied gas between two parallel plates*, J. Appl. Phys., **34** (1963), 3509–3513.

13 C. Cercignani, M. Lampis and S. Lorenzani, *Flow of a rarefied gas between parallel and almost parallel plates*, in "Rarefied Gas Dynamics" (ed. M. Capitelli), AIP, (2005), 719–724.

14 P. Charrier and B. Dubroca, *Asymptotic transport models for heat and mass transfer in reactive porous media*, Multiscale Model. Simul., **2** (2003), 124–157.

15 C.-C. Chen, I.-K. Chen, T.-P. Liu and Y. Sone, *Thermal transpiration for the linearized Boltzmann equation*, Commn. Pure Appl. Math., **60** (2007), 147–163.

16 P. Degond, V. Latocha, S. Mancini and A. Mellet, *Diffusion dynamics of an electron gas confined between two plates*, Methods and Applications of Analysis, **9** (2002), 127–150.

17 S. Fukui and R. Kaneko, *Analysis of ultra-thin gas film lubrication based on linearized Boltzmann equation including thermal creep flow*, J. Tribol., **110** (1988), 253–262.

18 F. Golse, *Anomalous diffusion limit for the Knudsen gas*, Asymptotic Analysis, **17** (1998), 1–12.

19 Y.-L. Han, *Thermal-creep-driven flows in Knudsen compressors and related nano/microscale gas transport channels*, J. Microelectromech. Systems, **17** (2008), 984–997.

20 Y.-L. Han, M. Young, E. P. Muntz and G. Shiflett, *Knudsen compressor performance at low pressures*, in "Rarefied Gas Dynamics" (ed. M. Capitelli), AIP, (2005), 162–167.

21 L. H. Holway, Jr., "Approximation Procedures for Kinetic Theory," Ph.D. Thesis, Harvard University, 1963.

22 L. H. Holway, Jr., *New statistical models for kinetic theory: Methods of construction*, Phys. Fluids, **9** (1966), 1658–1673.

23 M. L. Hudson and T. J. Bartel, *DSMC simulation of thermal transpiration and accommodation pumps*, in "Rarefied Gas Dynamics, vol. **1**" (eds. R. Brun, R. Campargue, R. Gatignol, J.-C. Lengrand), Cépaduès–Éditions, (1999), 719–726.

24 M. Knudsen, *Eine Revision der Gleichgewichtsbedingung der Gase. Thermische Molekularströmung*, Ann. Phys., **31** (1910), 205–229.

25 M. Knudsen, *Thermischer Molekulardruck der Gase in Röhren*, Ann. Phys., **33** (1910), 1435–1448.

26 F. J. McCormack, *Construction of linearized kinetic models for gaseous mixtures and molecular gases*, Phys. Fluids, **16** (1973), 2095–2105.

27 National Institutes of Natural Sciences and National Astronomical Observatory of Japan (eds.), "Chronological Scientific Tables," Marzen, Tokyo (1994) (in Japanese).

28 H. Niimi, *Thermal creep flow of rarefied gas between two parallel plates*, J. Phys. Soc. Jpn., **30** (1971), 572–574.

29 T. Ohwada, Y. Sone and K. Aoki, *Numerical analysis of the Poiseuille and thermal transpiration flows between two parallel plates on the basis of the Boltzmann equation for hard-sphere molecules*, Phys. Fluids A, **1** (1989), 2042–2049.

30 G. Pham-Van-Diep, P. Keeley, E. P. Muntz and D. P. Weaver, *A micromechanical Knudsen compressor*, in "Rarefied Gas Dynamics" (eds. J. Harvey and G. Lord), Oxford University Press, (1995), 715–721.

31 G. J. Prangsma, A. H. Alberga and J. J. M. Beenakker, *Ultrasonic determination of the volume viscosity of* N_2*,* CO*,* CH_4 *and* CD_4 *between 77 and 300 K*, Physica, **64** (1973), 278–288.

32 F. Sharipov and V. Seleznev, *Data on internal rarefied gas flows*, J. Phys. Chem. Ref. Data, **27** (1998), 657–706.

33 C. Shen, *Use of the degenerated Reynolds equation in solving the microchannel flow problem*, Phys. Fluids, **17** (2005), 046101.

34 C. E. Siewert, *The linearized Boltzmann equation: Concise and accurate solutions to basic flow problems*, Z. angew. Math. Phys., **54** (2003), 273–303.

35 Y. Sone, "Kinetic Theory and Fluid Dynamics," Birkhäuser, Boston, 2002; Supplementary Notes and Errata: Kyoto University Research Information Repository (http://hdl.handle.net/2433/66099).

36 Y. Sone, "Molecular Gas Dynamics: Theory, Techniques, and Applications," Birkhäuser, Boston, 2007; Supplementary Notes and Errata: Kyoto University Research Information Repository (http://hdl.handle.net/2433/66098).

37 Y. Sone, T. Fukuda, T. Hokazono and H. Sugimoto, *Experiment on a one-way flow of a rarefied gas through a straight circular pipe without average temperature and pressure gradients*, in "Rarefied Gas Dynamics" (eds. T. J. Bartel and M. A. Gallis), AIP, (2001), 948–955.

38 Y. Sone and E. Itakura, *Analysis of Poiseuille and thermal transpiration flows for arbitrary Knudsen numbers by a modified Knudsen number expansion and their database*, J. Vac. Soc. Jpn., **33** (1990), 92–94 (in Japanese) (the software package, based on this reference, made by Y. Sone, E. Itakura and M. Handa, can be downloaded from the webpage http://www.mfd.me.kyoto-u.ac.jp/Sone/database-e.html).

39 Y. Sone and K. Sato, *Demonstration of a one-way flow of a rarefied gas induced through a pipe without average pressure and temperature gradients*, Phys. Fluids, **12** (2000), 1864–1868.

40 Y. Sone and H. Sugimoto, *Vacuum pump without a moving part and its performance*, in "Rarefied Gas Dynamics" (eds. A. D. Ketsdever and E. P. Muntz), AIP, (2003), 1041–1048.

41 Y. Sone, Y. Waniguchi and K. Aoki, *One-way flow of a rarefied gas induced in a channel with a periodic temperature distribution*, Phys. Fluids, **8** (1996), 2227–2235.

42 S. Takata, H. Sugimoto and S. Kosuge, *Gas separation by means of the Knudsen compressor*, Eur. J. Mech., B/Fluids, **26** (2007), 155–181.

43 S. E. Vargo and E. P. Muntz, *An evaluation of a multiple-stage micromechanical Knudsen compressor and vacuum pump*, in "Rarefied Gas Dynamics" (ed. C. Shen), Peking University Press, (1997), 995–1000.

44 P. Welander, *On the temperature jump in a rarefied gas*, Ark. Fys., **7** (1954), 507–553.

Chapter 2

Poiseuille flow and thermal transpiration of a rarefied polyatomic gas through a circular tube with applications to microflows

2.1 Introduction

The Poiseuille flow and thermal transpiration of a rarefied gas through a long tube are fundamental and classical problems in rarefied gas dynamics. The former is a flow driven by a small and uniform pressure gradient imposed along the tube, and the latter, which is peculiar to a rarefied gas, is a flow caused by a small and uniform temperature gradient along the tube. Since 1960's, these flows have been the subjects of many papers. From 1960's to 1980's, the linearized model Boltzmann equation, in particular, the Bhatnagar-Gross-Krook (BGK) model [7,42], was used mainly both for theoretical and numerical analyses (see, for example, Refs. [10,11,37,23,17] for the Poiseuille flow and Refs. [37,23,17,22,26] for the thermal transpiration). But after around 1990, accurate numerical analysis based on the linearized Boltzmann equation became possible (see, for example, Refs. [27] and [31]). The reader is referred to Ref. [30], which contains an extensive review of the works earlier than this reference. Mention should also be made of the recent development [31,29], in particular, the mathematical study of the thermal transpiration [12].

The importance of these fundamental flows has rapidly been increased in connection with the recent progress of micro-mechanical systems because the small characteristic length leads the effect of rarefied gas to manifest itself even under atmospheric conditions. In practical applications, one encounters microscale systems with complex geometry, so that the direct application of kinetic theory, such as numerical simulations using the direct simulation Monte Carlo (DSMC) method, is computationally expensive and is not an efficient approach. Therefore, some heuristic macroscopic equations, which are intended to cover the transition regimes with non-small Knudsen numbers, have been proposed. The accurate numerical results for the Poiseuille flow and thermal transpiration provide a good standard for the

assessment of these macroscopic equations.

On the other hand, in many microscale applications, gas-flow channels or pipes are very thin compared with their length. This property enables us to derive simple macroscopic equations systematically from kinetic theory without any ambiguity. Such an approach has been taken in some different applications (see, for example, Ref. [15] for a thin-gap slider bearing and Refs. [13] and [14] for plasma thrusters). Recently, macroscopic equations of the same type were constructed for the purpose of analyzing the property of the Knudsen compressor [2,5], showing its applicability to gas separation [40], and investigating gas flows in a curved channel [4]. According to Ref. [5], the behavior of a gas in a thin pipe with an arbitrary but slowly-varying temperature distribution in the axial direction is described by a diffusion-type equation for any Knudsen number. The equation contains two functions, which correspond to the mass-flow rate of the Poiseuille flow and that of the thermal transpiration through the same pipe regarded as functions of the Knudsen number. Therefore, obtaining accurate data for the mass-flow rates of the Poiseuille flow and thermal transpiration for the whole range of the Knudsen number is essential for the application of the diffusion-type equation. Actually, in Ref. [5], the diffusion-type equation is applied to obtain the mass-flow rate and pressure distribution for the Knudsen pump, consisting of alternately arranged narrow and wide two-dimensional (2D) channels with a saw-tooth temperature distribution. In this application, use has been made of the database of the mass-flow rates of the Poiseuille flow and thermal transpiration between two parallel plates, constructed by the modified Knudsen-number expansion on the basis of the linearized BGK model [33].

Recently in Ref. [39], the macroscopic system of Ref. [5] was extended to a single polyatomic gas in the case of 2D channels, using the polyatomic version [1] of the Ellipsoidal Statistical (ES) model [18,19] of the Boltzmann equation. In the present study, we carry out the same extension in the case of circular tubes and apply the resulting system to the Knudsen compressor consisting of circular pipes with different radii, as well as to the flow through a long circular tube driven by a large pressure difference at both ends. Since the extension is essentially the same as in the case of 2D channels, we will just summarize the result. However, since the Poiseuille flow and thermal transpiration in a circular tube, the mass-flow rates of which give the two coefficients occurring in the macroscopic system, are the problems of fundamental importance, we will spend more space to discuss these flows. In

fact, as in the case of 2D channels, it turns out that the solution of the thermal transpiration through a circular tube based on the ES model for a polyatomic gas is identical with that based on the BGK model for a monatomic gas, and that the solution of the Poiseuille flow through a circular tube based on the ES model for a polyatomic gas is obtained by a simple conversion formula from that based on the BGK model for a monatomic gas.

The paper is organized as follows. In Sec. 2.2, we investigate Poiseuille flow and thermal transpiration of a rarefied polyatomic gas through an infinitely long straight tube with circular cross section on the basis of the linearized ES model for a polyatomic gas. After the formulation of the problems and some preliminary analysis (Secs. 2.2.1–2.2.3), we show that the problems can be reduced to the corresponding problems for the BGK model for a polyatomic gas (Sec. 2.2.4). Then, after some discussions of the properties of the mass-flow and heat-flow rates (Sec. 2.2.5), we show some numerical results (Sec. 2.2.6). In Sec. 2.3, we consider a rarefied polyatomic gas in a long circular tube with arbitrary and large temperature variation along the tube wall. The radius of the circular cross section may change discontinuously if the portion with a constant radius is long enough. The macroscopic equation of diffusion-type for such a tube, based on the ES model for a polyatomic gas, is summarized, together with the condition at the junction where the radius changes discontinuously. In Sec. 2.4, the macroscopic system is applied to a gas flow through a long circular pipe caused by a large pressure difference (Sec. 2.4.1) and to a Knudsen compressor composed of many long circular tubes (Sec. 2.4.2). Finally concluding remarks are given in Sec. 2.5.

2.2 Poiseuille flow and thermal transpiration through a circular tube

2.2.1 Problem, assumptions, and notations

Let us consider a rarefied polyatomic gas in an infinitely long and straight circular tube, and let δ be the number of degrees of freedom of a gas molecule. We take the X_3 axis (of a rectangular coordinate system X_i) along the tube axis and let the radius of the tube be R_0. A uniform pressure gradient in the X_3 direction is imposed in the gas, and a uniform temperature gradient in the same direction is imposed along the tube wall. That is, the pressure p and the temperature of the tube wall T_w are expressed as $p_0(1 + \alpha X_3/R_*)$ and

$T_0(1+\beta X_3/R_*)$, respectively, where R_* is a reference length (one may naturally let $R_* = R_0$, but we do not do so for later convenience). The fact that p is uniform in the cross section will be found later. We investigate the steady flow of the gas induced in the tube under the following assumptions.

(i) The behavior of the gas is described by the ES model [18,19] of the Boltzmann equation for a polyatomic gas [1].

(ii) The gas molecules undergo diffuse reflection on the tube wall.

(iii) The imposed pressure gradient α and temperature gradient β are so small that the equation and boundary condition can be linearized around an equilibrium state at rest.

Before presenting the basic equations, we summarize other notations used in Sec. 2.2 (see also Sec. 2.6). The symbol $\rho_0 = p_0/\mathcal{R}T_0$ denotes the density of the gas at $X_3 = 0$, $\mathcal{R}$ the gas constant per unit mass (the Boltzmann constant divided by the mass of a molecule), l_0 the mean free path of the gas molecules in the equilibrium state at rest at density ρ_0 and temperature T_0 (thus pressure p_0), and $\mathrm{Kn} = l_0/R_*$ the Knudsen number. Further, $x_i = X_i/R_*$, $(2\mathcal{R}T_0)^{1/2}\zeta_i$ is the molecular velocity, $\mathcal{R}T_0\mathcal{E}$ the energy related to the internal degree of freedom, $\Lambda_\delta \mathcal{E}^{\delta/2-1}(2\pi\mathcal{R}T_0)^{-3/2}(\mathcal{R}T_0)^{-1}\exp(-\zeta_i^2-\mathcal{E})\rho_0(1+\phi)$ the molecular velocity distribution function, Λ_δ the dimensionless constant defined by Eq. (2.48), $\rho_0(1+\omega)$ the density of the gas, $T_0(1+\tau)$ the temperature, $T_0(1+\tau_{\mathrm{tr}})$ the temperature related to the translational energy, $T_0(1+\tau_{\mathrm{int}})$ the temperature related to energy of the internal degree of freedom, $p_0(1+P)$ the pressure, $(2\mathcal{R}T_0)^{1/2}u_i$ the flow velocity, $p_0(\delta_{ij}+P_{ij})$ the stress tensor, and $p_0(2\mathcal{R}T_0)^{1/2}Q_i$ the heat-flow vector. The quantities $|\phi|$, $|\omega|$, $|\tau|$, $|\tau_{\mathrm{tr}}|$, $|\tau_{\mathrm{int}}|$, $|P|$, $|u_i|$, $|P_{ij}|$, and $|Q_i|$ are assumed to be small. We introduce the cylindrical coordinate system (r, θ, x_3) in the dimensionless x_i space and denote by a_i and b_i the unit vector in the r direction and that in the θ direction, respectively. Then, we denote $\zeta_r = \zeta_i a_i$, $\zeta_\theta = \zeta_i b_i$, $u_r = u_i a_i$, $u_\theta = u_i b_i$, $Q_r = Q_i a_i$, $Q_\theta = Q_i b_i$, $P_{rr} = P_{ij}a_i a_j$, $P_{\theta\theta} = P_{ij}b_i b_j$, $P_{r\theta} = P_{\theta r} = P_{ij}a_i b_j$, $P_{r3} = P_{3r} = P_{i3}a_i$, $P_{\theta 3} = P_{3\theta} = P_{i3}b_i$. In addition, $\zeta = (\zeta_i^2)^{1/2} = (\zeta_r^2+\zeta_\theta^2+\zeta_3^2)^{1/2}$, and $E(\zeta, \mathcal{E}) = \pi^{-3/2}\Lambda_\delta \exp(-\zeta^2-\mathcal{E})$. The summation convention (e.g., $\zeta_i a_i = \sum_{i=1}^3 \zeta_i a_i$) is used throughout the paper. We assume that the flow field is axisymmetric, i.e., ϕ in the cylindrical coordinate system does not depend on θ.

2.2.2 Basic equations

The linearized version of the ES model reads (see Sec. 2.6 for the original form of the model)

$$\zeta_r \frac{\partial \phi}{\partial r} + \frac{\zeta_\theta^2}{r}\frac{\partial \phi}{\partial \zeta_r} - \frac{\zeta_r \zeta_\theta}{r}\frac{\partial \phi}{\partial \zeta_\theta} + \zeta_3 \frac{\partial \phi}{\partial x_3} = \frac{2}{\sqrt{\pi}}\frac{1}{\mathrm{Kn}}(\phi_g - \phi), \tag{2.1}$$

with

$$\begin{aligned}
\phi_g &= \omega + 2\zeta_i u_i + \left(\zeta^2 - \frac{3}{2}\right)[(1-\eta)\tau_{\mathrm{tr}} + \eta\tau] + \left(\mathcal{E} - \frac{\delta}{2}\right)\tau_{\mathrm{rel}} \\
&\qquad + (1-\eta)\nu[P_{ij}\zeta_i\zeta_j - (\omega + \tau_{\mathrm{tr}})\zeta^2], && \text{(2.2a)}\\
\omega &= \iint_0^\infty \mathcal{E}^{\delta/2-1}\phi E d\mathcal{E} d^3\zeta, && \text{(2.2b)}\\
u_i &= \iint_0^\infty \zeta_i \mathcal{E}^{\delta/2-1}\phi E d\mathcal{E} d^3\zeta, && \text{(2.2c)}\\
\tau_{\mathrm{tr}} &= \frac{2}{3}\iint_0^\infty \zeta^2 \mathcal{E}^{\delta/2-1}\phi E d\mathcal{E} d^3\zeta - \omega, && \text{(2.2d)}\\
\tau_{\mathrm{int}} &= \frac{2}{\delta}\iint_0^\infty \mathcal{E}^{\delta/2}\phi E d\mathcal{E} d^3\zeta - \omega, && \text{(2.2e)}\\
\tau &= \frac{3\tau_{\mathrm{tr}} + \delta\tau_{\mathrm{int}}}{3+\delta}, && \text{(2.2f)}\\
\tau_{\mathrm{rel}} &= \eta\tau + (1-\eta)\tau_{\mathrm{int}}, && \text{(2.2g)}\\
P_{ij} &= \iint_0^\infty 2\zeta_i\zeta_j \mathcal{E}^{\delta/2-1}\phi E d\mathcal{E} d^3\zeta, && \text{(2.2h)}
\end{aligned}$$

where $d^3\zeta = d\zeta_1 d\zeta_2 d\zeta_3 = d\zeta_r d\zeta_\theta d\zeta_3$, and ν and η are parameters to adjust the Prandtl number. The Knudsen number Kn is expressed as

$$\mathrm{Kn} = \frac{2}{\sqrt{\pi}}(1 - \nu + \eta\nu)\frac{(2\mathcal{R}T_0)^{1/2}\mu_0}{p_0 R_*}, \tag{2.3}$$

in terms of ν, η, and the viscosity μ_0 corresponding to the temperature T_0 [see Sec. 2.6, Eq. (2.54a)]. In Eqs. (2.2b)–(2.2h) and in what follows, the domain of the integration with respect to ζ_i is its whole space, unless the contrary is stated.

The diffuse-reflection condition on the tube wall is written as

$$\phi = 2\sqrt{\pi}\int_{\zeta_r>0}\int_0^\infty \zeta_r \mathcal{E}^{\delta/2-1}\phi E d\mathcal{E} d^3\zeta + \left(\zeta^2 - 2 + \mathcal{E} - \frac{\delta}{2}\right)\beta x_3, \qquad (r = R_0/R_*,\ \zeta_r < 0), \tag{2.4}$$

where $T_0(1+\beta x_3)$ is the temperature of the tube wall.

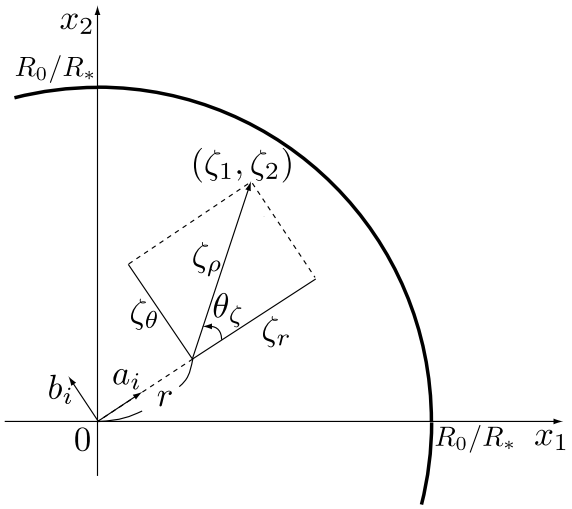

Figure 2.1: Coordinate system.

The linearized equation of state and the heat-flow vector are expressed as

$$P = \omega + \tau, \tag{2.5a}$$

$$Q_i = \iint_0^\infty \zeta_i(\zeta_j^2 + \mathcal{E})\mathcal{E}^{\delta/2-1}\phi E d\mathcal{E} d^3\zeta - \frac{5+\delta}{2}u_i. \tag{2.5b}$$

In addition, if we denote by $\rho_0(2\mathcal{R}T_0)^{1/2}\pi R_*^2 M$ the (dimensional) mass-flow rate (per unit time) through the tube, we have

$$M = 2\int_0^{R_0/R_*} u_3 r dr. \tag{2.6}$$

2.2.3 Similarity solutions

Let us introduce ζ_ρ and θ_ζ that express ζ_r and ζ_θ as

$$\zeta_r = \zeta_\rho \cos\theta_\zeta, \qquad \zeta_\theta = \zeta_\rho \sin\theta_\zeta, \tag{2.7}$$

(see Fig. 2.1) and transform the molecular velocity variables from $(\zeta_r,\, \zeta_\theta,\, \zeta_3)$ to $(\zeta_\rho,\, \theta_\zeta,\, \zeta_3)$. Note that $\zeta_\rho = (\zeta_r^2 + \zeta_\theta^2)^{1/2} = (\zeta_1^2 + \zeta_2^2)^{1/2}$ and $0 \le \zeta_\rho < \infty$, $-\pi < \theta_\zeta \le \pi$, and $-\infty < \zeta_3 < \infty$. Then, we seek the solution in the following form:

$$\phi = \left[\alpha + \beta\left(\zeta_\rho^2 + \zeta_3^2 + \mathcal{E} - \frac{5+\delta}{2}\right)\right] x_3 + \zeta_3\,[\,\alpha\,\Phi_P(r,\, \zeta_\rho,\, |\theta_\zeta|,\, \zeta_3^2,\, \mathcal{E}) + \beta\,\Phi_T(r,\, \zeta_\rho,\, |\theta_\zeta|,\, \zeta_3^2,\, \mathcal{E})]. \tag{2.8}$$

Actually, substitution of Eq. (2.8) into Eqs. (2.1) and (2.4) shows the consistency of Eq. (2.8) and leads to the following equation and boundary condition for Φ_J, where $J = P$ or T: The

equation is

$$\zeta_\rho \cos\theta_\zeta \frac{\partial \Phi_J}{\partial r} - \frac{\zeta_\rho}{r} \sin\theta_\zeta \frac{\partial \Phi_J}{\partial \theta_\zeta}$$
$$= \frac{2}{\sqrt{\pi}} \frac{1}{\mathrm{Kn}} [-\Phi_J + 2u_J + 2(1-\eta)\nu\zeta_\rho \cos\theta_\zeta \Pi_J] - I_J,$$
$$(0 \le r < R_0/R_*,\ 0 \le \zeta_\rho < \infty,\ 0 \le \theta_\zeta \le \pi,\ -\infty < \zeta_3 < \infty,\ 0 \le \mathcal{E} < \infty), \quad (2.9)$$

where

$$I_P = 1, \qquad I_T = \zeta_\rho^2 + \zeta_3^2 + \mathcal{E} - \frac{5+\delta}{2}, \quad (2.10a)$$
$$u_J = 2\int_{-\infty}^{\infty}\int_0^{\pi}\int_0^{\infty}\int_0^{\infty} \zeta_\rho \zeta_3^2 \mathcal{E}^{\delta/2-1} \Phi_J E d\mathcal{E} d\zeta_\rho d\theta_\zeta d\zeta_3, \quad (2.10b)$$
$$\Pi_J = 4\int_{-\infty}^{\infty}\int_0^{\pi}\int_0^{\infty}\int_0^{\infty} \zeta_\rho^2 \zeta_3^2 \cos\theta_\zeta \mathcal{E}^{\delta/2-1} \Phi_J E d\mathcal{E} d\zeta_\rho d\theta_\zeta d\zeta_3, \quad (2.10c)$$
$$E(\zeta, \mathcal{E}) = \Lambda_\delta \pi^{-3/2} \exp(-\zeta_\rho^2 - \zeta_3^2 - \mathcal{E}), \quad (2.10d)$$

and the boundary condition is

$$\Phi_J = 0,$$
$$(r = R_0/R_*,\ 0 \le \zeta_\rho < \infty,\ \pi/2 < \theta_\zeta \le \pi,\ -\infty < \zeta_3 < \infty,\ 0 \le \mathcal{E} < \infty). \quad (2.11)$$

In Eqs. (2.9)–(2.11), the range of θ_ζ has been reduced to $0 \le \theta_\zeta \le \pi$ by the use of the fact that Φ_J is an even function of θ_ζ.

The macroscopic quantities corresponding to Eq. (2.8) are obtained from Eqs. (2.2b)–(2.2h), (2.5a), and (2.5b) as follows.

$$\omega = (\alpha - \beta)x_3, \qquad P = \alpha x_3, \quad (2.12a)$$
$$u_r = u_\theta = 0, \qquad u_3 = \alpha u_P + \beta u_T, \quad (2.12b)$$
$$\tau_{\mathrm{tr}} = \tau_{\mathrm{int}} = \tau = \tau_{\mathrm{rel}} = \beta x_3, \quad (2.12c)$$
$$P_{rr} = P_{\theta\theta} = P_{33} = \alpha x_3, \qquad P_{r\theta} = P_{\theta 3} = 0, \qquad P_{r3} = \alpha \Pi_P + \beta \Pi_T, \quad (2.12d)$$
$$Q_r = Q_\theta = 0, \qquad Q_3 = \alpha Q_P + \beta Q_T, \quad (2.12e)$$

where u_J and Π_J are given in Eqs. (2.10b) and (2.10c), and Q_J by

$$Q_J = 2\int_{-\infty}^{\infty}\int_0^{\pi}\int_0^{\infty}\int_0^{\infty} \zeta_\rho \zeta_3^2 \left(\zeta_\rho^2 + \zeta_3^2 + \mathcal{E} - \frac{5+\delta}{2}\right) \mathcal{E}^{\delta/2-1} \Phi_J E d\mathcal{E} d\zeta_\rho d\theta_\zeta d\zeta_3. \quad (2.13)$$

That is, Eq. (2.8) indicates a flow in the axial direction with a uniform pressure and temperature gradients in the same direction. Note that the density, temperature, and pressure are

independent of r. The solution Φ_P corresponds to the Poiseuille flow, and Φ_T to the thermal transpiration. Correspondingly, the dimensionless mass-flow rate [Eq. (2.6)] is expressed as

$$M = \alpha M_P + \beta M_T, \tag{2.14a}$$

$$M_J = 2\int_0^{R_0/R_*} u_J r dr. \tag{2.14b}$$

If we multiply Eq. (2.9) by $\zeta_\rho \zeta_3^2 \mathcal{E}^{\delta/2-1} E$ and integrate it with respect to $\mathcal{E}$, ζ_ρ, θ_ζ, and ζ_3 over the domain $0 < \mathcal{E} < \infty$, $0 < \zeta_\rho < \infty$, $0 < \theta_\zeta < \pi$, and $-\infty < \zeta_3 < \infty$, we have

$$\frac{d\Pi_J}{dr} + \frac{\Pi_J}{r} = \begin{cases} -1 & (J = P), \\ 0 & (J = T). \end{cases} \tag{2.15}$$

Since Π_J should be finite at $r = 0$, it is obtained as

$$\Pi_P = -\frac{r}{2}, \qquad \Pi_T = 0. \tag{2.16}$$

Equation (2.16) simplifies Eq. (2.9) further.

2.2.4 Further transformation and reduction to the BGK model

The system, Eqs. (2.9) [with Eq. (2.16)] and (2.11), can be simplified further by multiplying by $(2/\sqrt{\pi})\Lambda_\delta \mathcal{E}^{\delta/2-1}\zeta_3^2 \exp(-\mathcal{E} - \zeta_3^2)$ and integrating with respect to $\mathcal{E}$ from 0 to ∞ and ζ_3 from $-\infty$ to ∞. The resulting system is as follows: The equation is

$$\zeta_\rho \cos\theta_\zeta \frac{\partial \Psi_J}{\partial r} - \frac{\zeta_\rho}{r}\sin\theta_\zeta \frac{\partial \Psi_J}{\partial \theta_\zeta} = \frac{2}{\sqrt{\pi}}\frac{1}{\mathrm{Kn}}\left[-\Psi_J + 2u_J[\Psi_J] + 2\left(1 - \frac{1}{\mathrm{Pr}}\right)\zeta_\rho \cos\theta_\zeta \Pi_J\right] - \tilde{I}_J, \quad (0 \le r < R_0/R_*,\ 0 \le \zeta_\rho < \infty,\ 0 \le \theta_\zeta \le \pi), \tag{2.17}$$

where

$$u_J[\Psi_J] = \frac{1}{\pi}\int_0^\pi \int_0^\infty \zeta_\rho \Psi_J \exp(-\zeta_\rho^2) d\zeta_\rho d\theta_\zeta, \tag{2.18a}$$

$$\Pi_P = -\frac{r}{2}, \qquad \Pi_T = 0, \tag{2.18b}$$

$$\tilde{I}_P = 1, \qquad \tilde{I}_T = \zeta_\rho^2 - 1, \tag{2.18c}$$

and the boundary condition is

$$\Psi_J = 0 \qquad (r = R_0/R_*,\ 0 \le \zeta_\rho < \infty,\ \pi/2 < \theta_\zeta \le \pi). \tag{2.19}$$

Here, Ψ_J is defined by

$$\Psi_J = \frac{2}{\sqrt{\pi}}\Lambda_\delta \int_{-\infty}^{\infty}\int_0^\infty \mathcal{E}^{\delta/2-1}\zeta_3^2\Phi_J \exp(-\mathcal{E}-\zeta_3^2)d\mathcal{E}d\zeta_3. \tag{2.20}$$

Once the solution Ψ_J (and thus u_J) of Eqs. (2.17)–(2.19) is obtained, one can reconstruct the original Φ_J by solving Eq. (2.9), which reduces to a partial differential equation for Φ_J, under the boundary condition (2.11). Therefore, any macroscopic quantity, such as Q_J in Eq. (2.13), can be obtained. For convenience of discussion below, we rewrite the mass-flow rates M_J [Eq. (2.14)] in the following form:

$$M_J[\Psi_J] = 2\int_0^{R_0/R_*} u_J[\Psi_J] r dr. \tag{2.21}$$

Here, we note that Eqs. (2.17)–(2.19) are of the same form as the corresponding equations and boundary conditions for the cylindrical Poiseuille flow and thermal transpiration based on the ES model for a monatomic gas [6]. The difference between monatomic and polyatomic gases arises only in the different values of Pr. Furthermore, Eqs. (2.17)–(2.19) with $J = T$, which do not contain Pr, are the same as the corresponding equation and boundary condition for the thermal transpiration based on the BGK model. As for the cylindrical Poiseuille flow, although Eqs. (2.17)–(2.19) with $J = P$ are different from the corresponding equation and boundary condition based on the BGK model, we can reduce the solution of the former to that of the latter by a simple conversion, as in the case of the plane Poiseuille flow. Let us put

$$\Psi_P = \Psi'_P - \frac{1}{\sqrt{\pi}}\frac{1}{\mathrm{Kn}}\left(1-\frac{1}{\mathrm{Pr}}\right)\left[r^2 - \left(\frac{R_0}{R_*}\right)^2\right]. \tag{2.22}$$

Then, it follows from Eqs. (2.17)–(2.19) with $J = P$ that Ψ'_P satisfies

$$\zeta_\rho \cos\theta_\zeta \frac{\partial \Psi'_P}{\partial r} - \frac{\zeta_\rho}{r}\sin\theta_\zeta \frac{\partial \Psi'_P}{\partial \theta_\zeta} = \frac{2}{\sqrt{\pi}}\frac{1}{\mathrm{Kn}}\left(-\Psi'_P + 2u_P[\Psi'_P]\right) - 1, \tag{2.23a}$$

$$\Psi'_P = 0 \qquad (r = R_0/R_*,\ \pi/2 < \theta_\zeta \le \pi), \tag{2.23b}$$

which are identical with the corresponding equation and boundary condition for the cylindrical Poiseuille flow based on the BGK model. To summarize these facts, we obtain the

following relations for the solutions, flow velocities, and mass-flow rates:

$$\Psi_P = \Psi_P^{\mathrm{BGK}} - \frac{1}{\sqrt{\pi}}\frac{1}{\mathrm{Kn}}\left(1-\frac{1}{\mathrm{Pr}}\right)\left[r^2 - \left(\frac{R_0}{R_*}\right)^2\right], \tag{2.24a}$$

$$u_P[\Psi_P] = u_P[\Psi_P^{\mathrm{BGK}}] - \frac{1}{2\sqrt{\pi}}\frac{1}{\mathrm{Kn}}\left(1-\frac{1}{\mathrm{Pr}}\right)\left[r^2 - \left(\frac{R_0}{R_*}\right)^2\right], \tag{2.24b}$$

$$u_T[\Psi_T] = u_T[\Psi_T^{\mathrm{BGK}}], \tag{2.24c}$$

$$M_P[\Psi_P] = M_P[\Psi_P^{\mathrm{BGK}}] + \frac{1}{4\sqrt{\pi}}\frac{1}{\mathrm{Kn}}\left(1-\frac{1}{\mathrm{Pr}}\right)\left(\frac{R_0}{R_*}\right)^4, \tag{2.24d}$$

$$M_T[\Psi_T] = M_T[\Psi_T^{\mathrm{BGK}}], \tag{2.24e}$$

where Ψ_P^{BGK} and Ψ_T^{BGK} are the solutions corresponding to Ψ_P and Ψ_T for the BGK model. As mentioned in Sec. 2.1, the database of $u_P[\Psi_P^{\mathrm{BGK}}]$, $u_T[\Psi_T^{\mathrm{BGK}}]$, $M_P[\Psi_P^{\mathrm{BGK}}]$, and $M_T[\Psi_T^{\mathrm{BGK}}]$, the original version of which was built by Sone and Itakura [33], has been constructed by Sone, Itakura, and Handa. From this, one can obtain an accurate values of these quantities instantaneously for an arbitrary Knudsen number. The database is available from the present authors (the software package can be downloaded from the webpage http://www.mfd.me.kyoto-u.ac.jp/Sone/database-e.html). Therefore, we do not need to carry out new computations to obtain u_P, u_T, M_P, and M_T for the ES model for a polyatomic gas. It should be noted that the conversion formula for the mass-flow rate of the Poiseuille flow between the ES model for a monatomic gas and the BGK model, corresponding to Eq. (2.24d), is given in Ref. [8].

2.2.5 Mass-flow and heat-flow rates

If we denote by $\mathcal{M}$ the total mass-flow rate in the X_3 direction per unit time, then it follows from Eqs. (2.6) and (2.14) that

$$\mathcal{M} = \pi\rho_0(2\mathcal{R}T_0)^{1/2}R_*^2\left[M_P(\mathrm{Kn};\, R_0/R_*)\frac{R_*}{p_0}\frac{dp}{dX_3} + M_T(\mathrm{Kn};\, R_0/R_*)\frac{R_*}{T_0}\frac{dT_w}{dX_3}\right], \tag{2.25}$$

where

$$M_J(\mathrm{Kn};\, R_0/R_*) = 2\int_0^{R_0/R_*} u_J\, r dr, \qquad (J = P,\, T). \tag{2.26}$$

Here, the fact that M_J depends on Kn and R_0/R_* is shown explicitly as arguments.

Now we take the radius of the circular tube R_0 as the reference length R_* and denote the corresponding Kn by Kn_0, i.e., $\mathrm{Kn} = (R_0/R_*)\,\mathrm{Kn}_0$. Then Eq. (2.25) becomes

$$\mathcal{M} = \pi\rho_0(2\mathcal{R}T_0)^{1/2}R_0^2\left[M_P(\mathrm{Kn}_0;\, 1)\frac{R_0}{p_0}\frac{dp}{dX_3} + M_T(\mathrm{Kn}_0;\, 1)\frac{R_0}{T_0}\frac{dT_w}{dX_3}\right]. \tag{2.27}$$

Since Eqs. (2.25) and (2.27) express the same quantity, we have the following relation:

$$M_J(\mathrm{Kn};\, R_0/R_*) = (R_0/R_*)^3 M_J(\mathrm{Kn}_0; 1). \tag{2.28}$$

Similarly, from the solution Φ_J (or Q_J), we can compute the heat-flow rate through the tube. Let $\mathcal{H}$ be the total heat-flow rate in the X_3 direction per unit time. Then we have

$$\mathcal{H} = \pi p_0 (2\mathcal{R}T_0)^{1/2} R_*^2 \left[H_P(\mathrm{Kn};\, R_0/R_*) \frac{R_*}{p_0} \frac{dp}{dX_3} + H_T(\mathrm{Kn};\, R_0/R_*) \frac{R_*}{T_0} \frac{dT_w}{dX_3} \right], \tag{2.29}$$

where

$$H_J(\mathrm{Kn};\, R_0/R_*) = 2 \int_0^{R_0/R_*} Q_J \, r dr, \qquad (J = P,\, T), \tag{2.30}$$

and it satisfies the following relation:

$$H_J(\mathrm{Kn};\, R_0/R_*) = (R_0/R_*)^3 H_J(\mathrm{Kn}_0; 1). \tag{2.31}$$

2.2.6 Numerical results

In this Sec. 2.2.6, we show the profiles of the velocity and heat flow and mass-flow rates for the Poiseuille flow and thermal transpiration obtained with the help of Eq. (2.24). The basic equation (2.1) contains the set of parameters (ν, η, δ) to characterize the polyatomic gas under consideration. In place of this set, we may also use another set (Pr, μ_b/μ, δ) because of relations (2.51c), (2.51d), and (2.52). Here, we consider the nitrogen gas (N_2; $\delta = 2$), for which experimental data for Pr and μ_b/μ are available (Pr = 0.718 [25] and $\mu_b/\mu = 0.731$ [28]). We set the values of ν and η in such a way that the resulting Pr and μ_b/μ are close to the above experimental values, that is, $\nu = -0.50$ and $\eta = 0.46$, which lead to Pr = 0.787 and $\mu_b/\mu = 0.722$. We also set $R_* = R_0$ and assume A_c in Eq. (2.47) to be constant.

Figures 2.2(a) and 2.2(b) show the velocity profile for the Poiseuille flow u_P and that for the thermal transpiration u_T for various values of Kn [cf. Eq. (2.12b)]. Figures 2.3(a) and 2.3(b) show the corresponding profiles of the heat-flow vectors Q_P and Q_T [cf. Eq. (2.12e)]. Tables 2.1 and 2.2 show the mass-flow rates M_P and M_T versus Kn, respectively. In Table 2.1, the result for a monatomic gas (Pr = 2/3) is also shown for comparison (M_T in Table 2.2 does not depend on the value of Pr and is the same as that for the BGK model).

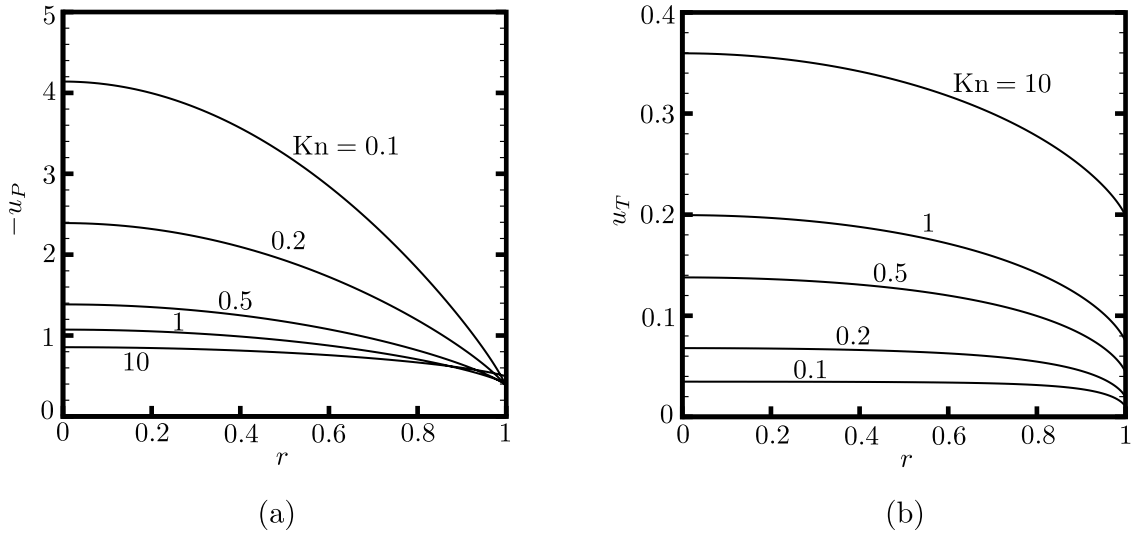

Figure 2.2: Profiles of the flow velocities for the Poiseuille flow and thermal transpiration through a circular tube. (a) Dimensionless flow velocity u_P for the Poiseuille flow. (b) Dimensionless flow velocity u_T for the thermal transpiration.

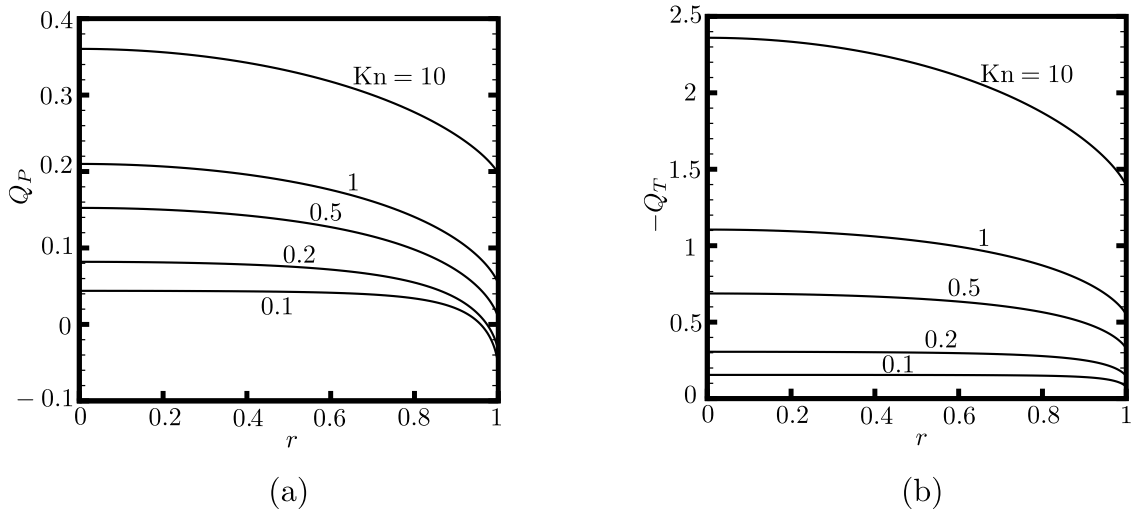

Figure 2.3: Profiles of the heat-flow vectors for the Poiseuille flow and thermal transpiration through a circular tube. (a) Dimensionless heat-flow vector Q_P for the Poiseuille flow. (b) Dimensionless heat-flow vector Q_T for the thermal transpiration.

Table 2.1: Dimensionless mass-flow rate M_P for the Poiseuille flow.

Kn	$-M_P\vert_{\mathrm{Pr}=2/3}$	$-M_P\vert_{\mathrm{Pr}=0.787}$
10^{-2}	0.2167(2)*	0.1843(2)
2×10^{-2}	0.1109(2)	0.9474(1)
3×10^{-2}	0.7567(1)	0.6489(1)
4×10^{-2}	0.5807(1)	0.4998(1)
6×10^{-2}	0.4048(1)	0.3509(1)
8×10^{-2}	0.3170(1)	0.2766(1)
10^{-1}	0.2645(1)	0.2322(1)
2×10^{-1}	0.1604(1)	0.1442(1)
3×10^{-1}	0.1263(1)	0.1155(1)
4×10^{-1}	0.1096(1)	0.1015(1)
6×10^{-1}	0.9336(0)	0.8797
8×10^{-1}	0.8558(0)	0.8154
1	0.8112	0.7788
5	0.7037	0.6972
10^1	0.7068	0.7035
10^2	0.7377	0.7373
10^3	0.7496	0.7495
10^4	0.7519	0.7519

* Read as 0.2167×10^2.

Table 2.2: Dimensionless mass-flow rate M_T for the thermal transpiration.

Kn	M_T
10^{-2}	0.3364(−2)*
2×10^{-2}	0.6665(−2)
3×10^{-2}	0.9903(−2)
4×10^{-2}	0.1308(−1)
6×10^{-2}	0.1923(−1)
8×10^{-2}	0.2514(−1)
10^{-1}	0.3079(−1)
2×10^{-1}	0.5558(−1)
3×10^{-1}	0.7555(−1)
4×10^{-1}	0.9197(−1)
6×10^{-1}	0.1176
8×10^{-1}	0.1370
1	0.1524
5	0.2579
10^1	0.2934
10^2	0.3573
10^3	0.3730
10^4	0.3757

* Read as 0.3364×10^{-2}.

2.3 Diffusion-type system

In this section, we consider a rarefied polyatomic gas in a straight pipe composed of long circular tubes connected longitudinally. The radius of each tube is different each other, as shown in Fig. 2.4. Therefore, the cross section of the pipe changes suddenly at the junctions of the tubes. We assume the following:

(i) The behavior of the gas is described by the ES model for a polyatomic gas.

(ii) The gas molecules undergo diffuse reflection on the pipe wall (including the walls at the junctions).

(iii) The length of each circular tube is much longer than its diameter.

(iv) The temperature of the pipe wall is uniform at each cross section (and at each junction). The distribution of the wall temperature along the pipe axis is arbitrary but continuous (its derivative may be discontinuous at the junctions), and its variation may be large. However, the length scale of its variation is much longer than the diameters of the tubes.

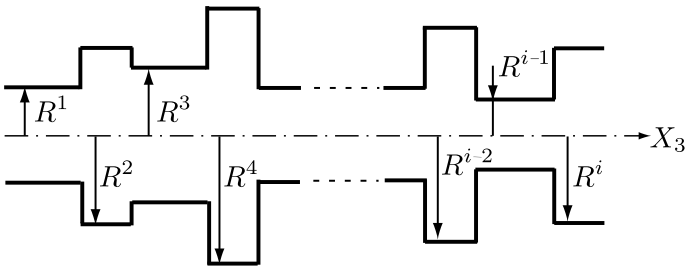

Figure 2.4: Schematic of the straight pipe.

In this situation, one can derive, by a systematic asymptotic analysis of the kinetic system, a macroscopic system consisting of a diffusion-type equation in each tube and a connection condition at each junction that describes the (slow) time evolution of the distribution of the pressure (or density) of the gas along the pipe axis. In Ref. [5], such a system was derived for a single and monatomic gas for tubes with arbitrary (not necessarily circular) cross sections on the basis of the Boltzmann equation and a general form of the boundary condition. Here, we repeat the same analysis for the ES model for a polyatomic gas with the diffuse reflection condition and for circular tubes. Since analysis is basically the same as that in Refs. [40] and [5], we only summarize the result.

We assume that the axis of the pipe is set along the X_3 axis. Let t be the time variable, $T_w(X_3)$ the temperature of the pipe wall, T the temperature of the gas, ρ the density of the gas, $p = \mathcal{R}\rho T$ the pressure of the gas, and $\mathcal{M}$ is the mass-flow rate across the pipe in the X_3 direction per unit time. Let L_* denote the reference length in the axial direction (a typical length of the tubes, the length scale of variation of the temperature, etc.), R_* ($\ll L_*$) the reference length in the radial direction (a typical radius of the tubes), T_* the reference temperature, ρ_* the reference density, $p_* = \mathcal{R}\rho_* T_*$ the reference pressure, l_* the reference mean free path of the gas molecules defined as $l_* = (2/\sqrt{\pi})(2\mathcal{R}T_*)^{1/2}/A_c(T_*)\rho_*$ (see Sec. 2.6), and $K_* = l_*/R_*$ the reference Knudsen number. Furthermore, we introduce the following dimensionless quantities:

$$\hat{t} = t\,[L_*^2/(2\mathcal{R}T_*)^{1/2}R_*]^{-1}, \quad z = X_3/L_*, \tag{2.32a}$$

$$\hat{T}_w = T_w/T_*, \quad \hat{\rho} = \rho/\rho_*, \quad \hat{T} = T/T_*, \quad \hat{p} = p/p_* \ (= \hat{\rho}\hat{T}), \tag{2.32b}$$

$$M = \mathcal{M}/\pi\rho_*(2\mathcal{R}T_*)^{1/2}R_*^2. \tag{2.32c}$$

The quantities $\hat{\rho}$, $\hat{T}$, $\hat{p}$, and M are expanded in terms of a small parameter $\epsilon = R_*/L_*$ as

$$\hat{\rho} = \hat{\rho}_{(0)} + \hat{\rho}_{(1)}\epsilon + \cdots , \tag{2.33a}$$

$$\hat{T} = \hat{T}_{(0)} + \hat{T}_{(1)}\epsilon + \cdots , \tag{2.33b}$$

$$\hat{p} = \hat{p}_{(0)} + \hat{p}_{(1)}\epsilon + \cdots , \tag{2.33c}$$

$$M = M_{(1)}\epsilon + \cdots , \tag{2.33d}$$

and $\hat{\rho}_{(0)}$, $\hat{T}_{(0)}$, $\hat{p}_{(0)}$, and $M_{(1)}$ are found to be the functions of $\hat{t}$ and z (i.e., they do not depend on the radial coordinate). In addition, $\hat{T}_{(0)}(\hat{t},\, z) = \hat{T}_w(z)$ holds, so that $\hat{p}_{(0)}(\hat{t},\, z) = \hat{\rho}_{(0)}(\hat{t},\, z)\hat{T}_w(z)$.

Let us consider the ith tube and denote $\hat{p}_{(0)}$ and $M_{(1)}$ there by $\hat{p}^i_{(0)}$ and $M^i_{(1)}$, respectively. Let R^i and $\hat{R}^i = R^i/R_*$ be the dimensional and dimensionless radii of the ith tube, respectively. Then, $\hat{p}^i_{(0)}$ is governed, through $M^i_{(1)}$, by the following equation:

$$\frac{\partial \hat{p}^i_{(0)}}{\partial \hat{t}} + \frac{\hat{T}_w}{(\hat{R}^i)^2}\frac{\partial M^i_{(1)}}{\partial z} = 0, \tag{2.34a}$$

$$M^i_{(1)} = \frac{\hat{p}^i_{(0)}}{\hat{T}_w^{1/2}}\left[M^i_P(K^i)\frac{\partial \ln \hat{p}^i_{(0)}}{\partial z} + M^i_T(K^i)\frac{d \ln \hat{T}_w}{dz}\right], \tag{2.34b}$$

where

$$K^i = \frac{K_*\hat{T}_w^{3/2}}{\hat{A}_c(\hat{T}_w)\hat{p}^i_{(0)}}, \tag{2.35}$$

and we have assumed that $A_c(T)$ in Eq. (2.47) can be written as

$$A_c(T) = A_c(T_*\hat{T}) = A_c(T_*)\hat{A}_c(\hat{T}). \tag{2.36}$$

(If $A_c = \text{const} \times T^m$, then $\hat{A}_c = \hat{T}^m$.) Here, $M^i_P(K^i)$ and $M^i_T(K^i)$ correspond to the dimensionless mass-flow rate of the Poiseuille flow and that of the thermal transpiration through an infinitely long circular tube with radius R^i. More precisely, they are related to $M_P(\text{Kn};\, R_0/R_*)$ and $M_T(\text{Kn};\, R_0/R_*)$ in Sec. 2.2.5 [cf. Eqs. (2.26) and (2.28)] as

$$M^i_J(K^i) = M_J(K^i;\, \hat{R}^i) = (\hat{R}^i)^3 M_J(K^i/\hat{R}^i;\, 1) \qquad (J = P,\, T). \tag{2.37}$$

At the junction of the ith tube with the neighboring $(i+1)$th tube, the following connection condition has to be satisfied:

$$\hat{p}^i_{(0)} = \hat{p}^{i+1}_{(0)}, \qquad M^i_{(1)} = M^{i+1}_{(1)}. \tag{2.38}$$

Equations (2.34) and (2.38) are to be supplemented by an appropriate initial condition and end conditions (see Sec. 2.4.2). Once the solution of this system is found, the dimensional pressure p^i and the dimensional mass-flow rate $\mathcal{M}^i$ in the ith tube are given, respectively, by [cf. Eqs. (2.32) and (2.33)]

$$p^i = p_*[\hat{p}^i_{(0)} + O(\epsilon)], \tag{2.39a}$$

$$\mathcal{M}^i = \pi\rho_*(2\mathcal{R}T_*)^{1/2}R_*^2[M^i_{(1)}\epsilon + O(\epsilon^2)]. \tag{2.39b}$$

2.4 Applications of diffusion-type system

In this section, we apply the diffusion-type equation with the connection condition summarized in Sec. 2.3 to two problems. As in Sec. 2.2.6, we consider the nitrogen gas and let $\nu = -0.50$ and $\eta = 0.46$, which lead to $\mathrm{Pr} = 0.787$ and $\mu_b/\mu = 0.722$. We also assume A_c in Eq. (2.47) to be constant (thus $\hat{A}_c = 1$).

2.4.1 Flow caused by a large pressure difference

We first consider a single long circular tube of radius R_0 and length L kept at a uniform temperature T_0 and set in the interval $0 \le X_3 \le L$. Let both ends of the tube be open, and the pressure at $X_3 = 0$ and that at $X_3 = L$ be kept at p_0 and p_1, respectively. We investigate the steady flow of the gas through the tube.

Let us take p_0, T_0, R_0, and L as the reference quantities p_*, T_*, R_*, and L_*, respectively. Then, $\hat{T}_w = 1$, and K_* is the Knudsen number based on R_0, p_0, and T_0. In addition, we omit the superscript i in Eqs. (2.34), (2.35), (2.37), and (2.39). Then, the end conditions become

$$\hat{p}_{(0)} = 1 \ \ (\text{at} \ \ z = 0), \qquad \hat{p}_{(0)} = p_1/p_0 \ \ (\text{at} \ \ z = 1). \tag{2.40}$$

We solve Eq. (2.34) with end conditions (2.40) and an appropriate initial condition, e.g., $\hat{p}_{(0)} = 1$ at $\hat{t} = 0$ for $0 < z < 1$, and obtain the steady flow as the long-time limit of the solution. In the final steady state, since $\partial\hat{p}_{(0)}/\partial\hat{t} = 0$ holds, we have $M_{(1)} \equiv M_f = \text{const.}$, and the mass-flow rate $\mathcal{M}$ is given by [cf. Eq. (2.39b)]

$$\mathcal{M} = \pi\rho_0(2\mathcal{R}T_0)^{1/2}R_0^2\,[M_f\epsilon + O(\epsilon^2)], \tag{2.41}$$

where $\rho_0 = p_0/\mathcal{R}T_0$ and $\epsilon = R_0/L$. Since the numerical solution method is straightforward, we show only the result of analysis.

Figure 2.5 shows the reduced mass-flow rate G versus K_* for $p_1/p_0 = 10^{-2}$. Here, $G = \mathcal{M}/\mathcal{M}_{\rm FM} = (3\sqrt{\pi}/4)[1-(p_1/p_0)]^{-1}M_f \approx (3\sqrt{\pi}/4)M_f$ [with the term of $O(\epsilon^2)$ neglected in Eq. (2.41)], and $\mathcal{M}_{\rm FM}$ is the mass-flow rate for the free-molecular flow, i.e., $\mathcal{M}_{\rm FM} = (4\sqrt{\pi}/3)R_0^3[(p_0-p_1)/L](2/\mathcal{R}T_0)^{1/2}$. In the figure, the solid line indicates the numerical result for N_2 gas (Pr = 0.787 and $\mu_b/\mu = 0.722$), and the black square indicates the experimental result taken from Ref. [24], where the experiment of the same problem is carried out with the nitrogen gas, using a bundle of huge number of tiny circular tubes, under the condition that $p_1/p_0 \approx 0$ and $\epsilon = 1/2727$. Figure 2.5(a) shows the results for $0.005 \le K_* \le 20$ and Fig. 2.5(b) is the magnified figure for $0.1 \le K_* \le 20$. The pressure ratio p_1/p_0 in the present example might be too small to apply the diffusion-type system with confidence. Nevertheless, the numerical and experimental results show good agreement on the whole, except for the difference of 10% to 15% in the range $0.5 \le K_* \le 8$.

In Fig. 2.5, the experimental data are plotted after a suitable conversion of the Knudsen number, which is explained in the following. In Ref. [24], the mean free path l_0 is defined by $l_0 = kT_0/\sqrt{2}\pi d^2 p_0$ (with k the Boltzmann constant), assuming that an N_2 molecule is a hard sphere with effective diameter d. Therefore, it is expressed in terms of the viscosity μ_0 at temperature T_0 and pressure p_0 as $l_0 = (2/\sqrt{\pi})(\mu_0/\gamma_1)(2\mathcal{R}T_0)^{1/2}/p_0$ where $\gamma_1 = 1.270042$ [32]. On the other hand, from Eqs. (2.51c) and (2.54a), our l_0 is given by $l_0 = (2/\sqrt{\pi})(\mu_0/{\rm Pr})(2\mathcal{R}T_0)^{1/2}/p_0$. If we assume that the viscosity μ_0 is a common quantity and eliminate it from the two expressions for l_0, we obtain a conversion formula for l_0 between our numerical result and experimental data in Ref. [24]. That is, in terms of the Knudsen number, we have $K_* = (\gamma_1/{\rm Pr})\,{\rm Kn}_i = 1.613777\,{\rm Kn}_i$, where ${\rm Kn}_i$ is the Knudsen number (at temperature T_0 and pressure p_0) in Ref. [24]. For instance, the measured value for ${\rm Kn}_i = 1$ is plotted at $K_* = 1.613777$ in Fig. 2.5.

2.4.2 Knudsen compressor

The Knudsen compressor [20,21] is a non-mechanical device that produces a one-way gas flow with a pumping effect using the imbalance of the thermal transpiration caused by periodic temperature distribution and periodic structure of the device. It has been attracting attention as a microscale flow controller (e.g., Refs. [36,41,34,35,16]) and gas separator (e.g., Ref. [40]) without any moving parts, and its variants (e.g., Refs. [38] and [3]) have been

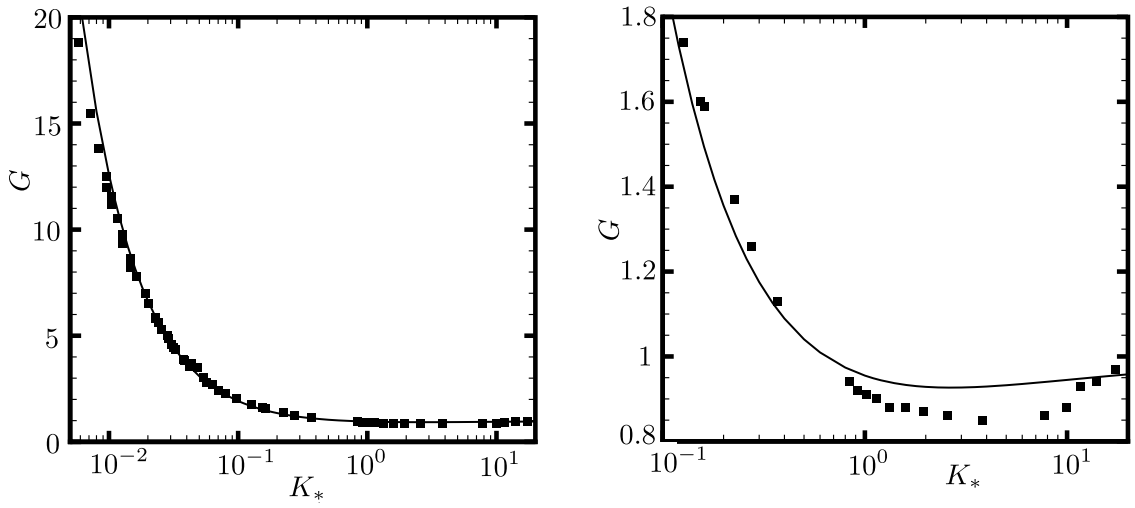

(a) (b)

Figure 2.5: Reduced mass-flow rate G [$\equiv (3\sqrt{\pi}/4)M_f$] vs K_* for N_2 gas in the case of $p_1/p_0 = 10^{-2}$. (a) $0.005 \le K_* \le 20$, (b) magnified figure for $0.1 \le K_* \le 20$. The solid line indicates the numerical result (Pr = 0.787 and $\mu_b/\mu = 0.722$), and the black square indicates the experimental result taken from Ref. [24].

proposed. A typical Knudsen pump is a long pipe with a periodic structure consisting of alternately arranged narrow and wide pipes. The temperature of the pipe is also periodic with the same period as the structure, such as a saw-tooth distribution increasing in the narrow segments and decreasing in the wide segments. The flow and its pumping effect have been studied numerically as well as experimentally. In practical applications, however, a large number of segments should be used, so that the estimate of the properties and performance of the compressor in various steady and unsteady situations by the DSMC computation or by experiment is a formidable task. Therefore, the simple macroscopic system summarized in Sec. 2.3 is useful for this purpose.

Let us consider the system shown in Fig. 2.6, that is, a pipe composed of alternately arranged m narrow circular tubes (radius R_0 and length aL) and m wide circular tubes [radius R_1 and length $(1-a)L$], set in the interval $0 \le X_3 \le mL$. The temperature $T_w(X_3)$ of the pipe wall has a saw-tooth shape as shown in the figure, i.e.,

$$T_w = \begin{cases} T_0, & \text{at } X_3 = nL \text{ and } mL, \\ T_1, & \text{at } X_3 = (a+n)L, \end{cases} \qquad (n = 0,\, 1,\, 2,\, ...,\, m-1), \tag{2.42}$$

and $T_w(X_3)$ is a piecewise linear function of X_3 joining T_0 and T_1. We assume that the assumptions (i)–(iii) of Sec. 2.3 are satisfied, so that (iv) there is also fulfilled. We consider

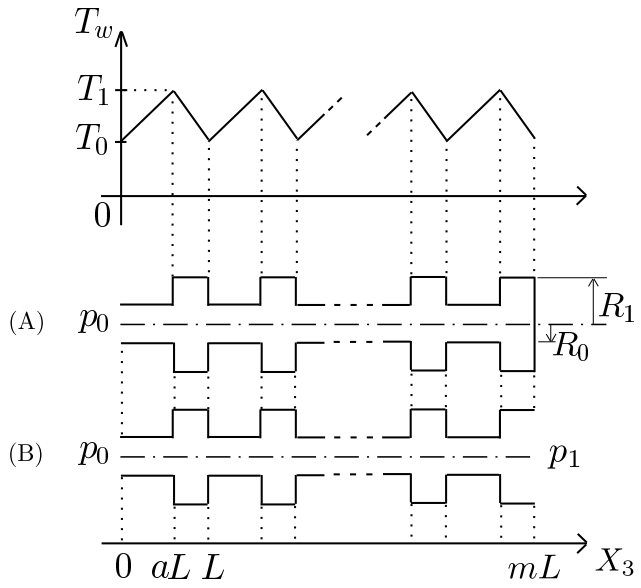

Figure 2.6: Knudsen compressor consisting of circular tubes.

the following two situations (Fig. 2.6):

(A) The pipe is closed at $X_3 = mL$, and the pressure at the open end $X_3 = 0$ is kept at p_0.

(B) Both ends are open, and the pressure at $X_3 = 0$ and that at $X_3 = mL$ are kept at p_0 and p_1, respectively.

We take p_0, T_0, R_0, and L as the reference quantities p_*, T_*, R_*, and L_*, respectively. Therefore, $\hat{T}_w(z) = 1$ at $z = n$ ($n = 0, 1, 2, ..., m-1$) and m, and $\hat{T}_w(z) = T_1/T_0$ at $z = a + n$, and K_* is the Knudsen number of the inlet condition. In addition, the end conditions become

$$\hat{p}_{(0)} = 1 \ \ (\text{at} \ \ z = 0), \quad M_{(1)} = 0 \ \ (\text{at} \ \ z = m) \quad \text{in Case (A)}, \tag{2.43a}$$

$$\hat{p}_{(0)} = 1 \ \ (\text{at} \ \ z = 0), \quad \hat{p}_{(0)} = p_1/p_0 \ \ (\text{at} \ \ z = m) \quad \text{in Case (B)}. \tag{2.43b}$$

We solve Eq. (2.34) with end conditions (2.43) and the initial condition

$$\hat{p}_{(0)} = 1, \quad \text{at} \ \ \hat{t} = 0, \ \ \text{for} \ \ 0 < z < 1, \tag{2.44}$$

and obtain the steady solution as the long-time limit of the unsteady solution. In the final steady state, $M^i_{(1)} = 0$ in case (A), and $M^i_{(1)} \equiv M_f = \text{const.}$ in case (B). In the latter case, the mass-flow rate $\mathcal{M}$ is given by [cf. Eq. (2.39b)]

$$\mathcal{M} = \pi\rho_0(2\mathcal{R}T_0)^{1/2}R_0^2 \, [M_f\epsilon + O(\epsilon^2)], \tag{2.45}$$

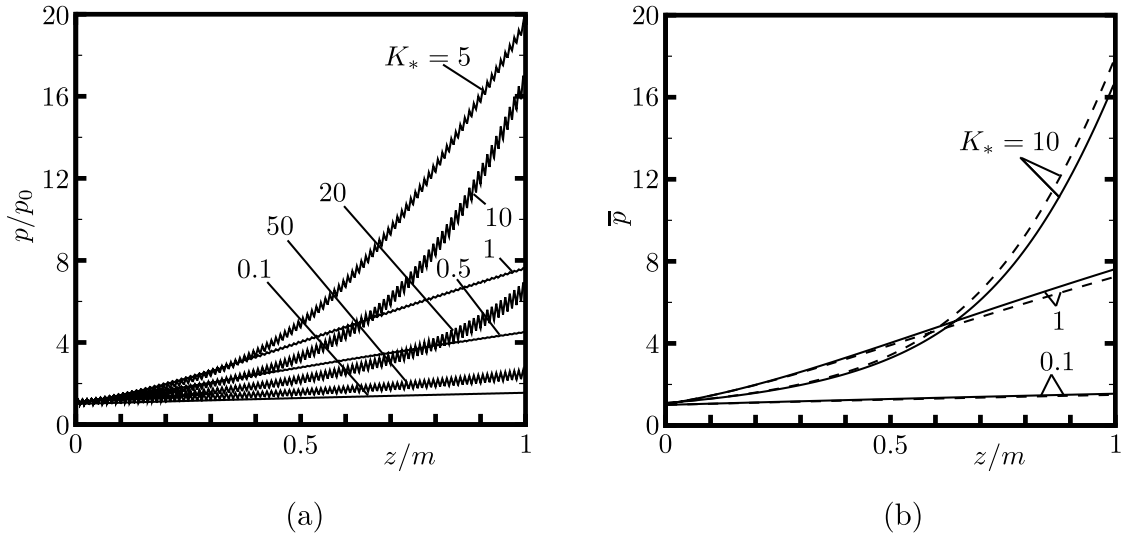

Figure 2.7: Steady pressure distribution along the pipe in Case (A) for $R_1/R_0 = 2$, $a = 0.5$, $T_1/T_0 = 1.5$, and $m = 100$ (N_2 gas: Pr = 0.787 and $\mu_b/\mu = 0.722$). (a) Various K_*, (b) Average pressure distribution for N_2 gas and monatomic gas (Pr = 2/3). In (b), the solid lines indicate the results for N_2 gas, and the dashed lines those for a monatomic gas.

where $\rho_0 = p_0/\mathcal{R}T_0$ and $\epsilon = R_0/L$.

Some numerical results for the steady pressure distribution along the pipe, i.e., p/p_0 versus z, in case (A) are shown in Figs. 2.7 and 2.8 for N_2 gas (Pr = 0.787 and $\mu_b/\mu = 0.722$). Figure 2.7 shows p/p_0 versus z for $m = 100$ in the case of $R_1/R_0 = 2$, $a = 0.5$, and $T_1/T_0 = 1.5$: Fig. 2.7(a) shows the effect of different K_*, and Fig. 2.7(b) the comparison between N_2 gas and a monatomic gas (Pr = 2/3) for $K_* = 0.1$, 1, and 10. In the latter figure, we show the average pressure $\overline{p}$ over each segment, rather than the pressure p itself, to make the difference clearer. A relatively high pressure rise at the closed end can be obtained for intermediate values of the entrance Knudsen number [Fig. 2.7(a)]. The pressure distribution for large numbers of the segments (i.e., large m) is shown in Fig. 2.8 for $R_1/R_0 = 2$, $a = 0.5$, $T_1/T_0 = 1.5$, and $K_* = 1$. In the case of $m = 1000$, the pressure at the closed end for N_2 gas becomes about 40 times the pressure at the open end.

An example of the manner of approach of the gas to the final steady state in Case (A) is shown in Fig. 2.9 for N_2 gas. More precisely, the time evolution of the pressure p_1 at the closed end ($z = m$ or $X_3 = mL$) versus $\hat{t}$ is plotted for $m = 10$ in the case of $R_1/R_0 = 2$, $a = 0.5$, and $T_1/T_0 = 1.5$. Figure 2.9(a) shows the global behavior ($0 \le \hat{t} \le 600$), and Fig. 2.9(b) the short-time behavior ($0 \le \hat{t} \le 1$). The approach is slower for intermediate

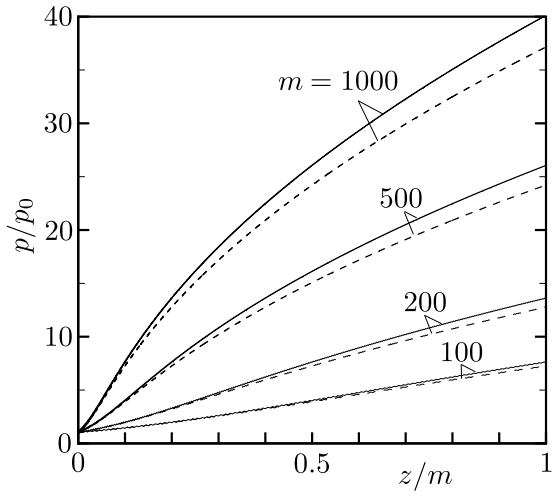

Figure 2.8: Steady pressure distribution along the pipe in Case (A) for $K_* = 1$, $T_1/T_0 = 1.5$, $a = 0.5$, and $R_1/R_0 = 2$. Various m for the N_2 gas and monatomic gas. The solid lines indicate the results for the N_2 gas, and the dashed lines those for the monatomic gas.

and large Knudsen numbers ($K_* = 1$ and 10).

Finally, we show in Table 2.3 the steady mass-flow rate M_f [Eq. (2.45)] in case (B) for different m and K_* in the case of $R_1/R_0 = 2$, $a = 0.5$, $T_1/T_0 = 1.5$, $p_1/p_0 = 2$, and $K_* = 1$. The results for N_2 (Pr = 0.787 and $\mu_b/\mu = 0.722$) as well as for a monatomic gas (Pr = 2/3) are shown in the table. For small Knudsen numbers ($K_* = 0.1$), the flow from the high-pressure end to the low-pressure end dominates (i.e., M_f is negative) even for $m = 200$. However, for intermediate and large Knudsen numbers ($K_* = 1$ and 10), the flow induced by the wall-temperature distribution overcomes the pressure-driven flow (i.e., M_f is positive).

2.5 Concluding remarks

In the present study, we considered two fundamental and classical problems of rarefied gas dynamics, Poiseuille flow and thermal transpiration through a circular tube for a polyatomic

Table 2.3: Steady mass-flow rates M_f versus the number of the units m in Case (B).

	$M_f\|_{\mathrm{Pr}=2/3}$			$M_f\|_{\mathrm{Pr}=0.787}$		
m	$K_* = 10$	$K_* = 1$	$K_* = 0.1$	$K_* = 10$	$K_* = 1$	$K_* = 0.1$
10	$-8.080(-2)^*$	$-7.037(-2)$	$-4.451(-1)$	$-8.161(-2)$	$-6.667(-2)$	$-3.875(-1)$
50	$1.096(-2)$	$3.382(-2)$	$-7.268(-2)$	$9.971(-3)$	$3.279(-2)$	$-6.127(-2)$
100	$1.935(-2)$	$4.286(-2)$	$-2.612(-2)$	$1.851(-2)$	$4.133(-2)$	$-2.049(-2)$
200	$2.127(-2)$	$4.439(-2)$	$-2.842(-3)$	$2.055(-2)$	$4.275(-2)$	$-1.082(-4)$

* Read as -8.080×10^{-2}.

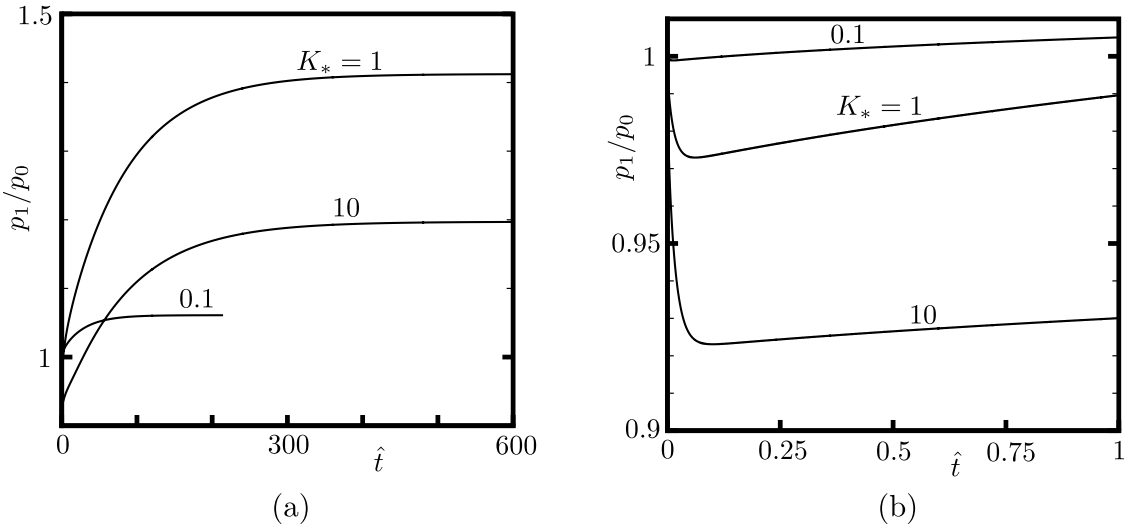

Figure 2.9: Time evolution of the pressure p_1 at the closed end ($X_3 = mL$) in Case (A) for $m = 10, T_1/T_0 = 1.5$, $a = 0.5$, and $R_1/R_0 = 2$. (a) $0 \le \hat{t} \le 600$, (b) $0 \le \hat{t} \le 1$.

gas. Our basic equation is the linearized version of the ES model of the Boltzmann equation for a polyatomic gas. But, we showed that the solution of the thermal transpiration through a circular tube based on the ES model for a polyatomic gas is identical with that based on the BGK model for a monatomic gas, and that the solution of the Poiseuille flow through a circular tube based on the ES model for a polyatomic gas is obtained by a simple conversion formula from that based on the BGK model for a monatomic gas. Therefore, we were able to obtain the profiles of the flow velocity and heat flow as well as the mass-flow rate for the present problem, exploiting the existing database for the BGK model for a monatomic gas (Sec. 2.2).

On the other hand, we derived a macroscopic equation of diffusion type and the connection conditions that describe the pressure distribution in a pipe consisting of many thin circular tubes with different radii connected one after another. The resulting macroscopic system is summarized in Sec. 2.3. With the database for the mass-flow rates mentioned above, the macroscopic system became applicable to practical problems of microscale gas flows when the pipe consists of circular tubes and the behavior of the gas is described by the ES model for a polyatomic gas.

Finally, we applied the macroscopic system to a gas flow through a single long circular tube caused by a large pressure difference imposed at both ends (Sec. 2.4.1) and to a Knudsen compressor consisting of many alternately arranged thinner and thicker circular tubes

(Sec. 2.4.2). With this procedure, we were able to obtain the pressure distribution along the pipe and the mass-flow rate through the pipe in the two problems easily.

It should be stressed that the direct numerical analysis of such problems, either by the DSMC method or by finite-difference methods based on the model Boltzmann equations, is a formidable task. Therefore, the present approach, using the diffusion-type system plus the database for the Poiseuille-flow and thermal-transpiration mass-flow rates, provides a useful and powerful tool. The applicability of the diffusion-type system can be extended easily just by constructing the corresponding database for the tubes with different cross sections.

2.6 Appendix A: ES model of the Boltzmann equation

In this appendix, we summarize the ES model of the Boltzmann equation for a polyatomic gas. Let us consider a gas consisting of molecules with internal degree of freedom δ. The number of the molecules with position in d^3X around $\boldsymbol{X}$, velocity in $d^3\xi$ around $\boldsymbol{\xi}$, and energy related to the internal degree of freedom in $d\widetilde{\mathcal{E}}$ around $\widetilde{\mathcal{E}}$ at time t is written as

$$\frac{1}{m} f(t,\, \boldsymbol{X},\, \boldsymbol{\xi},\, \widetilde{\mathcal{E}}) d^3X d^3\xi d\widetilde{\mathcal{E}}, \tag{2.46}$$

where f is the velocity and energy distribution function of the gas molecules, and m is the mass of a molecule. The ES model for a polyatomic gas can be written in the following form [1] (see the last paragraph of this appendix for the difference in notations between Ref. [1] and the present paper):

$$\frac{\partial f}{\partial t} + \xi_j \frac{\partial f}{\partial X_j} = A_c(T)\rho(\mathcal{G}[f] - f), \tag{2.47a}$$

$$\mathcal{G}[f] = \frac{\rho \Lambda_\delta \widetilde{\mathcal{E}}^{\delta/2-1}}{(2\pi)^{3/2} |\underline{\mathcal{T}}|^{1/2} (\mathcal{R}T_{\rm rel})^{\delta/2}} \times \exp\Big(-\frac{1}{2} {}^t(\boldsymbol{\xi} - \boldsymbol{v}) \cdot \underline{\mathcal{T}}^{-1} \cdot (\boldsymbol{\xi} - \boldsymbol{v}) - \frac{\widetilde{\mathcal{E}}}{\mathcal{R}T_{\rm rel}} \Big), \tag{2.47b}$$

$$\underline{\mathcal{T}} = (1-\eta)\Big[(1-\nu)\mathcal{R}T_{\rm tr}\underline{Id} + \nu\underline{\Theta}\Big] + \eta\mathcal{R}T\underline{Id}, \tag{2.47c}$$

$$\underline{\Theta} = \frac{1}{\rho}\iint_0^\infty (\boldsymbol{\xi} - \boldsymbol{v}) \cdot {}^t(\boldsymbol{\xi} - \boldsymbol{v}) f d\widetilde{\mathcal{E}} d^3\xi, \tag{2.47d}$$

$$\rho = \iint_0^\infty f d\widetilde{\mathcal{E}} d^3\xi, \tag{2.47e}$$

$$v_i = \frac{1}{\rho}\iint_0^\infty \xi_i f d\widetilde{\mathcal{E}} d^3\xi, \tag{2.47f}$$

$$T_{\rm tr} = \frac{1}{3\rho\mathcal{R}}\iint_0^\infty (\xi_i - v_i)^2 f d\widetilde{\mathcal{E}} d^3\xi, \tag{2.47g}$$

$$T_{\rm int} = \frac{2}{\delta\rho\mathcal{R}} \iint_0^\infty \widetilde{\mathcal{E}} f d\widetilde{\mathcal{E}} d^3\xi, \tag{2.47h}$$

$$T = \frac{3T_{\rm tr} + \delta T_{\rm int}}{3+\delta}, \tag{2.47i}$$

$$T_{\rm rel} = \eta T + (1-\eta) T_{\rm int}. \tag{2.47j}$$

Here, ρ is the mass density of the gas, v_i is the flow velocity, T is the temperature, $T_{\rm tr}$ is the temperature related to the translational energy, $T_{\rm int}$ is the temperature related to the energy of the internal degree of freedom, and $\mathcal{R}$ is the specific gas constant (the Boltzmann constant divided by the mass of a molecule); $\nu \in [-1/2, 1)$ and $\eta \in (0, 1]$ are the parameters to adjust the Prandtl number and the bulk viscosity to the gas under consideration [see Eqs. (2.51c) and (2.51d)]; $A_c(T)$ is a function of T such that $A_c(T)\rho$ is the collision frequency of the gas molecules, and Λ_δ is a dimensionless constant defined by

$$\Lambda_\delta^{-1} = \int_0^\infty s^{\delta/2-1} e^{-s} ds. \tag{2.48}$$

In addition, $\underline{\mathcal{I}}$ and $\underline{\Theta}$ are 3×3 symmetric matrices, $\underline{Id}$ is the 3×3 identity matrix, $|\underline{\mathcal{I}}|$ and $\underline{\mathcal{I}}^{-1}$ are the determinant and the inverse matrix of $\underline{\mathcal{I}}$, respectively, and the symbol ^{t} indicates the transpose operation. In what follows, for an arbitrary matrix $\underline{A}$, its (i, j) component, determinant, inverse matrix, and transposed matrix are denoted by A_{ij}, $|\underline{A}|$, $\underline{A}^{-1}$, and ${}^t\underline{A}$, respectively. In the above equations, $d^3\xi = d\xi_1 d\xi_2 d\xi_3$, and the domain of integration with respect to ξ_i is the whole space of ξ_i. It should be noted that the pressure p and the stress tensor p_{ij} are given by

$$p = \rho\mathcal{R}T, \tag{2.49a}$$

$$p_{ij} = \rho\Theta_{ij} = \iint_0^\infty (\xi_i - v_i)(\xi_j - v_j) f d\widetilde{\mathcal{E}} d^3\xi. \tag{2.49b}$$

The vanishing right-hand side of Eq. (2.47a) is equivalent to the fact that f is a local equilibrium distribution $f_{\rm eq}$ [1]:

$$f_{\rm eq} = \frac{\rho\Lambda_\delta}{(2\pi\mathcal{R}T)^{3/2}(\mathcal{R}T)^{\delta/2}} \widetilde{\mathcal{E}}^{\delta/2-1} \exp\Big(-\frac{(\xi_i - v_i)^2}{2\mathcal{R}T} - \frac{\widetilde{\mathcal{E}}}{\mathcal{R}T}\Big). \tag{2.50}$$

It is also known [1] that Eq. (2.47) leads to the viscosity μ, the thermal conductivity κ, the

Prandtl number Pr, and the bulk viscosity μ_b in the following form:

$$\mu = \frac{1}{1-\nu+\eta\nu}\frac{\mathcal{R}T}{A_c(T)}, \tag{2.51a}$$

$$\kappa = \frac{\gamma}{\gamma-1}\mathcal{R}\frac{\mathcal{R}T}{A_c(T)}, \tag{2.51b}$$

$$\mathrm{Pr} = \frac{\gamma}{\gamma-1}\frac{\mathcal{R}\mu}{\kappa} = \frac{1}{1-\nu+\eta\nu}, \tag{2.51c}$$

$$\mu_b = \frac{1}{\eta}\Big(\frac{5}{3}-\gamma\Big)\frac{\mu}{\mathrm{Pr}}, \tag{2.51d}$$

with γ the ratio of the specific heats given by

$$\gamma = \frac{\delta+5}{\delta+3}. \tag{2.52}$$

Equation (2.47) contains the set of parameters (ν, η, δ) characterizing the gas under consideration. In place of this set, we may use another set (Pr, μ_b/μ, δ) because of relations (2.51c), (2.51d), and (2.52).

The molecular mean free path l_0 in an equilibrium state at rest at temperature T_0 and density ρ_0 is defined as

$$l_0 = \frac{2}{\sqrt{\pi}}\frac{(2\mathcal{R}T_0)^{1/2}}{A_c(T_0)\rho_0}, \tag{2.53}$$

in terms of the mean molecular speed $(2/\sqrt{\pi})(2\mathcal{R}T_0)^{1/2}$ and the collision frequency $A_c(T_0)\rho_0$ in the equilibrium state. Therefore, the viscosity μ_0, the thermal conductivity κ_0, and the bulk viscosity μ_{b0} corresponding to the equilibrium state are expressed (in terms of l_0) as

$$\mu_0 = \frac{\sqrt{\pi}}{2}\frac{1}{1-\nu+\eta\nu}\frac{p_0}{(2\mathcal{R}T_0)^{1/2}}l_0, \tag{2.54a}$$

$$\kappa_0 = \frac{\sqrt{\pi}}{2}\frac{\gamma}{\gamma-1}\frac{\mathcal{R}p_0}{(2\mathcal{R}T_0)^{1/2}}l_0, \tag{2.54b}$$

$$\mu_{b0} = \frac{1}{\eta}\Big(\frac{5}{3}-\gamma\Big)\frac{\mu_0}{\mathrm{Pr}}. \tag{2.54c}$$

The diffuse-reflection condition [8,9,32], adapted to the present polyatomic case, on the boundary is expressed as

$$f = \frac{\rho_w\Lambda_\delta}{(2\pi\mathcal{R}T_w)^{3/2}(\mathcal{R}T_w)^{\delta/2}}\widetilde{\mathcal{E}}^{\delta/2-1}\exp\Big(-\frac{\xi_i^2}{2\mathcal{R}T_w}-\frac{\widetilde{\mathcal{E}}}{\mathcal{R}T_w}\Big), \quad (\boldsymbol{\xi}\cdot\boldsymbol{n}>0), \tag{2.55a}$$

$$\rho_w = -\Big(\frac{2\pi}{\mathcal{R}T_w}\Big)^{1/2}\int_{\boldsymbol{\xi}\cdot\boldsymbol{n}<0}\int_0^\infty \boldsymbol{\xi}\cdot\boldsymbol{n} f d\widetilde{\mathcal{E}}d^3\xi, \tag{2.55b}$$

where T_w is the temperature of the boundary, and $\boldsymbol{n}$ is the unit normal vector of the boundary pointed toward the gas.

In Ref. [1], the energy $\widetilde{\mathcal{E}}$, which is denoted by ε there, is assumed to be expressed as $\widetilde{\mathcal{E}} = I^{2/\delta}$ in terms of a variable I, and I is used as an independent variable. More specifically, the distribution function in Ref. [1], which we denote by $\overline{f}(t, \boldsymbol{X}, \boldsymbol{\xi}, I)$ here, is defined in such a way that

$$\frac{1}{m}\overline{f}(t, \boldsymbol{X}, \boldsymbol{\xi}, I) d^3X d^3\xi dI, \tag{2.56}$$

indicates the number of the molecules with position in d^3X around $\boldsymbol{X}$, velocity in $d^3\xi$ around $\boldsymbol{\xi}$, and the variable I in dI around I at time t. Therefore, the relation between $\overline{f}$ and the present f is as follows:

$$f(t, \boldsymbol{X}, \boldsymbol{\xi}, \widetilde{\mathcal{E}}) = (\delta/2)\widetilde{\mathcal{E}}^{\delta/2-1}\overline{f}(t, \boldsymbol{X}, \boldsymbol{\xi}, \widetilde{\mathcal{E}}^{\delta/2}). \tag{2.57}$$

In addition, Λ_δ in Ref. [1], which we denote by $\overline{\Lambda}_\delta$ here, is related to Λ_δ in Eq. (2.48) as

$$\Lambda_\delta^{-1} = (2/\delta)(\overline{\Lambda}_\delta)^{-1}. \tag{2.58}$$

References

1 P. Andries - P. Le Tallec - J.-P. Perlat - B. Perthame, *The Gaussian-BGK model of Boltzmann equation with small Prandtl number*, Eur. J. Mech. B/Fluids, **19** (2000), 813-830.

2 K. Aoki - P. Degond, *Homogenization of a flow in a periodic channel of small section*, Multiscale Model. Simul., **1** (2003), 304-334.

3 K. Aoki - P. Degond - L. Mieussens - M. Nishioka - S. Takata, *Numerical simulation of a Knudsen pump using the effect of curvature of the channel*, in *Rarefied Gas Dynamics*, M. S. Ivanov and A. K. Rebrov eds., Siberian Branch of the Russian Academy of Sciences, Novosibirsk, (2007), 1079-1084.

4 K. Aoki - P. Degond - L. Mieussens - S. Takata - H. Yoshida, *A diffusion model for rarefied flows in curved channels*, Multiscale Model. Simul., **6** (2008), 1281–1316.

5 K. Aoki - P. Degond - S. Takata - H. Yoshida, *Diffusion models for Knudsen compressors*, Phys. Fluids, **19** (2007), 117103.

6 K. Aoki - S. Takata - K. Kugimoto, *Diffusion approximation for the Knudsen compressor composed of circular tubes*, in *Rarefied Gas Dynamics*, T. Abe ed., AIP, Melville, (2009), 953-958.

7 P. L. Bhatnagar - E. P. Gross - M. Krook, *A model for collision processes in gases. I. Small amplitude processes in charged and neutral one-component systems*, Phys. Rev., **94** (1954), 511-525.

8 C. Cercignani, *The Boltzmann Equation and Its Applications*, Springer-Verlag, Berlin (1988).

9 C. Cercignani, *Rarefied Gas Dynamics, From Basic Concepts to Actual Calculations*, Cambridge Univ. Press, Cambridge (2000).

10 C. Cercignani - A. Daneri, *Flow of a rarefied gas between two parallel plates*, J. Appl. Phys., **34** (1963), 3509-3513.

11 C. Cercignani - F. Sernagiotto, *Cylindrical Poiseuille flow of a rarefied gas*, Phys. Fluids, **9** (1966), 40-44.

12 C.-C. Chen - I.-K. Chen - T.-P. Liu - Y. Sone, *Thermal transpiration for the linearized Boltzmann equation*, Commn. Pure Appl. Math., **60** (2007), 0147-0163.

13 P. Degond, *A model of near-wall conductivity and its application to plasma thrusters*, SIAM J. Applied Math., **58** (1998), 1138-1162.

14 P. Degond - V. Latocha - L. Garrigues - J. P. Boeuf, *Electron transport in stationary plasma thrusters*, Transp. Theory and Stat. Phys., **27** (1998), 203-221.

15 S. Fukui - R. Kaneko, *Analysis of ultra-thin gas film lubrication based on linearized Boltzmann equation including thermal creep flow*, J. Tribol., **110** (1988), 253-262.

16 Y. L. Han - M. Young - E. P. Muntz - G. Shiflett, *Knudsen compressor performance at low pressures*, in *Rarefied Gas Dynamics*, M. Capitelli ed., AIP, Melville, (2005), 162-167.

17 M. Hasegawa - Y. Sone, *Poiseuille and thermal transpiration flows of a rarefied gas for various pipes*, J. Vac. Soc. Jpn., **31** (1988), 416-419 (in Japanese).

18 L. H. Holway, Jr., *Approximation procedures for kinetic theory*, Ph.D. Thesis, Harvard University (1963).

19 L. H. Holway, Jr., *New statistical models for kinetic theory: Methods of construction*, Phys. Fluids, **9** (1966), 1658-1673.

20 M. Knudsen, *Eine Revision der Gleichgewichtsbedingung der Gase. Thermische Molekularströmung*, Ann. Phys., **31** (1910), 205-229.

21 M. Knudsen, *Thermischer Molekulardruck der Gase in Röhren*, Ann. Phys., **33** (1910), 1435-1448.

22 S. K. Loyalka, *Thermal transpiration in a cylindrical tube*, Phys. Fluids, **12** (1969), 2301-2305.

23 S. K. Loyalka - T. S. Storvick - H. S. Park, *Poiseuille flow and thermal creep flow in long, rectangular channels in the molecular and transition flow regimes*, J. Vac. Sci. Technol., **13** (1976), 1188-1192.

24 L. Marino, *Experiments on rarefied gas flows through tubes*, Microfluid Nanofluid, **6** (2009), 109-119.

25 National Institutes of Natural Sciences and National Astronomical Observatory of Japan (eds.), *Chronological Scientific Tables*, Maruzen, Tokyo, (1994) (in Japanese).

26 H. Niimi, *Thermal creep flow of rarefied gas between two parallel plates*, J. Phys. Soc. Jpn., **30** (1971), 572-574.

27 T. Ohwada - Y. Sone - K. Aoki, *Numerical analysis of the Poiseuille and thermal transpiration flows between two parallel plates on the basis of the Boltzmann equation for hard-sphere molecules*, Phys. Fluids A, **1** (1989), 2042-2049.

28 G. J. Prangsma - A. H. Alberga - J. J. M. Beenakker, *Ultrasonic determination of the volume viscosity of* N_2*,* CO*,* CH_4 *and* CD_4 *between 77 and 300 K*, Physica, **64** (1973), 278-288.

29 F. Sharipov - G. Bertoldo, *Poiseuille flow and thermal creep based on the Boltzmann equation with the Lennard–Jones potential over a wide range of the Knudsen number*, Phys. Fluids, **21** (2009), 067101.

30 F. Sharipov - V. Seleznev, *Data on internal rarefied gas flows*, J. Phys. Chem. Ref. Data, **27** (1998), 657-706.

31 C. E. Siewert, *The linearized Boltzmann equation: Concise and accurate solutions to basic flow problems*, Z. angew. Math. Phys., **54** (2003), 273-303.

32 Y. Sone, *Molecular Gas Dynamics: Theory, Techniques, and Applications*, Birkhäuser, Boston (2007).

33 Y. Sone - E. Itakura, *Analysis of Poiseuille and thermal transpiration flows for arbitrary Knudsen numbers by a modified Knudsen number expansion and their database*, J. Vac. Soc. Jpn., **33** (1990), 92-94 (in Japanese).

34 Y. Sone - K. Sato, *Demonstration of a one-way flow of a rarefied gas induced through a pipe without average pressure and temperature gradients*, Phys. Fluids, **12** (2000), 1864-1868.

35 Y. Sone - H. Sugimoto, *Vacuum pump without a moving part and its performance*, in *Rarefied Gas Dynamics*, A. Ketsdever and E. P. Muntz eds., AIP, Melville, (2003), 1041-1048.

36 Y. Sone - Y. Waniguchi - K. Aoki, *One-way flow of a rarefied gas induced in a channel with a periodic temperature distribution*, Phys. Fluids, **8** (1996), 2227-2235.

37 Y. Sone - K. Yamamoto, *Flow of rarefied gas through a circular pipe*, Phys. Fluids, **11** (1968), 1672-1678.

38 H. Sugimoto - Y. Sone, *Vacuum pump without a moving part driven by thermal edge flow*, in *Rarefied Gas Dynamics*, M. Capitelli ed., AIP, Melville, (2005), 168-173.

39 S. Takata - H. Funagane - K. Aoki, *Fluid modeling for the Knudsen compressor: Case of polyatomic gases*, Kinetic and Related Models, **3** (2010), 353-372.

40 S. Takata - H. Sugimoto - S. Kosuge, *Gas separation by means of the Knudsen compressor*, Eur. J. Mech. B/Fluids, **26** (2007), 155-181.

41 S. E. Vargo - E. P. Muntz, *An evaluation of a multiple-stage micromechanical Knudsen compressor and vacuum pump*, in *Rarefied Gas Dynamics*, C. Shen ed., Peking University Press, Peking, (1997), 995-1000.

42 P. Welander, *On the temperature jump in a rarefied gas*, Ark. Fys., **7** (1954), 507-553.

Chapter 3

Poiseuille and thermal transpiration flows of a highly rarefied gas: over-concentration in the velocity distribution function

3.1 Introduction

Poiseuille and thermal transpiration flows are among the most fundamental problems in rarefied gas dynamics or in microfluidics and have been investigated by many researchers. At the early stage of the modern rarefied gas dynamics, analyses were made by the use of arbitrary assumptions on the velocity distribution function, such as the variational and moment methods. Direct numerical computations were also carried out, first on the basis of the model equations, such as the Bhatnagar–Gross–Krook (BGK or Boltzmann–Krook–Welander) model [2,30], and then of the original Boltzmann equation. An exhaustive list of references is beyond the scope of the present paper. The reader is referred to, e.g., [7] and [26] and the references therein for the background and representative results. Some references rather directly related to the present work will be cited at proper occasions.

In the present paper we come back to the above classical problems, especially those in the two-dimensional channel, because there occurs an interesting phenomenon of the over-concentration of molecules on velocities parallel to the walls in the highly rarefied regime (see figures 3 and 6 in [23]). We shall focus on this issue and clarify its structure. We also propose a numerical method that handles the difficulty arising from this phenomenon. The method enables us to obtain the net mass flow through the channel in that regime accurately. For the linearized Boltzmann equation, an accurate deterministic numerical method was established in late 1980s ([27]) for the intermediate rarefied regime, and there is a general asymptotic theory for the slightly rarefied regime ([24,25]). Thus, the proposed method fills the last gap for preparing the database of net mass flow that covers the entire range of the Knudsen number Kn, i.e. from the continuum to the free molecular regime.

In the case of the two-dimensional channel, the flows in the highly rarefied regime have

been studied analytically by [5] for the Poiseuille flow and by [22] for the thermal transpiration on the basis of the BGK equation. They reported that the net mass flow grows logarithmically in Kn (Kn $\gg 1$) as Kn is increased. In the analyses, they used an advantageous property of the model equation that the basic equation and its boundary condition can be reduced to a set of integral equations for macroscopic quantities. The same reduction can be applied to more sophisticated model equations such as the ellipsoidal statistical model [11,12,1] and the McCormack model for gas mixtures [18]. It cannot, however, be applied to the original Boltzmann equation. As a result, analyses of the flows in the highly rarefied regime on the basis of the Boltzmann equation have not been carried out for a long time, though the logarithmic growth in Kn has been expected.

Recently, [9] studied the thermal transpiration in the highly rarefied regime on the basis of the linearized Boltzmann equation for hard-sphere (HS) molecules and proved rigorously mathematically the logarithmic growth of the induced mass flow. They introduced a pointwise estimate of the velocity distribution function in addition to the norm estimates that are widely used in mathematical studies of the Boltzmann equation. The pointwise estimate plays a key role in the proof of logarithmic growth. In the present paper, motivated by their result, we construct an iterative approximation method and clarify the behaviour of the gas in the highly rarefied regime for both the Poiseuille flow and thermal transpiration problems. The method is rather ordinary, but we will ensure its convergence and estimate the order of error at each stage of iteration explicitly. Consequently, we will have a clear view of practical numerical analyses, by which the structure of the over-concentration will be clarified.

The paper is organized as follows. We start from the statement and formulation of the problems in § 3.2 and summarize the mathematical estimates by [9] in § 3.3. Then in § 3.4.1 we present an iterative approximation procedure and show its convergence and explicit error estimates at each stage of iteration in the highly rarefied regime. In § 3.4.2, we clarify the structure of the over-concentration on the basis of § 3.4.1. In § 3.4.3, we present the actual numerical method to be adopted that is based on the procedure in § 3.4.1. Numerical results are shown in § 3.5. Finally in § 3.6 we present an asymptotic formula of the net mass flow through the channel for large Kn, which is available not only for HS molecules but also for any molecular model belonging to Grad's hard potential [10]. We will also point out that the profiles of the heat flow in Poiseuille flow and of the flow velocity in thermal transpiration

agree well with each other in the highly rarefied regime. The reason is also given.

3.2 Problem and formulation

Consider a rarefied gas between two parallel resting plates located respectively at $X_1 = \pm D/2$ ($D > 0$), where X_i are the Cartesian coordinates. The two plates are kept at the temperature $T_0(1 + \beta_T X_2/D)$ (β_T is a constant), and a uniform pressure gradient is imposed on the gas in the direction of X_2; i.e. the pressure is given by $p_0(1 + \beta_P X_2/D)$. (It can be shown that the pressure is independent of X_1.) We will investigate the behaviour of the gas under the following assumptions:

(i) The behaviour of the gas can be described by the Boltzmann equation for hard-sphere molecules with a common diameter σ and mass m. (The restriction to HS molecules will be relaxed later in § 3.6.1.)

(ii) The gas molecules are diffusely reflected on the surface of the plates.

(iii) $|\beta_T|$, $|\beta_P| \ll 1$, so that the equation and boundary condition can be linearized around the reference equilibrium state at rest with temperature T_0 and pressure p_0.

Usually, the above problem with $\beta_T = 0$ (the case that the plate temperature is uniform) is called the Poiseuille flow problem, while that with $\beta_P = 0$ (the case of no pressure gradient) is called the thermal transpiration problem. We call the gap between the plates occupied by the gas the (two-dimensional) channel. It is known that a flow is induced along the channel in both problems.

Let us denote the molecular velocity by $(2RT_0)^{1/2}\boldsymbol{\zeta}$ and the velocity distribution function by $\rho_0(2RT_0)^{-3/2}[1 + \phi(\boldsymbol{x}, \boldsymbol{\zeta})]E(|\boldsymbol{\zeta}|)$, where $\boldsymbol{x} = \boldsymbol{X}/D$, $E(t) = \pi^{-3/2}\exp(-t^2)$, $\rho_0 = p_0/RT_0$ and R is the specific gas constant. Then, the problem is described by the following boundary-value problem for ϕ:

$$\zeta_i \frac{\partial \phi}{\partial x_i} = -\frac{\nu}{k}\phi + \frac{1}{k}K(\phi), \tag{3.1}$$

$$\phi = (|\boldsymbol{\zeta}|^2 - 2)\beta_T x_2 \pm 2\sqrt{\pi}\int_{\zeta_1 \gtrless 0} \zeta_1 \phi E \mathrm{d}\boldsymbol{\zeta}, \qquad \text{for } \zeta_1 \lessgtr 0,\ x_1 = \pm\frac{1}{2}, \tag{3.2}$$

where

$$K(\phi) = \int \kappa(\boldsymbol{\zeta}_*, \boldsymbol{\zeta})\phi(\boldsymbol{\zeta}_*)E(|\boldsymbol{\zeta}_*|)\mathrm{d}\boldsymbol{\zeta}_*, \tag{3.3}$$

$$\kappa(\boldsymbol{\zeta}_*, \boldsymbol{\zeta}) = \frac{\sqrt{\pi}}{\sqrt{2}}\frac{1}{|\boldsymbol{\zeta} - \boldsymbol{\zeta}_*|}\exp\left(\frac{|\boldsymbol{\zeta}_* \times \boldsymbol{\zeta}|^2}{|\boldsymbol{\zeta}_* - \boldsymbol{\zeta}|^2}\right) - \frac{\sqrt{\pi}}{2\sqrt{2}}|\boldsymbol{\zeta} - \boldsymbol{\zeta}_*|, \tag{3.4}$$

$$\nu(|\boldsymbol{\zeta}|) = \frac{1}{2\sqrt{2}}\left[\exp(-|\boldsymbol{\zeta}|^2) + \left(2|\boldsymbol{\zeta}| + \frac{1}{|\boldsymbol{\zeta}|}\right)\int_0^{|\boldsymbol{\zeta}|}\exp(-s^2)\mathrm{d}s\right], \tag{3.5}$$

$$k = \frac{\sqrt{\pi}}{2}\frac{\ell_0}{D}, \quad \ell_0 = \frac{1}{\sqrt{2}\pi\sigma^2(\rho_0/m)}, \tag{3.6}$$

and ℓ_0 is the mean free path of a gas molecule at the reference equilibrium state. Note that we shall use k in place of the Knudsen number $\mathrm{Kn}(= \ell_0/D)$ to indicate the degree of gas rarefaction (see (3.6)). The above ϕ should be consistent with the imposed pressure field $p_0(1 + \beta_P X_2/D)$, which is reduced to the following condition:

$$\frac{2}{3}\int |\boldsymbol{\zeta}|^2\phi E\mathrm{d}\boldsymbol{\zeta} = \beta_P x_2. \tag{3.7}$$

Since the problem is linear, we can seek the solution ϕ, independent of x_3, in the form

$$\phi = \beta_P[x_2 + \phi_P(x_1, \boldsymbol{\zeta})] + \beta_T[(|\boldsymbol{\zeta}|^2 - \frac{5}{2})x_2 + \phi_T(x_1, \boldsymbol{\zeta})], \tag{3.8}$$

where $\phi_J(x_1, \boldsymbol{\zeta})$ $(J = P, T)$ is a solution of the following boundary-value problem:

$$\zeta_1\frac{\partial\phi_J}{\partial x_1} = -\frac{\nu}{k}\phi_J + \frac{1}{k}K(\phi_J) - I_J \quad (J = P, T), \tag{3.9a}$$

$$\phi_J = 0, \qquad \text{for } \zeta_1 \lessgtr 0,\ x_1 = \pm\frac{1}{2}, \tag{3.9b}$$

$$I_P = \zeta_2, \quad I_T = \zeta_2(|\boldsymbol{\zeta}|^2 - \frac{5}{2}). \tag{3.9c}$$

Throughout this paper, the subscript J represents the problem indicator P or T: the former indicates the Poiseuille flow and the latter the thermal transpiration. Here ϕ_J is considered to be odd in ζ_2, even in ζ_3 and symmetric in the following sense:

$$\phi_J(x_1, \zeta_1, \zeta_2, \zeta_3) = \phi_J(-x_1, -\zeta_1, \zeta_2, \zeta_3). \tag{3.10}$$

Macroscopic quantities can be obtained once ϕ is known. Because of (3.8), the density, temperature, pressure and stress tensor of the gas are simply expressed as $\rho_0[1+(\beta_P-\beta_T)x_2]$, $T_0(1 + \beta_T x_2)$, $p_0(1 + \beta_P x_2)$ and

$$p_0(1 + \beta_P x_2)\mathbf{I} - p_0\beta_P x_1\begin{bmatrix} 0 & 1 & 0 \\ 1 & 0 & 0 \\ 0 & 0 & 0 \end{bmatrix}, \qquad (\mathbf{I}\text{: the identity matrix}), \tag{3.11}$$

while the flow velocity $(2RT_0)^{1/2}\boldsymbol{u}$ and the heat flow vector $\frac{1}{2}\rho_0(2RT_0)^{3/2}\boldsymbol{Q}$ have their x_2-components only, which are expressed as a moment of ϕ as follows:

$$u_2 = \int \zeta_2 \phi E \mathrm{d}\boldsymbol{\zeta}, \quad Q_2 = \int \zeta_2 (|\boldsymbol{\zeta}|^2 - \frac{5}{2}) \phi E \mathrm{d}\boldsymbol{\zeta}. \tag{3.12}$$

For the sake of later convenience, we introduce the notation convention that

$$u[f] = \int \zeta_2 f E \mathrm{d}\boldsymbol{\zeta}, \quad Q[f] = \int \zeta_2 (|\boldsymbol{\zeta}|^2 - \frac{5}{2}) f E \mathrm{d}\boldsymbol{\zeta}, \quad M[f] = \int_{-1/2}^{1/2} u[f] \mathrm{d}x_1. \tag{3.13}$$

Then, u_2 and Q_2 may be rewritten by $u_2 = u[\phi] = \beta_P u[\phi_P] + \beta_T u[\phi_T]$ and $Q_2 = Q[\phi] = \beta_P Q[\phi_P] + \beta_T Q[\phi_T]$. The net mass flow through the channel per unit length in X_3 is expressed by $\rho_0 D(2RT_0)^{1/2} M[\phi]$, where $M[\phi] = \beta_P M[\phi_P] + \beta_T M[\phi_T]$.

3.3 Preliminary arguments

The problem (3.9) can be solved formally as

$$\phi_J = \phi_J^{(0)} + \phi_J^R, \tag{3.14a}$$

$$\phi_J^{(0)} = -\frac{k}{\nu}\left[1 - \exp\left(-\frac{\nu}{k}\frac{|x_1 \pm (1/2)|}{|\zeta_1|}\right)\right] I_J, \quad \zeta_1 \gtrless 0, \tag{3.14b}$$

$$\phi_J^R = \frac{1}{k\zeta_1}\int_{\mp 1/2}^{x_1} \exp\left(-\frac{\nu}{k}\frac{|s - x_1|}{|\zeta_1|}\right) K(\phi_J) \mathrm{d}s, \quad \zeta_1 \gtrless 0. \tag{3.14c}$$

In accordance with (3.14a), u, M and Q may be written as

$$u[\phi_J] = u[\phi_J^{(0)}] + u[\phi_J^R], \quad M[\phi_J] = M[\phi_J^{(0)}] + M[\phi_J^R], \quad Q[\phi_J] = Q[\phi_J^{(0)}] + Q[\phi_J^R]. \tag{3.15}$$

We primarily discuss the former two quantities; Q will be considered in § 3.6.2.

Chen *et al.* [9] studied the thermal transpiration problem ϕ_T by the use of the formal solution (3.14) and proved mathematically the following for $k \gg 1$:

(i) There is a unique solution $\phi_T \in L^\infty$, where L^∞ is defined with the norm $\|f\|_\infty = \sup_{\boldsymbol{\zeta}} |f| E^{1/2}$ for each x_1.

(ii) There is a constant $C > 0$ independent of k such that

$$|\phi_T E^{1/2}| \le C\left(|\zeta_1| + \frac{1}{k}\right)^{-1}, \qquad |K(\phi_T) E^{1/2}| \le C(1 + \ln k). \tag{3.16}$$

(iii) There are constants $C_2 \ge C_1 > 0$ and $C_3 > 0$ independent of k such that

$$C_1 \ln k \le u[\phi_T^{(0)}] \le C_2 \ln k, \qquad |u[\phi_T^R]| < C_3 (1 + \ln k)^2 / k. \tag{3.17}$$

The last estimate (3.17) implies that in the highly rarefied regime the flow $u[\phi_T^{(0)}]$ induced by the known inhomogeneous term corresponding to the temperature gradient is predominant, and the contribution of the remainder $u[\phi_T^R]$ is much smaller than $u[\phi_T^{(0)}]$, i.e. $O(k^{-1}\ln k)$ relative to $u[\phi_T^{(0)}]$. Since (3.17) is a uniform estimate in x_1, $M[\phi_T^R]$ and $M[\phi_T^{(0)}]$ follow the same estimate as (3.17).

By the analysis parallel to that of [9], we can show for the Poiseuille flow problem that the statements (i) and (ii) with ϕ_T being replaced by ϕ_P hold as they are and that (iii) is replaced by the following:

(iii)$'$ There are constants $C_2 \geq C_1 > 0$ and $C_3 > 0$ independent of k such that

$$-C_1 \ln k \geq u[\phi_P^{(0)}] \geq -C_2 \ln k, \qquad |u[\phi_P^R]| < C_3(1+\ln k)^2/k \tag{3.18}$$

(see Sec. 3.8). Again, because of the uniform estimate in x_1, $M[\phi_P^R]$ and $M[\phi_P^{(0)}]$ follow the same estimate as (3.18).

Remark 1 *One may think that dropping the first two terms on the right-hand side of* (3.9a) *would give a reasonable approximation in the highly rarefied regime. It, however, leads to the divergence of flow velocity, which has been known for a long time. Physically, the divergence is caused by completely neglecting the scattering of molecules with a velocity parallel to the walls ($\zeta_1 = 0$). In the dominant part $\phi_J^{(0)}$ of the solution, the effect of such a scattering is partially included (only the term $K(\phi_J)/k$ is dropped from* (3.9a)*), which prevents the divergence for every fixed k and captures the asymptotic behaviour as $k \to \infty$. See, e.g., [6] and [26] for related discussions.*

Figure 3.1 shows $M[\phi_J^{(0)}]$, the expression of which is eventually reduced to (3.24) that appears later. The direct numerical solution of $M[\phi_J]$ by Ohwada *et al.* [23] is also shown for comparison. The relative error of $M[\phi_T^{(0)}]$ to $M[\phi_T]$ is less than 17%, 13% and 11% for $k = 10$, 15 and 20, while that of $M[\phi_P^{(0)}]$ to $M[\phi_P]$ is less than 19%, 15% and 12% for $k = 10$, 15 and 20. Thus, it is strongly suggested that the use of $\phi_J^{(0)}$ as the initial guess is effective for an iterative solution method in the highly rarefied regime.

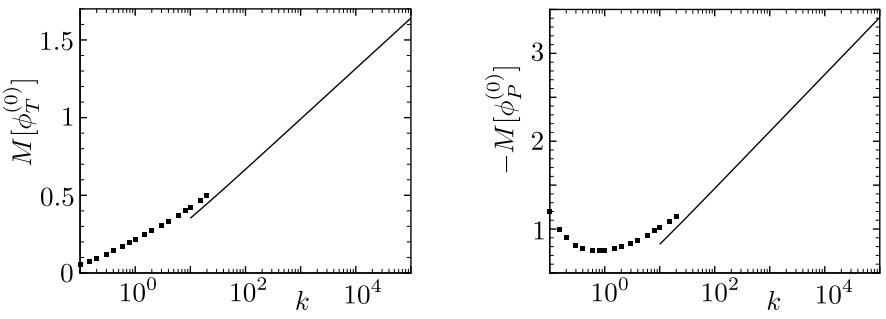

(a) (b)

Figure 3.1: $M[\phi_J^{(0)}]$ for large Knudsen numbers. (a) $M[\phi_T^{(0)}]$ versus k and (b) $M[\phi_P^{(0)}]$ versus k. In each panel, $M[\phi_J^{(0)}]$ is shown by a solid line. Numerical results of $M[\phi_J]$ by Ohwada *et al.* [23] for intermediate Knudsen numbers are also shown for comparison by the closed symbols.

3.4 Structure of the over-concentration and solution method

3.4.1 Iterative approximation: method and error estimate

Motivated by the result shown in figure 3.1, we consider a sequence of functions $\phi_J^{(0)}$, $\phi_J^{(1)}$, $\phi_J^{(2)}, \dots$ generated by the following procedure:

$$\phi_J^{(n)} = \phi_J^{(0)} + \int_{\mp 1/2}^{x_1} \frac{1}{k\zeta_1} \exp\Big(-\frac{\nu}{k}\frac{|s-x_1|}{|\zeta_1|}\Big) K(\phi_J^{(n-1)}) \mathrm{d}s, \quad \zeta_1 \gtrless 0, \quad (n = 1, 2, \dots). \tag{3.19}$$

By using both the norm and pointwise estimates following [9], we can prove the following for $k \gg 1$ (see Sec. 3.8):

(*a*) $\{\phi_J^{(n)}\}$ is a Cauchy sequence in L^∞ and thus has a limit in L^∞. Further, this limiting function is a solution of (3.14): $\phi_J = \lim_{n\to\infty} \phi_J^{(n)}$.

(*b*) By introducing $\psi_J^{(0)} = \phi_J^{(0)}$ and $\psi_J^{(n)} = \phi_J^{(n)} - \phi_J^{(n-1)}$ $(n = 1, 2, \dots)$, $\phi_J^{(n)}$ is rewritten as $\phi_J^{(n)} = \sum_{i=0}^{n} \psi_J^{(i)}$. In order to have the sequence $\{\phi_J^{(n)}\}$, we may use the following generating procedure for $\{\psi_J^{(n)}\}$ in place of (3.19):

$$\psi_J^{(n)} = \int_{\mp 1/2}^{x_1} \frac{1}{k\zeta_1} \exp\Big(-\frac{\nu}{k}\frac{|s-x_1|}{|\zeta_1|}\Big) K(\psi_J^{(n-1)}) \mathrm{d}s, \quad \zeta_1 \gtrless 0. \tag{3.20}$$

Then there are positive constants C_0 and C_1 independent of k such that

$$|\psi_J^{(i)} E^{1/2}| \le C_0(|\zeta_1| + k^{-1})^{-1}[C_1 k^{-1}(\ln k + 1)]^i, \tag{3.21a}$$

$$\|\psi_J^{(i)}\|_\infty \le C_0 k\,[C_1 k^{-1}(\ln k+1)]^i, \tag{3.21b}$$

$$|K(\psi_J^{(i)})E^{1/2}| \le C_0(\ln k+1)\,[C_1 k^{-1}(\ln k+1)]^i, \tag{3.21c}$$

where $i = 0, 1, 2, \ldots$. Thus the error of $\phi_J^{(i)}E^{1/2}$ is $O(k^{-i}(1+\ln k)^{i+1})$.

(c) There are positive constants C_0 and C_1 independent of k such that

$$|u[\psi_J^{(i)}]|,\ |M[\psi_J^{(i)}]| \le C_0[C_1 k^{-1}(\ln k+1)]^i(\ln k+1). \tag{3.22}$$

Remark 2 *Equation* (3.19) *or* (3.20) *is a rather common iterative approximation procedure. Here the point is that we can prove* (a)–(c) *in the present problems, which have not been known so far. Incidentally, the above convergence rates* (3.21a) *and* (3.22) *of the sequences are faster than those suggested in remark 4.4 of [9]. This is because we make use of* (3.21c) *at each stage of iteration in the estimate (see Sec. 3.8).*

3.4.2 Structure of over-concentration

Estimate (3.21a) clearly shows the structure of the over-concentration of molecules on $\zeta_1 \sim 0$. Further, $\phi_J^{(0)}E^{1/2}$ (or $\psi_J^{(0)}E^{1/2}$) has a peak $O(k)$ around $\zeta_1 = 0$, remains $O(k)$ for $|\zeta_1| = O(k^{-1})$ and decreases down to $O(1)$ for $|\zeta_1| \sim 1$. As a result, its L^∞ norm, which picks up the peak value, is $O(k)$, while its averages such as $u[\phi_J^{(0)}]$ and $M[\phi_J^{(0)}]$ are smaller quantities $O(\ln k+1)$. At each stage of iteration, $\psi_J^{(n)}E^{1/2}$ is scaled down by the factor $O(k^{-1}(\ln k+1))$ with the peak position essentially unchanged.

In summary, the over-concentration in the highly rarefied regime occurs in the range of $|\zeta_1| = O(k^{-1})$. This phenomenon should be captured correctly by taking into account the first correction $\psi_J^{(1)}$ to the initial guess $\phi_J^{(0)}$ in the present iterative procedure, because $\psi_J^{(2)}E^{1/2}$ and higher-order corrections decrease with the rate $O(k^{-1}(\ln k+1)^2)$ as k increased, as is clear from the above estimates. The feature is schematically shown in figure 3.2. Strictly speaking, estimate (3.21a) is not necessarily optimal, so that the actual peak and the range of over-concentration may be smaller and thinner than estimated. However, figure 3.3 and the data to be shown in § 3.5, which we obtained numerically, demonstrate that the estimate is actually optimal.

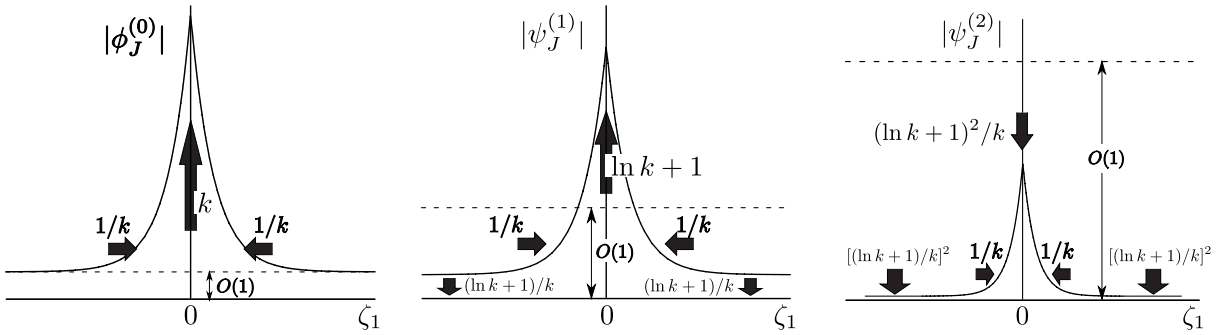

(a) (b) (c)

Figure 3.2: Change of (a) $\phi_J^{(0)}$, (b) $\psi_J^{(1)}$ and (c) $\psi_J^{(2)}$ for small $|\zeta_1|$ as k is increased ($k \gg 1$). In each panel, the rate and the direction of change when k is increased are shown.

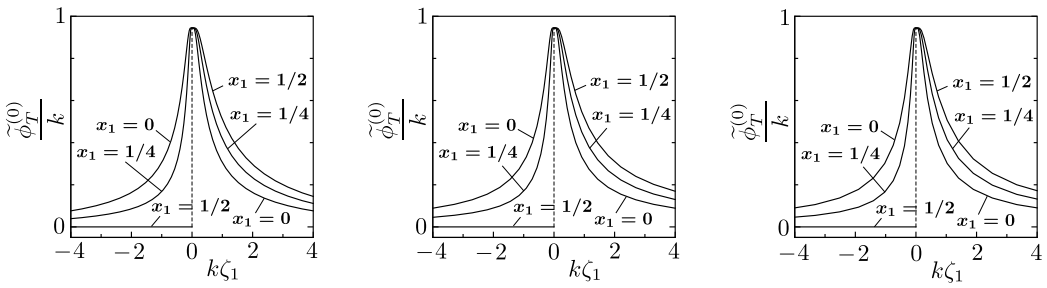

(a) (b) (c)

Figure 3.3: $\widetilde{\phi}_T^{(0)}/k$ versus $k\zeta_1$ at $\zeta_\rho = 0.611$ on three spatial points ($x_1 = 0$, 1/4 and 1/2), where $\zeta_\rho = (|\boldsymbol{\zeta}|^2 - \zeta_1^2)^{1/2}$. (a) $k = 10$, (b) $k = 10^2$ and (c) $k = 10^3$. Here, $\widetilde{\phi}_T^{(0)} \equiv \phi_T^{(0)} E^{1/2}/\zeta_2$ is a function of x_1, ζ_1 and ζ_ρ.

3.4.3 Overview of computational method

Most plainly, a straightforward iterative finite-difference scheme would be used for numerical computation, especially for intermediate Knudsen numbers. The scheme is obtained by discretizing in both x_1 and $\boldsymbol{\zeta}$ the following equation arising from (3.9):

$$\zeta_1 \frac{\partial \phi_J^{(n)}}{\partial x_1} = -\frac{\nu}{k}\phi_J^{(n)} + \frac{1}{k}K(\phi_J^{(n-1)}) - I_J, \tag{3.23a}$$

$$\phi_J^{(n)} = 0, \qquad \text{for } \zeta_1 \lessgtr 0,\ x_1 = \pm\frac{1}{2}. \tag{3.23b}$$

Equation (3.19), which was the basis of the discussion of § 3.4.2, is also obtained by analytical integration of (3.23) with respect to x_1. Thus, the sequence of functions $\phi_J^{(0)}, \phi_J^{(1)}, \dots$ generated by (3.19) is identical to that generated by (3.23) with $\phi_J^{(-1)} = 0$. Thus, the finite-difference scheme that is based on (3.23) should converge also with the rate $O(k^{-1}(\ln k + 1))$ in the highly rarefied regime, which actually gives a numerical solution in that regime only by several (or even a few) iterations. Nevertheless, the straightforward finite-difference approach will be faced with a difficulty. The difficulty lies in the discretization. As described before, $M[\phi_J]$ is a quantity $O(\ln k)$ (see (3.17) and (3.18)). The contribution from the region in ζ_1 where ϕ_J decreases down from $O(k)$ to $O(1)$ is $O(\ln k)$, while the contribution from the remaining region is $O(1)$ (see (3.16)). Thus, a well-balanced arrangement of grid points both to the thin over-concentration part and to the remaining part is required, which becomes difficult to realize for large k, especially when the knowledge in § 3.4.2 is lacking. (Note that, in practice, $\ln k$ is not so different from 1 when k is large. Compare 1, $\ln k$ and k when $k = 10^3$.)

Because of the above observation, we carry out the numerical computations in the following way. Here the main concern is the net mass flow $M[\phi_J]$. We first calculate the zeroth and first approximations, which are responsible for the over-concentration, analytically as much as possible. In this step, thanks to the simple form of $\phi_J^{(0)}$ (see (3.14b)), $M[\phi_J^{(0)}]$ is eventually reduced to

$$M[\phi_J^{(0)}] = \frac{1}{\sqrt{\pi}}\int_0^\infty \Bigg[\Big(1 - \frac{a^2}{12k^2}\Big)\mathrm{Ei}\Big(-\frac{a}{k}\Big) + \frac{1}{12}\Big(1 - \frac{a}{k}\Big)\mathrm{e}^{-\frac{a}{k}} - \frac{1}{2}\frac{k}{a}\Big\{1 + \Big(\frac{5}{3} - \frac{k}{a}\Big)(1 - \mathrm{e}^{-\frac{a}{k}})\Big\}\Bigg] t^3 \tilde{I}_J \mathrm{e}^{-t^2}\mathrm{d}t, \tag{3.24}$$

where Ei is the exponential integral defined by $\mathrm{Ei}(-x) = -\int_x^\infty t^{-1}\exp(-t)\mathrm{d}t$ $(x > 0)$ and

$$a = \frac{\nu(t)}{t}, \quad \tilde{I}_P = 1, \quad \tilde{I}_T = \Big(t^2 - \frac{5}{2}\Big). \tag{3.25}$$

The remaining integration with respect to t is easily performed numerically. The results shown in figure 3.1 are thus obtained. For $n \geq 1$, $\psi_J^{(n)}$ is expressed by (3.20). The corresponding net mass flow is expressed as

$$M[\psi_J^{(n)}] = 2\int_{-1/2}^{1/2}\int_{\zeta_1>0} \frac{\zeta_2}{\nu}\Big(1 - \exp\Big(-\frac{\nu}{k}\frac{(1/2)-s}{\zeta_1}\Big)\Big)K(\psi_J^{(n-1)})E(|\boldsymbol{\zeta}|)\mathrm{d}\boldsymbol{\zeta}\mathrm{d}s, \tag{3.26}$$

because the integration with respect to x_1 from $-1/2$ to $1/2$ can be performed analytically after changing the order of integration. As to $\psi_J^{(1)}$ and $M[\psi_J^{(1)}]$, the integration with respect to s and a part of the others can be performed analytically, thanks to the simple form of $\phi_J^{(0)}$ (see (3.14b)). As a result, (3.20) and (3.26) are eventually reduced to three- and fivefold integrations of a given function respectively. These integrations are performed numerically by first applying the double exponential transformation [28,20,19] and then using the trapezoid formula for transformed variables.

By the method in the previous paragraph, we can deal with the over-concentration and its contribution to the net mass flow accurately. In the extremely highly rarefied regime, the first (or even zeroth) approximation is accurate enough, thanks to the convergence rate $O(k^{-1}(\ln k + 1))$ in one iteration. Further iterations are required only in the regime close to the intermediate rarefied regime. The required number of iterations increases as k is decreased, because the convergence rate $O(k^{-1}(\ln k + 1))$ becomes worse. Fortunately, however, we do not expect a serious numerical difficulty in that regime, because the range of the over-concentration in ζ_1, which is $O(k^{-1})$, is no longer too thin. The main technical problem in solving $\psi_J^{(2)}$ and higher-order corrections is that only the discretized data of $\psi_J^{(n-1)}$ are available in (3.20) and (3.26) and that the integration with respect to s cannot be carried out analytically. The integration with respect to $\boldsymbol{\zeta}$ is performed by using the trapezoid formula after the double exponential transformation. As to the integration with respect to s, $K(\psi_J^{(n-1)})$ is approximated by the piecewise quadratic interpolation of the data on grid points. Then the integration of the approximated $K(\psi_J^{(n-1)})$ multiplied by $1-\exp(-\nu((1/2)-s)/(k\zeta_1))$ in (3.26) or $\exp(-\nu|s-x_1|/(k|\zeta_1|))$ in (3.20) is carried out analytically. In the actual numerical computations, we seek $\psi_J^{(n)}(x_1, \boldsymbol{\zeta})$ in the form of $(\zeta_2/\zeta_\rho)\Psi_J^{(n)}(x_1, \zeta_1, \zeta_\rho)$ $(\zeta_\rho = \sqrt{|\boldsymbol{\zeta}|^2 - \zeta_1^2}$),

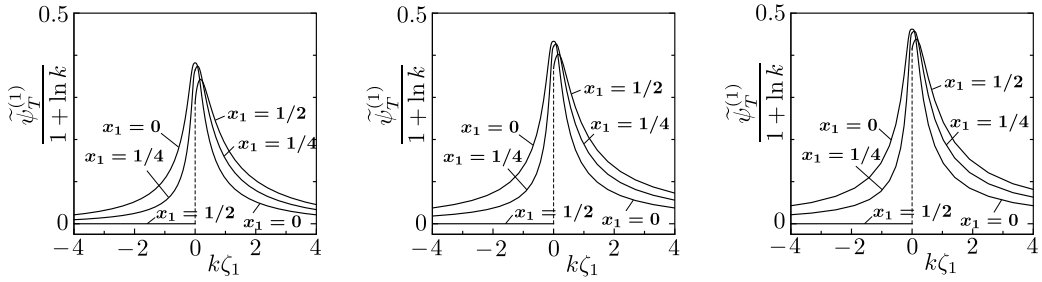

(a) (b) (c)

Figure 3.4: $\widetilde{\psi}_T^{(1)}/(1+\ln k)$ versus $k\zeta_1$ at $\zeta_\rho = 0.611$ $[\zeta_\rho = (|\boldsymbol{\zeta}|^2 - \zeta_1^2)^{1/2}]$ on three spatial points ($x_1 = 0$, 1/4 and 1/2), where $\widetilde{\psi}_T^{(1)} \equiv \psi_T^{(1)} E^{1/2}/\zeta_2$ is a function of x_1, ζ_1 and ζ_ρ. (a) $k = 10$, (b) $k = 10^2$ and (c) $k = 10^3$.

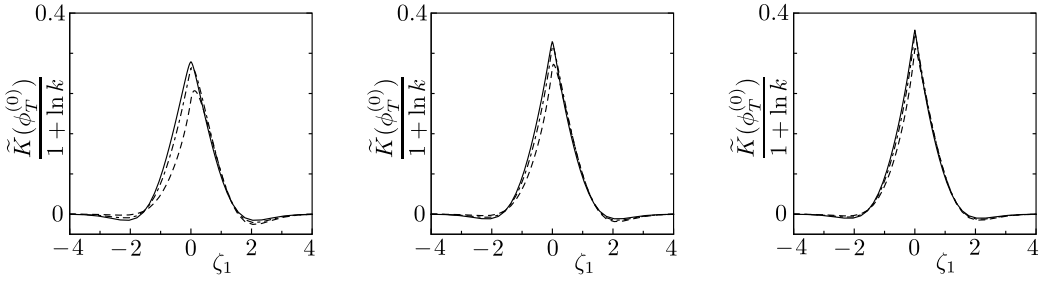

(a) (b) (c)

Figure 3.5: $\widetilde{K}(\phi_T^{(0)})/(1+\ln k)$ versus ζ_1 at $\zeta_\rho = 0.611$ $[\zeta_\rho = (|\boldsymbol{\zeta}|^2 - \zeta_1^2)^{1/2}]$ on three spatial points ($x_1 = 0$, 1/4 and 1/2), where $\widetilde{K}(\phi_T^{(0)}) \equiv K(\phi_T^{(0)}) E^{1/2}/\zeta_2$ is a function of x_1, ζ_1 and ζ_ρ. (a) $k = 10$, (b) $k = 10^2$ and (c) $k = 10^3$. In each panel, the solid, dash-dotted and dashed lines indicate the profile at $x_1 = 0$, 0.25 and 0.5, respectively.

following [23]. The same similarity applies to $K(\psi_J^{(n)})$. Thus, the computations have been carried out for functions of x_1, ζ_1 and ζ_ρ. In the computations, 11, 97 and 113 grid points have been arranged in the half-ranges of x_1 and ζ_1 (i.e., $0 \le x_1 \le 1/2$ and $\zeta_1 > 0$) and in the whole range of $\zeta_\rho (> 0)$. Grid points in $-1/2 \le x_1 \le 0$ and $\zeta_1 < 0$ have been arranged symmetrically with respect to $x_1 = 0$ and $\zeta_1 = 0$.

3.5 Numerical results and discussions

3.5.1 Velocity distribution functions

Figures 3.4 and 3.5 show an example of $\psi_T^{(1)}$ and $K(\phi_T^{(0)})$ obtained numerically. The behaviour of $K(\phi_T^{(0)})$ and $\psi_T^{(1)}$ in the figures actually follows the estimate (3.21). That is, as

	Present results							
	Thermal transpiration			Poiseuille flow			Literature[a]	
k	$M[\phi_T^{(0)}]$	$M[\phi_T^{(1)}]$	$M[\phi_T^{(n)}]$	$M[\phi_P^{(0)}]$	$M[\phi_P^{(1)}]$	$M[\phi_P^{(n)}]$	$M[\phi_T]$	$M[\phi_P]$
10	0.3530	0.4117	$0.4241^{(7)b}$	−0.8267	−0.9805	$-1.0159^{(7)}$	0.4241	−1.0159
15	0.4064	–	–	−0.9360	–	–	0.4668	−1.0907
20	0.4451	0.4924	$0.4982^{(5)}$	−1.0146	−1.1322	$-1.1477^{(5)}$	0.4982	−1.1477
10^2	0.6673	0.6893	$0.6900^{(3)}$	−1.4621	−1.5125	$-1.5143^{(3)}$	–	–
10^3	0.9910	0.9960	$0.9960^{(2)}$	−2.1102	−2.1210	$-2.1210^{(2)}$	–	–
10^4	1.3157	1.3166	$1.3166^{(1)}$	−2.7596	−2.7615	$-2.7615^{(1)}$	–	–
10^5	1.6404	1.6406	$1.6406^{(1)}$	−3.4091	−3.4094	$-3.4094^{(1)}$	–	–
10^6	1.9652	1.9652	$1.9652^{(1)}$	−4.0587	−4.0587	$-4.0587^{(1)}$	–	–

[a]Direct numerical solution by Ohwada *et al.* [23]. The data refined by Kosuge *et al.* [14], which may differ at most by 2 at the last digit from those of [23], are shown in the table.
[b]Converged data. The superscript number in parentheses indicates the order of approximation n.

Table 3.1: Net mass flows in the highly rarefied regime

is seen in figure 3.4, $\psi_T^{(1)}$ is $O(\ln k + 1)$ and is localized in the range of $|k\zeta_1| \lesssim 1$. On the other hand, as is seen in figure 3.5, $K(\phi_T^{(0)})$ is also $O(\ln k + 1)$, but there is no trace of the over-concentration observed in $\phi_T^{(0)}$; i.e. $K(\phi_T^{(0)})$ behaves moderately in ζ_1. These facts mean that the localization of $\phi_T^{(0)}$ disappears by the action of K but is reproduced by the action of integration (3.20). Note that $\psi_T^{(1)}$ and $\phi_T^{(0)}$ are similar to each other (see figures 3.3 and 3.4). Thus, roughly speaking, with the action of integration (3.20) after K as a unit process, the original distribution is reproduced with the scale reduced by the factor of $k^{-1}(\ln k + 1)$. Figure 3.6 shows the transition from $\phi_T^{(0)}$ to $\psi_T^{(4)}$ that is obtained numerically for $k = 10$. The figure shows the expected invariance of the form of $\psi_J^{(n)}$ in the iterative process. This implies that estimate (3.21a) is actually optimal, as mentioned at the end of § 3.4.2.

3.5.2 Net mass flows

The net mass flows that have been obtained numerically for several values of k are shown in table 3.1. In table 3.1, the zeroth-, first- and higher-order iterative approximation solutions ($M[\phi_J^{(0)}]$, $M[\phi_J^{(1)}]$ and $M[\phi_J^{(n)}]$) are presented, where the data in the columns of $M[\phi_J^{(n)}]$ have converged to five digits. We have also prepared a database that promptly gives the net mass flows for arbitrary values of $k \geq 10$ in the same way as [15]. The details are given in Sec. 3.9.

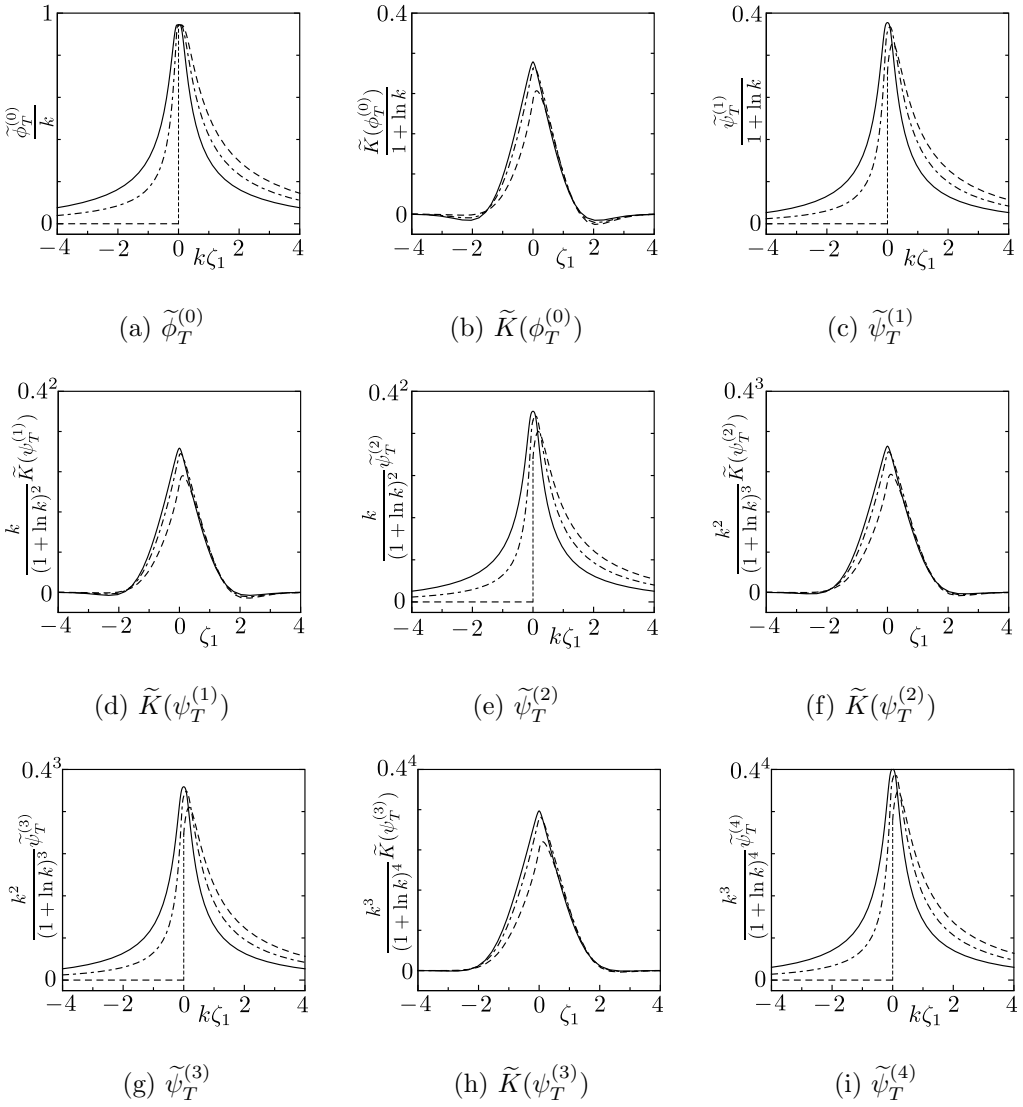

Figure 3.6: Transition from $\phi_T^{(0)}$ to $\psi_T^{(4)}$ ($\phi_T^{(0)} \to K(\phi_T^{(0)}) \to \psi_T^{(1)} \to K(\psi_T^{(1)}) \to \psi_T^{(2)} \to K(\psi_T^{(2)}) \to \psi_T^{(3)} \to K(\psi_T^{(3)}) \to \psi_T^{(4)}$) in the case of $k = 10$ at $\zeta_\rho = 0.611$ ($\zeta_\rho = (|\boldsymbol{\zeta}|^2 - \zeta_1^2)^{1/2}$). In each panel, rescaled $\widetilde{\phi}_T^{(0)} = \phi_T^{(0)} E^{1/2}/\zeta_2$, $\widetilde{\psi}_T^{(n)} = \psi_T^{(n)} E^{1/2}/\zeta_2$ ($n = 1, \ldots, 4$) or $\widetilde{K}(\cdot) = K(\cdot)E^{1/2}/\zeta_2$, which is a function of x_1, ζ_1 and ζ_ρ, is shown in place of $\phi_T^{(0)}$, $\psi_T^{(n)}$ or $K(\cdot)$. The solid, dash-dotted and dashed lines indicate the profile at $x_1 = 0$, 0.25 and 0.5, respectively. Note the difference of the scale of abscissa between two groups of panels, i.e. (a), (c), (e), (g) and (i) versus (b), (d), (f) and (h). The factor 0.4 in the ordinate corresponds to the constant C_1 in (3.21).

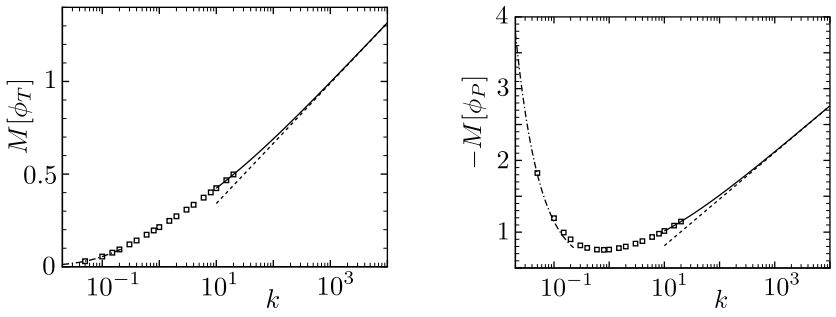

(a) (b)

Figure 3.7: Net mass flows as a function of k. (a) $M[\phi_T]$ vs k and (b) $M[\phi_P]$ vs k. The solid lines indicate the data taken from the present database (see (3.42)), the dashed lines the asymptotic formula (3.27a), dash-dot lines the asymptotic theory for small k [26] and open symbols the numerical data by [23,14].

The data taken from the database are shown by the solid lines in figure 3.7, together with the numerical results by Ohwada *et al.* [23] and Kosuge *et al.* [14] for intermediate Knudsen numbers (open symbols), the asymptotic solutions in [26] for small Knudsen numbers (dash–dotted lines) and the asymptotic formula (3.27) for large Knudsen numbers that appears later (dashed lines). As is clear from the table and the figure, the present results (solid lines) are smoothly connected to those of [23] and [14] for intermediate Knudsen numbers. (Kosuge *et al.* [14], who studied the case of binary gas mixtures, obtained the data for a pure gas as a special case, though they are not shown in the paper. Those data are mentioned when the work of [14] is cited in the present paper.)

3.6 Further discussions on asymptotic behaviour as $k \to \infty$

3.6.1 Grad's hard potential and asymptotic formula for $M[\phi_J]$

In obtaining (3.24), we have changed the order of integration, which is allowed because there is a positive constant ν_* such that $\nu \geq \nu_* > 0$. The expression (3.24) is valid for any molecular model if its $\nu(|\boldsymbol{\zeta}|)$ has a positive lower bound. Grad [10] showed that such a positive lower bound exists for his hard-potential model (Grad's hard potential; see Sec. 3.10), which contains the HS model as a special case. Further, by using the mathematical estimates of [10], we can show that the estimates (a)–(c) in § 3.4.1 are valid also for Grad's hard

potential. Thus, the discussion so far also applies to Grad's hard potential. Besides the HS model, various practical models such as the cutoff inverse-power-law (IPL) model with the exponent $s \geq 5$ ($s = 5$ is the cutoff Maxwell molecule), the variable hard-sphere (VHS) model ([3]) with the viscosity index $1/2 \leq \omega \leq 1$ and the variable soft-sphere (VSS) model ([16]) with $1/2 \leq \omega \leq 1$ and the exponent of cosine of deflection angle $\alpha \geq 1$ belong to Grad's hard potential. (As to the notation ω and α we follow [3], while as to s we follow [10]. The viscosity index of the IPL model with the exponent s is given by $\omega = (s+3)/[2(s-1)]$.)

One useful consequence of the above facts is that $M[\phi_J]$ can be expressed by the right-hand side of (3.24) for any molecular model belonging to Grad's hard potential within the error $O(k^{-1}(\ln k)^2)$. Examining the behaviour of the integrand in (3.24) as $k \to \infty$ leads to the following simple asymptotic formula for $M[\phi_J]$ for Grad's hard potential:

$$M[\phi_J] = C_{J0} \ln k + C_{J1} + C_J[\nu] + O(k^{-1}(\ln k)^2), \tag{3.27a}$$

where

$$C_{P0} = -\frac{1}{2\sqrt{\pi}}, \quad C_{P1} = -\frac{3}{4}\frac{1}{\sqrt{\pi}}(1-\gamma), \quad C_{T0} = \frac{1}{4\sqrt{\pi}}, \quad C_{T1} = \frac{1}{8\sqrt{\pi}}(1-3\gamma), \tag{3.27b}$$

$$C_J[\nu] = \frac{1}{\sqrt{\pi}} \int_0^\infty t^3 \ln \nu(t) \tilde{I}_J \mathrm{e}^{-t^2} \mathrm{d}t, \tag{3.27c}$$

and γ is the Euler constant ($\gamma = 0.577216$). Note that C_{P0} and C_{T0} are independent of molecular models. Thus, as far as the leading order is concerned, $M[\phi_J]$ is independent of molecular models in the highly rarefied regime. This is not obvious from (3.14b).

Further, $C_P[\nu]$ and $C_T[\nu]$ can be obtained easily. Some examples are shown in table 3.2, where ν is normalized in such a way that $\overline{\nu}$ defined by $\overline{\nu} := (4/\sqrt{\pi}) \int_0^\infty t^2 \nu(t) \mathrm{e}^{-t^2} \mathrm{d}t$ is unity. For instance, for the VHS and IPL models with the viscosity index ω, ν is commonly given by

$$\nu(t) = \frac{2^{\omega-2}}{\Gamma(-\omega + (5/2))} \frac{1}{t} \int_0^\infty r^{3-2\omega} (\exp(-|t-r|^2) - \exp(-|t+r|^2)) \mathrm{d}r. \tag{3.28}$$

Thus, the formula (3.27a) for the VHS model is identical to that for the IPL model with the same viscosity index. They can be different from each other at $O(k^{-1}(\ln k)^2)$ or higher order of k^{-1}, because of the difference of K in (3.9a). Incidentally, if ν is normalized in such a way that $\overline{\nu} \neq 1$, we rewrite (3.27a) as $M[\phi_J] = C_{J0} \ln(k/\overline{\nu}) + C_{J1} + C_J[\nu/\overline{\nu}] + O(k^{-1}(\ln k)^2)$ and identify the values of $\sqrt{\pi} C_J[\nu/\overline{\nu}]$ with those of $\sqrt{\pi} C_J[\nu]$ in table 3.2.

Molecular model	Viscosity index ω^a	$\sqrt{\pi}C_P[\nu]$	$\sqrt{\pi}C_T[\nu]$
HS	1/2	0.0310229	0.120791
VHS (helium or neon)	0.66	0.0237010	0.0832157
VHS (argon)	0.81	0.0147201	0.0471379
VHS (xenon)	0.85	0.0119477	0.0373583
Pseudo-Maxwell	1	0	0

[a]Taken from table A1 in [3]

Table 3.2: Coefficients $C_P[\nu]$ and $C_T[\nu]$ in (3.27)

In the case of the HS model, the actual error of formula (3.27) (the first three terms) is less than 20%, 3.6%, 0.52% and 0.073% for $k = 10$, 10^2, 10^3 and 10^4, respectively. For $k \geq 10^4$, formula (3.27) gives the same values as those of $M[\phi_J^{(0)}]$ at least to five digits.

The asymptotic formula corresponding to (3.27) can be obtained along the same lines for Poiseuille and thermal transpiration flows in a circular tube. Let us denote by D a radius of the pipe cross-section and by $\rho_0(\pi D^2)(2RT_0)^{1/2}M[\phi]$ the net mass flow through the pipe cross-section, where ϕ is written as $\phi = \beta_P[x_2 + \phi_P(x_1, x_3, \boldsymbol{\zeta})] + \beta_T[(|\boldsymbol{\zeta}|^2 - 5/2)x_2 + \phi_T(x_1, x_3, \boldsymbol{\zeta})]$. Then, we can show that $M[\phi_J]$ is given by

$$M[\phi_P] = -\frac{4}{3}\frac{1}{\sqrt{\pi}} + O(k^{-1}\ln k), \quad M[\phi_T] = \frac{2}{3\sqrt{\pi}} + O(k^{-1}\ln k), \tag{3.29}$$

for $k \gg 1$, irrespective of the molecular model as long as it belongs to Grad's hard potential. It should be noted that (3.29) agrees with the classical results for the BGK model, including the order of the error terms ([8,21]; see also [13]).

3.6.2 Similarity between $u[\phi_T]$ and $Q[\phi_P]$

It is known that the dimensionless net mass flow of the thermal transpiration is identical to the dimensionless net heat flow of the Poiseuille flow for arbitrary Knudsen numbers ([17]; see also [29]):

$$\int_{-1/2}^{1/2} u[\phi_T]\mathrm{d}x_1 = \int_{-1/2}^{1/2} Q[\phi_P]\mathrm{d}x_1. \tag{3.30}$$

It is, however, seen from (3.14b) that $u[\phi_T^{(0)}]$ and $Q[\phi_P^{(0)}]$ are identical even at the level of spatial profile:

$$u[\phi_T^{(0)}] = Q[\phi_P^{(0)}]. \tag{3.31}$$

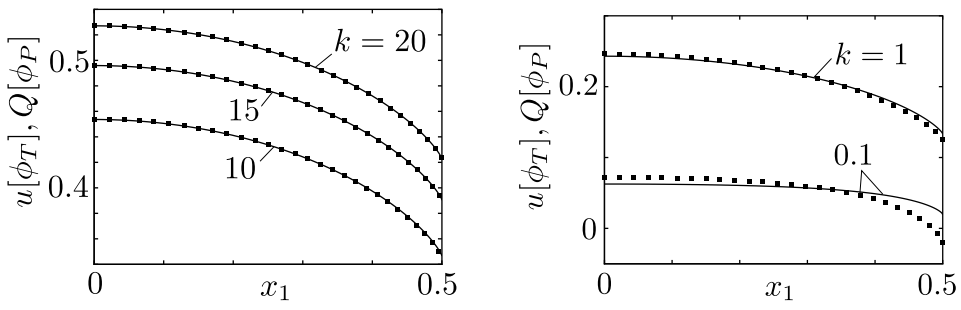

Figure 3.8: Profiles of $u[\phi_T]$ and $Q[\phi_P]$ in the half-range of the channel ($0 \le x_1 \le 1/2$). (a) Large k and (b) small and intermediate k. The solid lines indicate $u[\phi_T]$, while the closed symbols indicate $Q[\phi_P]$. The data shown were obtained by Kosuge *et al.* [14].

That is, the profile of dimensionless flow velocity of thermal transpiration agrees with that of dimensionless heat flow of Poiseuille flow within the error of $O(k^{-1}(\ln k)^2)$ for large k:

$$u[\phi_T] = Q[\phi_P] + O(k^{-1}(\ln k)^2) \qquad (k \gg 1). \tag{3.32}$$

Figure 3.8(a) shows the profiles of $u[\phi_T]$ and $Q[\phi_P]$ for $k = 10$, 15 and 20 obtained by [14]. In the figure, $u[\phi_T]$ is indicated by the solid lines, while $Q[\phi_P]$ is indicated by the closed symbols. They agree well with each other, which is explained by relation (3.32). As shown in figure 3.8(b), the profiles do not agree for small and intermediate Knudsen numbers.

3.7 Conclusion

In the present paper, we have investigated the Poiseuille and thermal transpiration flows of a highly rarefied gas, with a special interest in the over-concentration of molecules on velocities parallel to the walls. Making use of the mathematical estimate given in [9] and [10], we have constructed an iterative approximation scheme with an explicit convergence estimate for the highly rarefied regime and have clarified the structure of the over-concentration in the velocity distribution function. We have also constructed a database for both problems that promptly gives the accurate data of the net mass flow for an arbitrary value of $k \ge 10$ for an HS molecular gas. In addition, we have presented an explicit simple asymptotic formula for the net mass flows for large Knudsen numbers, which is valid up to $O(1)$ and is applicable to any molecular model belonging to Grad's hard potential. Finally, we have pointed out that the profiles of the heat flow of Poiseuille flow and of the flow velocity of thermal transpiration

agree with each other in the highly rarefied regime and have clarified the reason.

3.8 Appendix A: Sketch of proofs of the statements in § 3.3 and § 3.4.1

The difference between the Poiseuille flow and thermal transpiration problems lies only in the form of I_J. This difference requires a few minor changes in the course of the proof in [9] to reach statements (i), (ii), and (iii)$'$ of § 3.3. Thus, we shall provide below only the sketch of proof of the statements in § 3.4.1.

Part (b). By using lemma 4.2 of [9], we first easily obtain that there is a positive constant C_0 such that

$$|\psi_J^{(0)} E^{1/2}| \le C_0 (\frac{1}{k} + |\zeta_1|)^{-1}, \quad ||\psi_J^{(0)}||_\infty \le C_0 k, \tag{3.33}$$

where $||\cdot||_\infty = \sup_{\boldsymbol{\zeta}} |\cdot E^{1/2}|$. Then, by following the proof of lemma 4.3 of [9], we have from the above estimate that there is a positive constant C such that

$$|K(\psi_J^{(0)}) E^{1/2}| \le C C_0 (\ln k + 1). \tag{3.34}$$

Using this estimate in (3.20), we obtain

$$|\psi_J^{(1)} E^{1/2}| \le C_0^2 C k^{-1} (\ln k + 1) \Big(\frac{1}{k} + |\zeta_1|\Big)^{-1}, \quad ||\psi_J^{(1)}||_\infty \le C_0^2 C (\ln k + 1). \tag{3.35}$$

Note that $\psi_J^{(1)}$ follows the same estimate as $\psi_J^{(0)}$ as a function of $\boldsymbol{\zeta}$ and x_1. Thus, by repeating the above process, we have

$$|K(\psi_J^{(1)}) E^{1/2}| \le (C C_0)^2 k^{-1} (\ln k + 1)^2 \tag{3.36}$$

and further conclude (3.21) in § 3.4.1. (The $\max(C_0, C C_0)$ and $C C_0$ here are the C_0 and C_1 in (3.21).) Since the above constants C and C_0 are independent of k, $||\psi_J^{(n)}||_\infty \to 0$ as $n \to \infty$.

Part (a). By the use of estimate (3.21a), we see that $||\phi_J^{(n)}||_\infty \le C_0 k / [1 - C C_0 k^{-1} (\ln k + 1)] < \infty$ and that for $\forall n > m$,

$$|(\phi_J^{(n)} - \phi_J^{(m)}) E^{1/2}| \le C_0 \Big(\frac{1}{k} + |\zeta_1|\Big)^{-1} \frac{[C C_0 k^{-1} (\ln k + 1)]^{m+1}}{1 - C C_0 k^{-1} (\ln k + 1)}. \tag{3.37}$$

For sufficiently large k, the right-hand side tends to zero as $m \to \infty$, so that $||\phi_J^{(n)} - \phi_J^{(m)}||_\infty \to 0$. Thus $\{\phi_J^{(n)}\}$ is a Cauchy sequence in L^∞. Now denote $\lim_{n\to\infty} \phi_J^{(n)}$ by Φ_J and define a function R_J by

$$R_J \equiv \Phi_J - \phi_J^{(0)} - \int_{\mp 1/2}^{x_1} \frac{1}{k\zeta_1} \exp\Big(-\frac{\nu}{k}\frac{|s-x_1|}{|\zeta_1|}\Big) K(\Phi_J)\mathrm{d}s, \quad \zeta_1 \gtrless 0. \tag{3.38}$$

Since this equation can be rewritten as

$$R_J = \Phi_J - \phi_J^{(n)} - \int_{\mp 1/2}^{x_1} \frac{1}{k\zeta_1} \exp\Big(-\frac{\nu}{k}\frac{|s-x_1|}{|\zeta_1|}\Big) K(\Phi_J - \phi_J^{(n-1)})\mathrm{d}s, \quad \zeta_1 \gtrless 0, \tag{3.39}$$

we obtain $||R_J||_\infty \le ||\Phi_J - \phi_J^{(n)}||_\infty + C_0||K(\Phi_J - \phi_J^{(n-1)})||_\infty \to 0$ as $n \to \infty$, where lemma 4.1 of [9] has been used. Thus Φ_J is a solution of (3.14) in L^∞.

Part (c). First, $u[\psi_J^{(n)}]$ is expressed as

$$\begin{aligned} u[\psi_J^{(n)}] = &\int_{-\infty}^{\infty}\int_{-\infty}^{\infty}\int_{0}^{\infty}\int_{-1/2}^{x_1} \frac{\zeta_2}{\zeta_1} \exp\Big(-\frac{\nu}{k|\zeta_1|}|s-x_1|\Big)\frac{1}{k} K(\psi_J^{(n-1)}) E \mathrm{d}s\mathrm{d}\zeta_1\mathrm{d}\zeta_2\mathrm{d}\zeta_3 \\ &+ \int_{-\infty}^{\infty}\int_{-\infty}^{\infty}\int_{-\infty}^{0}\int_{1/2}^{x_1} \frac{\zeta_2}{\zeta_1} \exp\Big(-\frac{\nu}{k|\zeta_1|}|s-x_1|\Big)\frac{1}{k} K(\psi_J^{(n-1)}) E \mathrm{d}s\mathrm{d}\zeta_1\mathrm{d}\zeta_2\mathrm{d}\zeta_3. \end{aligned} \tag{3.40}$$

Then, in the same way as the estimate of A_1 in [9], we have, by using (3.21c),

$$\begin{aligned} |u[\psi_J^{(n)}]| &\le C'[C_1 k^{-1}(\ln k + 1)]^n \int_{-\infty}^{\infty}\int_{-\infty}^{\infty}\int_{0}^{\infty}\int_{-1/2}^{1/2} \frac{|\zeta_2|}{\zeta_1} \exp\Big(-\frac{\nu}{k\zeta_1}|s-x_1|\Big) E^{1/2} \mathrm{d}s\mathrm{d}\zeta_1\mathrm{d}\zeta_2\mathrm{d}\zeta_3 \\ &\le C''[C_1 k^{-1}(\ln k + 1)]^n (\ln k + 1), \end{aligned} \tag{3.41}$$

where C' and C'' are some positive constants. The estimate for $M[\psi_J^{(n)}]$ can be obtained in the same way.

3.9 Appendix B: Database of the net mass flows for the HS model

The database of the net mass flows for $k \ge 10$ that has been constructed in the present work makes use of the Chebyshev polynomial interpolation (see [4]) for $10 \le k < 10^7$:

$$M[\phi_J] = \sum_{j=0}^{N} a_J^{(j)} P^{(j)}\Big(\frac{\ln(k^2/(k_{max}k_{min}))}{\ln(k_{max}/k_{min})}\Big), \tag{3.42}$$

where $P^{(j)}$ is the following polynomial of degree j of its argument:

$$P^{(0)}(x) = 1, \quad P^{(1)}(x) = x, \quad P^{(n)}(x) = 2xP^{(n-1)}(x) - P^{(n-2)}(x), \tag{3.43}$$

j	$a_P^{(j)}$	$a_T^{(j)}$	j	$a_P^{(j)}$	$a_T^{(j)}$
0	$-1.84790018(+0)^a$	8.54825701(−1)	9	1.49228707(−7)	−1.25559087(−7)
1	−8.83316631(−1)	4.49679688(−1)	10	2.60089118(−7)	−8.99270022(−8)
2	−3.92650101(−2)	1.52324109(−2)	11	−1.14839592(−7)	3.11987783(−8)
3	1.05217018(−2)	−3.54414570(−3)	12	−2.17698962(−8)	8.08859477(−9)
4	−1.57787850(−3)	3.01542071(−4)	13	9.70450516(−8)	−3.18197288(−8)
5	2.70953882(−5)	8.62335466(−5)	14	−2.15201321(−7)	6.99137082(−8)
6	3.90220820(−5)	−3.32236013(−5)	15	2.68421948(−7)	−1.00798691(−7)
7	−5.19294709(−6)	3.56117808(−6)	16	−1.68935567(−7)	5.64147556(−8)
8	−1.00587844(−6)	5.59709749(−7)			

[a] Read as $-1.84790018 \times 10^{+0}$.

Table 3.3: Coefficients $a_P^{(j)}$ and $a_T^{(j)}$ in (3.42) for $10 \le k < 10^4$.

j	$a_P^{(j)}$	$a_T^{(j)}$	j	$a_P^{(j)}$	$a_T^{(j)}$
0	$-3.73438354(+0)^a$	1.80303014(+0)	5	1.25230608(−5)	−5.76967764(−6)
1	−9.73557111(−1)	4.86790137(−1)	6	−2.45021285(−6)	1.09473993(−6)
2	−4.16662892(−4)	2.00691591(−4)	7	3.79936917(−7)	−1.61013000(−7)
3	1.66673351(−4)	−7.94789372(−5)	8	−4.39077230(−8)	1.66539324(−8)
4	−5.13184520(−5)	2.41268625(−5)			

[a] Read as $-3.73438354 \times 10^{+0}$.

Table 3.4: Coefficients $a_P^{(j)}$ and $a_T^{(j)}$ in (3.42) for $10^4 \le k < 10^7$.

for $n \ge 2$ and $-1 \le x \le 1$, $(N, k_{min}, k_{max}) = (16, 10, 10^4)$ for $10 \le k < 10^4$ and $(N, k_{min}, k_{max}) = (8, 10^4, 10^7)$ for $10^4 \le k < 10^7$. The coefficients $a_J^{(j)}$ have been determined by the numerical data of $M[\phi_J]$ computed for $N+1$ different values of k, say $k^{(l)}$, such that $\ln(k^{(l)2}/(k_{max}k_{min}))/\ln(k_{max}/k_{min}) = -\cos((2l+1)\pi/(2N+2))$ $(l = 0, \ldots, N)$. They are shown in tables 3.3 and 3.4. For economy of computation, the values of $a_T^{(j)}$ in the tables have been determined from the heat flow of the Poiseuille flow by using relation (3.30). (Note that the data of $M[\phi_T^{(i)}]$ and $M[\phi_P^{(i)}]$ $(i = 0, 1, n)$ in table 3.1 have been computed independently of each other.)

For $k \ge 10^7$, the database makes use of the first three terms of (3.27a):

$$M[\phi_J] = C_{J0} \ln k + C_{J1} + C_J[\nu], \tag{3.44}$$

where C_{J0} and C_{J1} are those in (3.27b) and $C_J[\nu]$ that for the HS model in table 3.2.

3.10 Appendix C: Grad's hard potential

In general, the collision frequency ν is written as

$$\nu(|\boldsymbol{\zeta}|) = 2\pi \int \int_0^{\pi/2} B(\theta, |\boldsymbol{\zeta}_* - \boldsymbol{\zeta}|) E(|\boldsymbol{\zeta}_*|) \mathrm{d}\theta \mathrm{d}\boldsymbol{\zeta}_*. \tag{3.45}$$

The hard potential introduced by Grad [10] (Grad's hard potential) is defined as the potential satisfying the condition that

$$\frac{B(\theta, V)}{|\cos\theta \sin\theta|} < C(V + V^{-1+\epsilon}), \quad B_0(V) \geq C\frac{V}{1+V}, \tag{3.46}$$

where C and $\epsilon < 1$ are positive constants and

$$B_0(V) = \int_0^{\pi/2} B(\theta, V) \mathrm{d}\theta. \tag{3.47}$$

For Grad's hard potential, Grad [10] showed that there are positive constants ν_0 and ν_1 such that $\nu_1(1 + |\boldsymbol{\zeta}|^2)^{1/2} \geq \nu(|\boldsymbol{\zeta}|) \geq \nu_0 > 0$, that $\nu(|\boldsymbol{\zeta}|)$ is a monotonic increasing function of $|\boldsymbol{\zeta}|$ and that $\hat{K}$ defined by $\hat{K}(\hat{\phi}) = K(\phi)E^{1/2}$ with $\hat{\phi} = \phi E^{1/2}$ is a compact operator on L^2.

References

1 P. Andries, P. Le Tallec, J. P. Perlat and B. Perthame, *The Gaussian-BGK model of Boltzmann equation with small Prandtl number*, Eur. J. Mech. B Fluids, **19** (2000), 813–830.

2 P. L. Bhatnagar, E. P. Gross and M. Krook, *A model for collision processes in gases. Part I. Small amplitude processes in charged and neutral one-component systems*, Phys. Rev., **94** (1954), 511–525.

3 G. A. Bird, *Molecular Gas Dynamics and the Direct Simulation of Gas Flows*, Oxford University Press, 1994.

4 J. P. Boyd, *Chebyshev and Fourier Spectral Methods*, Dover, second (revised), 2001.

5 C. Cercignani, *Plane Poiseuille flow and Knudsen minimum effect*, in *Rarefied Gas Dynamics*, (ed. J. A. Laurmann), vol. II, pp. 92–101, Academic, 1963.

6 C. Cercignani, *The Boltzmann Equation and its Applications*, Springer, 1988.

7 C. Cercignani, *Slow Rarefied Flows*, Birkhäuser, 2006.

8 C. Cercignani and F. Sernagiotto, *Cylindrical Poiseuille flow of a rarefied gas*, Phys. Fluids, **9** (1966), 40–44.

9 C.-C. Chen, I.-K. Chen, T.-P. Liu and Y. Sone, *Thermal transpiration for the linearized Boltzmann equation*, Commun. Pure Appl. Math., **60** (2007), 0147–0163.

10 H. Grad, *Asymptotic theory of the Boltzmann equation. Part II*, in *Rarefied Gas Dynamics*, (ed. J. A. Laurmann), vol. I, pp. 26–59, Academic, 1963.

11 L. H. Holway, Jr., *Approximation Procedures for Kinetic Theory*, Ph.D. thesis, Harvard University, Cambridge, MA, 1963.

12 L. H. Holway, Jr., *New statistical models for kinetic theory: methods of construction*, Phys. Fluids, **9** (1966), 1658–1673.

13 E. H. Kennard, *Kinetic Theory of Gases*, McGraw-Hill, 1938.

14 S. Kosuge, K. Sato, S. Takata and K. Aoki, *Flows of a binary mixture of rarefied gases between two parallel plates*, in *Rarefied Gas Dynamics*, (ed. M. Capitelli), pp. 150–155, AIP, 2005.

15 S. Kosuge and S. Takata, *Database for flows of binary gas mixtures through a plane microchannel*, Eur. J. Mech. B Fluids, **27** (2008), 444–465.

16 K. Koura and H. Matsumoto, *Variable soft sphere molecular model for inverse-power-law or Lennard-Jones potential*, Phys. Fluids A, **3** (1991), 2459-2465.

17 S. K. Loyalka, *Kinetic theory of thermal transpiration and mechanocaloric effect. Part I*, J. Chem. Phys., **55** (1971), 4497-4503.

18 F. J. McCormack, *Construction of linearized kinetic models for gaseous mixtures and molecular gases*, Phys. Fluids, **16** (1973), 2095–2105.

19 M. Mori, *Discovery of the double exponential transformation and its developments*, Publ. RIMS Kyoto Univ., **41** (2005), 897–935.

20 M. Mori and M. Sugihara, *The double-exponential transformation in numerical analysis*, J. Comput. Appl. Math., **127** (2001), 287–296.

21 H. Niimi, *Thermal creep flow of rarefied gas through a cylindrical tube*, J. Phys. Soc. Japan, **24** (1968), 225.

22 H. Niimi, *Thermal creep flow of rarefied gas between two parallel plates*, J. Phys. Soc. Japan, **30** (1971), 572–574.

23 T. Ohwada, Y. Sone and K. Aoki, *Numerical analysis of the Poiseuille and thermal transpiration flows between two parallel plates on the basis of the Boltzmann equation for hard-sphere molecules*, Phys. Fluids A, **1** (1989), 2042–2049.

24 Y. Sone, *Asymptotic theory of flow of rarefied gas over a smooth boundary. Part I*, in *Rarefied Gas Dynamics* (ed. L. Trilling and H. Y. Wachman), vol. I, pp. 243–253, Academic, 1969.

25 Y. Sone, *Asymptotic theory of a steady flow of a rarefied gas past bodies for small Knudsen numbers*, in Advances in Kinetic Theory and Continuum Mechanics (ed. R. Gatignol and Soubbaramayer), pp. 19–31, Springer, 1991.

26 Y. Sone, *Molecular Gas Dynamics*, Birkhäuser, 2007. supplemental notes and errata are available at: http://hdl.handle.net/2433/66098.

27 Y. Sone, T. Ohwada and K. Aoki, *Temperature jump and Knudsen layer in a rarefied gas over a plane wall: numerical analysis of the linearized Boltzmann equation for hard-sphere molecules*, Phys. Fluids A, **1** (1989), 363–370.

28 H. Takahasi and M. Mori, *Double exponential formulas for numerical integration*, Publ. RIMS Kyoto Univ., **9** (1974), 721-741.

29 S. Takata, *Symmetry of the linearized Boltzmann equation and its application*, J. Stat. Phys., **136** (2009), 751-784. ($(5/2)\gamma_2$ on line 18, p. 762 and line 24, p. 763, in this reference is a misprint of $(5/4)\gamma_2$).

30 P. Welander, *On the temperature jump in a rarefied gas*, Ark. Fys., **7** (1954), 507–553.

Conclusion

The present thesis contains some studies on internal rarefied gas flows based on kinetic theory of gases. In Chapter 1, we have investigated properties of a Knudsen compressor (or pump) when the gas is a polyatomic gas. In Chapter 2, we have investigated rarefied polyatomic gas flows through a long circular pipe in some situations. In Chapter 3, we have investigated Poiseuille and thermal transpiration flows of a highly rarefied gas for the purpose of clarifying the physical properties based on a mathematical basis.

In Chapter 1, we have considered the Knudsen compressor consisting of many alternately arranged thin and thick two-dimensional channels, and have investigated its properties when the gas is a polyatomic gas. We have derived a simple fluid-dynamic-type system, describing a pressure distribution in the Knudsen compressor, together with an appropriate connection condition at junctions, on the basis of a polyatomic version of the ellipsoidal statistical (ES) model of the Boltzmann equation, by a systematic asymptotic analysis under the assumption that the channel width is much smaller than the length of the pump. The difference from the corresponding fluid-dynamic-type equation for a monatomic gas is confined in the transport coefficients occurring in the equation. The transport coefficients can be obtained readily from those corresponding to the Bhatnagar-Gross-Krook (BGK) model for a monatomic gas. We have showed by some numerical simulations that the polyatomic-gas effect on the performance of the Knudsen compressor is quite limited, so that the existing fluid-dynamic-type system for a monatomic gas can be applied safely to a polyatomic gas in the level of practical applications.

In Chapter 2, we have investigated the Poiseuille and thermal transpiration flows of a rarefied polyatomic gas through a long circular tube on the basis of the linearized ES model of the Boltzmann equation for a polyatomic gas. We have derived a simple conversion formula by which the solutions of the Poiseuille and thermal transpiration flows based on the ES model for a polyatomic gas are obtained from those based on the BGK model for a monatomic gas. We have obtained the numerical results of the flow velocities, mass-flow rates, etc. for the Nitrogen gas. Furthermore, we have considered a rarefied polyatomic gas in a long circular pipe under the following assumptions: (i) the pressure and temperature

variations along the pipe can be arbitrary and large; (ii) the length scale of variations is much longer than the radius of the pipe; (iii) the pipe may consist of circular tubes with different radii. We have shown that the pressure distribution along the pipe is described by a fluid-dynamic-type equation with the transport coefficients consisting of the mass-flow rates of the Poiseuille and thermal transpiration flows by the same way as in Chapter 1. We have applied the system to a gas flow through a single long circular tube caused by a large pressure difference imposed at both ends (Sec. 2.4.1) and to a Knudsen compressor consisting of many alternately arranged thinner and thicker circular tubes (Sec. 2.4.2). With this procedure, we have obtained, by easy computations, the pressure distribution along the pipe and the mass-flow rate through the pipe in the two problems.

In Chapter 3, we have investigated the Poiseuille and thermal transpiration flows of a highly rarefied gas between two parallel plates, with a special interest in the over-concentration of gas molecules on velocities parallel to the walls. Making use of the mathematical estimate, we have constructed an iterative approximation scheme with an explicit convergence estimate in the highly rarefied regime and have clarified the structure of the over-concentration in the velocity distribution function. We have also carried out numerical computations based on the scheme for a hard-sphere molecular gas and have constructed a database for both problems that promptly gives the accurate data of the net mass flow for an arbitrary value of large Knudsen numbers. In addition, we have presented an explicit and simple asymptotic formula for the net mass flows in the highly rarefied regime, which is applicable to any molecular model belonging to Grad's hard potential. Finally, we have pointed out that the profiles of the heat flow of Poiseuille flow and of the flow velocity of thermal transpiration agree with each other in the highly rarefied regime and have clarified the reason.

Acknowledgment

I would like to express my heartfelt thanks to my supervisors, Professor Kazuo Aoki and Associate Professor Shigeru Takata, who offered me interesting and challenging works. I appreciate Professor Kazuo Aoki's kind guidance and advices. I also appreciate Associate Professor Shigeru Takata's kind guidance, fruitful discussions and encouragement. I would like to express my thanks to Assistant Professor Shingo Kosuge for his kind support for research and technical problems.

I am grateful to coworkers at our laboratory for providing good environment for university life. Finally, I am so grateful to my parents for supporting me for a long time.

List of Publications

Chapter 1

Shigeru Takata, Hitoshi Funagane and Kazuo Aoki, *Fluid modeling for the Knudsen compressor: Case of polyatomic gases*, Kinetic and Related Models, **3** (2010), pp. 353–372.

Chapter 2

Hitoshi Funagane, Shigeru Takata, Kazuo Aoki and Ko Kugimoto, *Poiseuille flow and thermal transpiration of a rarefied polyatomic gas through a circular tube with applications to microflows*, Bollettino U.M.I., (9) **IV** (2011), pp. 19–46.

Chapter 3

Shigeru Takata and Hitoshi Funagane, *Poiseuille and thermal transpiration flows of a highly rarefied gas: over-concentration in the velocity distribution function*, J. Fluid Mech., **669** (2011), pp. 242–259.